Western Graduate&PostdoctoralStudies

Western University
Scholarship@Western

Electronic Thesis and Dissertation Repository

2-25-2021 11:00 AM

# Study of Recyclable and Repairable Dynamic Covalent Polymers for Sustainable 3D Printing Development

Mingyue Zheng, *The University of Western Ontario*

Supervisor: Jun Yang, *The University of Western Ontario*

A thesis submitted in partial fulfillment of the requirements for the Doctor of Philosophy degree in Mechanical and Materials Engineering

© Mingyue Zheng 2021

Follow this and additional works at: https://ir.lib.uwo.ca/etd

Part of the Other Materials Science and Engineering Commons

## Recommended Citation

Zheng, Mingyue, "Study of Recyclable and Repairable Dynamic Covalent Polymers for Sustainable 3D Printing Development" (2021). *Electronic Thesis and Dissertation Repository*. 7673.
https://ir.lib.uwo.ca/etd/7673

This Dissertation/Thesis is brought to you for free and open access by Scholarship@Western. It has been accepted for inclusion in Electronic Thesis and Dissertation Repository by an authorized administrator of Scholarship@Western. For more information, please contact wlswadmin@uwo.ca.

# Abstract

3D printing technology with valuable features, including cost-saving, easy access, and unlimited structure design, has attracted significant attention and been employed for production use. This technology has also been considered as a sustainable manufacturing method and quickly developed in recent years. However, the development of sustainable 3D printing is still facing challenges, especially in waste management. Thanks to the flexibility of 3D printing and diversified printing mechanisms, the big step forward can be approachable by the transformation from materials. This dissertation presents a variety of strategies designed for sustainable 3D printing development based on the combination of dynamic covalent chemistry and 3D printing technique. Dynamic covalent bonds provide polymers, including thermosets, with responsive covalent adaptable networks, allowing the materials to be reversible, leading to a recyclable material technology. Through synthesizing epoxy and polyurethane based dynamic covalent polymers as 3D printing materials, together with developing a corresponding 3D printing technique, the strength of green 3D printing is explored.

In this study, OH functionalized multi-walled carbon nanotubes (MWCNTs-OH) are incorporated in the printing material to improve the mechanical property and tailor the photothermal conversion capability of the developed materials. Due to the super high strength and minuscule size of MWCNTs, they are widely used to reinforce polymer as fillers. With MWCNTs-OH incorporating, the ultimate tensile strength and Young's modulus of samples both increased. In particular, young's modulus of 2 wt% DTDA-PU was about 8.6 times higher than the pure sample. Furthermore, MWCNTs are functioning as an excellent photothermal converter to allow the heat triggering to be replaced with a laser light. Therefore, near-infrared (NIR) laser source is utilized as the heat source for targeting the damaged spot of printing parts precisely for in-situ repair application. After the sample is cut in half and repaired, the mechanical properties recover to 86.3% after three times NIR laser-triggered in-site repair. In addition, a creative approach of contactless supporting structure removal is explored to promote post-processing automation and reduce printing parts defective rate. Our sustainable 3D printing strategy has developed an environmentally friendly and energy-efficient technology, which paves the way toward a circular economy.

# Keywords

3D printing, sustainable manufacturing, dynamic covalent chemistry, in-situ repairable, recyclable, disulfide bond, transesterification, polyurethane, epoxy, MWCNTs-OH

# Summary of Lay Audience

Sustainable manufacturing aims to reduce the consumption of finite natural resources and the negative impact on our environment. 3D printing technology, also known as additive manufacturing, is a process to fabricate 3D objects directly from a digital 3D model via computers. This technology can effectively reduce waste by avoiding conventional centralized mass productions. However, as 3D printing polymers being the major player in the current printing materials market, their waste disposal has caused an environmental burden. This work takes the further step of sustainable 3D printing development by developing the fully recyclable and repairable 3D printing technology.

Dynamic covalent bonds are the key to solving the problem. These are the covalent bonds that can exchange or switch between several molecules under certain conditions. Therefore, dynamic covalent bonds allow polymers, including thermosets, to be reversible, leading to a recyclable and repairable materials technology. In this work, disulfide bonds and transesterification, as two of the most widely studied dynamic covalent bonds, were utilized for our recyclable and repairable printing materials development.

The relatively low mechanical properties of pure polymers are another issue that limit the applications of 3D printing polymer products. Therefore, carbon nanotubes (CNTs), as the strongest and stiffest materials yet discovered, were incorporated in our recyclable and repairable printing materials to improve their mechanical performance. Furthermore, CNTs can be employed as light to heat convertors that can generate large amounts of heat by absorbing light. The stimulus to trigger the above dynamic covalent bonds usually is heat. However, heat energy is not easy to control, especially during the repair process for complex structures. The dynamic covalent

polymers with CNTs incorporated can convert the stimulus from heat to light. Therefore, the repairing processes of damaged complex structures can be precisely and remotely operated with laser aiding. In addition, support structures are always necessary for 3D printing parts with overhang structures and need to be removed after printing. Traditional support removal processes by mechanical force are labor-intensive and prone to error. The laser-aid technique can effectively reduce defective rate by achieving contactless removal, which can also reduce the waste of resource.

# Co-Authorship Statement

Chapter 2-6 in this thesis are based on the following papers:

Title: Direct ink writing of recyclable and in situ repairable photothermal polyurethane for sustainable 3D printing development†

Authors: Mingyue Zheng, Qiuquan Guo, Xiangyu Yin, Nuwansiri Nirosh Getangama, John R. de Bruyn, Junfeng Xiao, Yang Bai, Mei Liu, Jun Yang

All the experimental and theoretical work was carried out by Mingyue Zheng under the supervision of Dr. Jun Yang. The initial draft and following modification of this manuscript were conducted by Mingyue Zheng under the supervision of Dr. Jun Yang. The other co-authors contributed to the formation of the final version with discussion and related characterization. The paper has been published by J. Mater. Chem. A.

**Title:** 3D Printable Bis(2,2,6,6,-tetramethylpoperidin-1-yl)disulfide Cross-linked Polyurethane Network

**Authors:** Mingyue Zheng, Qiuquan Guo, Xiangyu Yin, Junfeng Xiao, Jun Yang

All the experimental and theoretical work was carried out by Mingyue Zheng under the supervision of Dr. Jun Yang. The initial draft and following modification of this manuscript were conducted by Mingyue Zheng under the supervision of Dr. Jun Yang. The other co-authors contributed to the formation of the final version with discussion and related characterization. The paper co-authored by Mingyue Zheng, Qiuquan Guo, Xiangyu Yin, Junfeng Xiao and Jun Yang is to be submitted.

For the other content of this thesis, all the preparation for experimental testing and set-up was undertaken by Mingyue Zheng under the supervision of Dr. Jun Yang. Experimental testing was performed by Mingyue Zheng under the supervision of Dr. Jun Yang. The initial draft and following modification of this manuscript were conducted by Mingyue Zheng under the supervision of Dr. Jun Yang.

# Acknowledgments

Throughout five years of research experience and writing this dissertation, I have received a great deal of support and assistance. It is a pleasure to have this chance to express my great appreciation to everyone who supported and made this work possible.

Foremost, I would like to express my sincere gratitude to my supervisor-Professor Jun Yang, for his guidance through each stage of the progress. His insightful advice, forward guidance and continuous support pushed me to sharpen my thinking and encouraged me to face the challenges. He is instrumental in defining the path of my research. I deeply know that this thesis could not have been possible without him. I also would like to thank my supervisor committees, Prof. Ovidiu-Remus Tutunea-Fatan and Prof. George K Knopf, for their kind advice on my studies at every stage.

I also wish to extend my heartfelt appreciation to all my colleagues in Yang's group. Their cooperation, friendship and help delighted my research and life. I would like to give my special thanks to Dr. Xiangyu Yin and Dr. Qiuquan Guo. Their seasoned advice and constructive comments always led me to overcome the difficulties in my experiments.

I am very grateful to Western Nanofabrication Facility for training me to use SEM imaging from Dr. Tim Goldhawk and Dr. Todd Simpson. I would like to show my thanks to Prof. John R. de Bruyn and Nirosh Getangama for their help in material rheological behavior testing. I also want to thank the Institute for Chemicals and Fuels from Alternative Resources (ICFAR) for the generous help in material characterization from Fang (Flora) Cao and Dr. Hongwei (Lilly) Li.

Words are not enough to express my gratitude toward my family. I would not have been able to do this without their support. I would like to sincerely thank my parents for their understanding,

encouragement, and support. I feel extremely grateful for meeting my husband, Mengze Yang, at Western University. It is his company that makes my life full of love and energy. It simply would not have been possible without him.

# Table of Contents

Abstract ........ ii

Summary of Lay Audience ........ iv

Co-Authorship Statement ........ vi

Acknowledgments ........ viii

Table of Contents ........ x

List of Tables ........ xv

List of Figures ........ xvi

List of Appendices ........ xxv

Glossary of Terms ........ xxvi

Chapter 1 ........ 1

1 Introduction ........ 1

  1.1 Development of Sustainable Manufacturing ........ 2

  1.2 Development of 3D Printing ........ 4

    1.2.1 Review of 3D Printing Technologies ........ 4

    1.2.2 Review of 3D Printing Materials ........ 13

    1.2.3 Perspectives and Challenges for 3D Printing ........ 24

1.3 The Solutions with Dynamic Covalent Chemistry ............................................. 26

1.3.1 Introduction to Dynamic Covalent Chemistry ......................................... 26

1.3.2 Development of 3D printing Technology Based on Dynamic Covalent Chemistry ........................................................................................ 34

1.3.3 Thesis Objectives ........................................................................ 39

1.4 Thesis Outline ........................................................................................ 41

Chapter 2 ........................................................................................................ 44

2 Experimental and Characterization Techniques .......................................... 44

2.1 Introduction ........................................................................................... 44

2.2 Materials and Chemicals ....................................................................... 46

2.3 Materials Synthesis and Fabrication ...................................................... 47

2.3.1 Synthesis of FA-Epoxy ............................................................... 47

2.3.2 Synthesis of CADH-Epoxy .......................................................... 47

2.3.3 Synthesis of TEMPS-PU .............................................................. 48

2.3.4 Synthesis of DTDA-PU ............................................................... 50

2.3.5 Synthesis of DTDA-PU/MWCNTs-OH ...................................... 51

2.4 DIW 3D Printing Technology ................................................................. 51

2.5 Instruments and Characterization .......................................................... 53

Chapter 3 ................................................................................................ 57

3 Synthesis and Characterization of 3D Printable Dynamic Covalent Polymers ........... 57

3.1 Introduction ............................................................................................ 58

3.2 Result and Discussion ............................................................................ 61

3.2.1 Materials Synthesis ........................................................................ 61

3.2.2 Thermal Properties of FA-Epoxy, CADH-Epoxy, TEMPS-PU and DTDA-PU...72

3.2.3 Mechanical Properties of FA-Epoxy, CADH-Epoxy, TEMPS-PU and DTDA-PU ........................................................................................... 77

3.3 Summary ................................................................................................ 79

Chapter 4 ................................................................................................ 81

4 Recyclable 3D Printing of Polyurethanes based on Heterocyclic Disulfide Bonds and Aromatic Disulfide Bonds ............................................................................ 81

4.1 Introduction ............................................................................................ 82

4.2 Result and Discussion ............................................................................ 84

4.2.1 Rheological Behavior of TEMPS-PU and DTDA-PU............................. 84

4.2.2 3D Printability of TEMPS-PU and DTDA-PU........................................ 87

4.2.3 Recyclability of TEMPS-PU and DTDA-PU .......................................... 90

4.3 Summary ........................................................................................... 94

Chapter 5 ............................................................................................... 96

5 Recyclable 3D Printing of MWCNTs-OH Reinforced Polyurethane Composites Based on Dynamic Disulfide Bonds ........................................................................... 96

5.1 Introduction ....................................................................................... 97

5.2 Result and Discussion .......................................................................... 99

5.2.1 DTDA-PU/MWCNTs-OH Composite Synthesis .................................... 99

5.2.2 Physical Properties of DTDA-PU/MWCNTs-OH Composites ............. 101

5.2.3 Rheological Behavior of DTDA-PU/MWCNTs-OH Composites .......... 108

5.2.4 3D Printability and Recyclability of DTDA-PU/MWCNTs-OH Composites.....111

5.3 Summary ......................................................................................... 116

Chapter 6 ............................................................................................. 118

6 Photothermal Conversion Triggered Dynamic Disulfide Bonds of 3D Printed Polyurethane Composite ............................................................................ 118

6.1 Introduction ..................................................................................... 118

6.2 Result and Discussion ........................................................................ 121

6.2.1 Photothermal Behavior of DTDA-PU Composites ................................ 121

6.2.2 In-situ Repairability of DTDA-PU Composite Printed Samples ........... 127

6.2.3 Laser Assisted Non-physical Support Removal Technique ................... 132

6.3 Summary ........................................................................................... 133

Chapter 7 ........................................................................................... 135

7 Conclusions and Future Work ......................................................................... 135

7.1 Conclusions ........................................................................................... 135

7.2 Future Work ........................................................................................... 138

References ........................................................................................... 140

Appendices ........................................................................................... 175

Curriculum Vitae ........................................................................................... 178

# List of Tables

Table 1-1. Summary of 3D printing processes based on the ASTM classifications [16]. ........ 7

Table 2-1. Summary of instruments used in experiments...................................................... 56

Table 3-1. Thermogravimetric analysis data of synthesized materials. .................................. 73

Table 3-2. Tensile properties of FA-Epoxy, CADH-Epoxy, TEMPS-PU and DTDA-PU. ... 79

Table 4-1. Printing parameters of DIW 3D printing processes for TEMPS-PU and DTDA-PU. ........................................................................................................................ 88

Table 5-1. Young's modulus, tensile strength at break, and elongation at break of DTDA-PU composites and pure samples. ........................................................................................ 107

# List of Figures

Figure 1-1. Four different manufacturing concepts and their contributions to stakeholder value. ........ 3

Figure 1-2. The fundamental working process of three different types of vat polymerization 3D printing technologies (a) SLA, (b) DLP and (c) CLIP. ........ 6

Figure 1-3. The fundamental working process of LOM. ........ 8

Figure 1-4. Printing system of (a) PBF and (b) BJ technology. ........ 9

Figure 1-5. The working process of directed energy deposition. The form of metal feedstock can be (a) a wire or (b) a powder stream. ........ 10

Figure 1-6. Basic working principle of PolyJet 3D printer. ........ 11

Figure 1-7. The working process of (a) FDM and (b) DIW. ........ 12

Figure 1-8. (a) The comparison between standard alloy(left) and nanoparticle-enhanced alloy (right) solidification process during metal 3D printing. (b)The schematic of the Initiator-Integrated 3D printing process and the photo image of 3D Printed Ni-coated Eiffel tower. ........ 15

Figure 1-9. The 3D printing process of transparent polycrystalline yttrium aluminum garnet. (a) Scheme of the ink synthesis and printing mechanism. (b) Printed ceramic structures after post-heating treatment. ........ 17

Figure 1-10. The 3D magnetic printing process. (a) The 3D magnetic printing setup combined a DLP based 3D printer with a magnetic field that applied via electromagnetic solenoids. (b) The schematic of the 3D magnetic printing process. Fillers systematically align, then resin selectively polymerizes following voxels programming to have specific reinforcement orientation. .... 19

Figure 1-11. The integrated tissue-organ printing system. (a) The integrated tissue-organ printer was composed of three parts: a 3-axis stage controller, a dispensing module and a closed chamber. (b) Schematic of 3D printing patterning with multiple cell-laden hydrogels and supporting PCL polymer. (c) CAD/CAM process for the integrated tissue-organ printing system. ............... 21

Figure 1-12. Images of macroscopic shape memory performance of trachea stent. The time taken for the stent transiting from the temporary state to the permanent shape was 14 s. (a) Dorsal view. (b) On end view. ........................................................................................................ 22

Figure 1-13. The biomimetic 4D printing process. (a) One-step shear-induced alignment of fibrils during DIW printing of hydrogel composite ink and the influence of swelling strain $\alpha$ and anisotropic stiffness $E$. (b) Morphologies of 4D printed flowers composed of 90°/0° (left) and -45°/45° (right) bilayers during the swelling process. .......................................................... 23

Figure 1-14. The comparison between additive and subtractive manufacturing. (a) Subtractive manufacturing relies on material-removing machining processes (milling, sawing, drilling, etc.). (b) Additive manufacturing applies a layer-by-layer fabrication method via different 3D printing machines (SLA, DIW, FDM, SLS, etc.). ............................................................................. 25

Figure 1-15. The process of Diels-Alder reaction. .............................................................. 29

Figure 1-16. Topographical rearrangement mechanism via transesterification. .................... 30

Figure 1-17. Different mechanistic pathways for dynamic disulfide exchange. ................... 32

Figure 1-18. Materials based on dynamic disulfide chemistry. (a) A pristine sample cut in half then healed by staying in contact for 2 h. (b) Shape memory and self-healing behavior of polysulfide materials. ........................................................................................................ 33

Figure 1-19. 3D printing materials based on the DA reaction. (a) DA enhanced PLA based 3D printing material. (i) Illustration and photographs of pure PLA and PLA with DA adducts. (ii) Ultimate strength results of pure PLA and PLA with 10% and 20% DA adducts in X/Y/Z printing directions. (b) DA reversible thermoset printing material. Comparison of microscope pictures (i) and macro surface roughness (ii) of the cross-section of printed parts from different materials. ........................................................................................................................................ 35

Figure 1-20. Examples of the 3D printing process utilized dynamic covalent bonds. (a) Schematic illustration of the plastic deformation and pyrolysis in the mechano-plastic pyrolysis process. (b) The colored disulfide based polyurethane acrylate samples were cut into two pieces and healed. Images of sample deformation under manual stretching and 5 kg weightlifting. .................. 37

Figure 1-21. (a) The crosslinking-dissolution-recrosslinking cycle of recyclable DIW 3D printing of nanoclay-reinforced vitrimer epoxy. (b) The repairability and recyclability of photopolymerization-based printing material. ...................................................................... 38

Figure 2-1 A picture of Engine SR 3D printer with KR2 15 modular printing heads from Hyrel 3D. ........................................................................................................................................ 52

Figure 3-1. Free energy profile illustrating kinetically (A to C) and thermodynamically (A to B) controlled reaction. ............................................................................................................ 59

Figure 3-2. Scheme graphs showing the polymerization and repolymerization mechanisms. (a) Synthetic scheme for FA-Epoxy. (b) The dissolution and repolymerization process of FA-Epoxy with EG aiding. .......... 62

Figure 3-3. (a) Image of the as-prepare FA-Epoxy sample. (b) The FTIR spectra diagram of BADGE, fatty acid and FA-Epoxy. (c) The recycling process of FA-Epoxy. .......... 63

Figure 3-4. (a) Compounds that have been used in CADH-Epoxy synthesized. (b) Network formation of CADH-Epoxy during the disulfide bond metathesis. .......... 65

Figure 3-5. (a) The photograph of a synthesized CADH-Epoxy sample. (b) The FTIR spectra diagram of BADGE, CADH and CADH-Epoxy. .......... 66

Figure 3-6. The illustration of the recycling cycle of CADH-Epoxy. .......... 67

Figure 3-7. Synthesised route of (a) Bi-TEMPS-OH and (b) Bi-TEMPS-OH incorporated polyurethane. .......... 69

Figure 3-8. (a) The photograph of the synthesized TEMPS-PU sample. (b) The FTIR spectra of monomers and TEMPS-PU .......... 70

Figure 3-9. (a) Synthetic scheme for DTDA-PU. (b) Image of the as-prepared DTDA-PU sample. (c) FTIR spectra of PTMEG, DTDA, IPDI and synthesized DTDA-PU. .......... 71

Figure 3-10. TGA curves of (a) FA-Epoxy, (b) CADH-Epoxy, (c) TEMPS-PU and (d) DTDA-PU. Their temperatures at 5% weight loss ($T_{d5}$) are labelled out in the diagrams. .......... 74

Figure 3-11. The thermogram of as-prepared samples via differential scanning calorimetry. 75

Figure 3-12. Loss tangent and storage modulus data depending on the temperature of (a) TEMPS-PU and (b) DTDA-PU measured using a dynamic mechanical analysis machine. ................ 76

Figure 3-13. The mechanical properties of synthesized materials. The stress-strain curves of (a) FA-Epoxy, (b) CADH-Epoxy, (c) TEMPS-PU and (d) DTDA-PU. .................................... 78

Figure 4-1. Schema of polymer printing via a DIW extrusion printer................................... 82

Figure 4-2. Temperature-dependent viscosity curves of (a) TEMPS-PU and (b) DTDA-PU with a fixed share rate (share rate=1 $s^{-1}$) in heating process from 120 to 150 °C............................. 85

Figure 4-3. Temperature-dependent viscosity curves of (a) TEMPS-PU and (b) DTDA-PU with a fixed share rate (share rate=1 $s^{-1}$) in cooling process from 150 to 120 °C. ............................ 86

Figure 4-4. The ink filaments extruded from the DIW printer with different nozzle diameters. The ink filament diameters are approximately equal to the nozzle size. ....................................... 88

Figure 4-5. (a) Photographs of 3D printed octopus and Eiffel tower demos from TEMPS-PU. Scale bars: 10 mm. (b) Photographs of 3D printed Tiantan and the Arc de Triomphe demos from DTDA-PU. Scale bars: 10 mm.......................................................................................... 90

Figure 4-6. An illustration of the reprinting process of disulfide-based 3D printing materials. ........................................................................................................................... 91

Figure 4-7. Photographs showing the re-printability of TEMPS-PU and DTDA-PU. (a) Three cycles of printed parts from TEMPS-PU. Scale bars: 10 mm. (b) Three cycles of printed parts from DTDA-PU. Scale bars: 10 mm. ........................................................................................ 92

Figure 4-8. The experiment results of uniaxial tensile tests for multiple times recycled. (a) Typical stress-strain curves for TEMPS-PU samples of three recycled cycles, and their corresponding values of (b) tensile strength at break and (c) elongation at break. (d) Typical stress-strain curves for DTDA-PU, and their corresponding values of their (e) tensile strength at break and (f) elongation at break. .......... 93

Figure 5-1. SEM images of the distribution of MWCNTs without (left) and with (right) hydroxy functionalization in DMF (imaged after drying). Scale bars: 1 μm. .......... 99

Figure 5-2. SEM images of DTDA-PU composites with different contents of MWCNTs-OH. Scale bars: 1 μm. .......... 100

Figure 5-3. TGA curves of DTDA-PU/MWCNTs-OH composites at a heating rate of 5 °C/min from 30 °C to 600 °C under $N_2$ environment. Inset on the top right is the detailed curves from 375 to 425 °C. .......... 102

Figure 5-4. DSC curves of DTDA-PU/MWCNTs-OH composites at a heat rate of 10 °C/min from -70 °C to 180 °C. .......... 103

Figure 5-5. DMA analysis of DTDA-PU/MWCNTs-OH composites from -80 °C to 80 °C. Solid lines represent storage modulus, and dashed lines represent loss tangent delta. .......... 104

Figure 5-6. (a) Swelling ratio for 0 wt%, 1 wt%, 2 wt% and 3 wt% DTDA-PU samples at room temperature. (b-c) Photographs of DTDA-PU with different MWCNTs-OH contents (b) before and (c) after being immersed in toluene for 6 hours at room temperature. .......... 105

Figure 5-7. (a) The tensile stress-strain curves of DTDA-PU composites. (b) Photographs showing the unstretched and stretched 2 wt% DTDA-PU.................................................. 106

Figure 5-8. (a) Temperature-dependent viscosity curves of DTDA-PU/ MWCNTs-OH. (b) The comparison of viscosities at 120 °C, 145 °C and 150 °C. The different colours and symbols indicate different MWCNTs-OH contents and different temperatures, as shown in the legends. ..... 109

Figure 5-9. (a) Share rate-dependent viscosity curves of DTDA-PU/ MWCNTs-OH. (b) The comparison of viscosities at 1 $s^{-1}$ and 10 $s^{-1}$. The different colours and symbols indicate different MWCNTs-OH contents and different share rate, as shown in the legends. ......................... 110

Figure 5-10. Photographs of DIW 3D printer working process. The beginning (left) and finishing (right) of the printing process. ......................................................................................... 112

Figure 5-11. (a) Photographs of the Hanging Gardens of Babylon model printed with pure (left) and 2 wt% DTDA-PU (right) with inset about bottom edge and the second-floor cantilever beam of the pure DTDA-PU printed sample. Scale bars: 10 mm. (b) Partial enlarged view of the 2 wt% DTDA-PU printed models captured by optical microscopy under different magnification. Scale bars: 1000 μm. .......................................................................................................... 113

Figure 5-12. Images of three cycles of printed architectures. From left to right are the printed models of Chichen Itza, Taj Mahal, the Great Wall of China. Scale bars: 10 mm.............. 114

Figure 5-13. (a) Typical tensile testing curves of the initial material and the third cycle recycled material, and their comparison of (b) tensile strength at break and (c) elongation at break. 115

Figure 6-1. Representation of the disulfide bond reaction during the in-situ repair process.120

Figure 6-2. Schematic illustration of the experimental setup. A 1 W 808nm NIR light source was used. The aluminum optical breadboard was used for vibration control. The operation stage was covered by an additional opaque case with a ventilation system for personal protection. ... 122

Figure 6-3. (a) Surface temperature elevation of the DTDA-PU and their composites samples as a function of time with NIR light turns on for 60 s, then off. (b) The maximum temperatures of samples after 60 s NIR light irradiation. (c)The cooling down temperatures after light turn off for 60 s. Light spot diameter = 6 mm; working distance = 30 cm. ........................................... 123

Figure 6-4. Photothermal properties of DTDA-PU composites. Thermographic images of samples before (a) and after (b) NIR irradiation for 10 s with digital images of samples inset. ........ 124

Figure 6-5. (a) Temperature elevation of 2 wt% DTDA-PU under H-laser (1 W) and L-laser (0.5 W); spot diameter = 6 mm; working distance = 30 cm. (b) Thermographic images of the 2 wt% DTDA-PU after H-Laser and L-Laser irradiation for 60 s. ................................................ 126

Figure 6-6. Top view (see pictures above) and cross-sectional view (see pictures below) of the SEM images of damaged 2 wt% DTDA-PU before and after being repaired. Scale bar: 100 µm. ........................................................................................................................ 128

Figure 6-7. (a) Stress-strain curves of 2 wt% DTDA-PU for three damaged-repaired cycles, and their comparison of (b) tensile strength at break and (c) elongation at break...................... 130

Figure 6-8 Repair processes of 2 wt% DTDA-PU printed parts. (a) Photographs of a damaged and repaired printed arch bridge sample. Scale bars: 10 mm. (b) Photographs of a damaged and repaired 2 wt% DTDA-PU printing honeycomb sample. The detailed images are shown as insets. . 131

Figure 6-9. The process of precisely removing the support structure of 2 wt% DTDA-PU printed the Arc de Triomphe model. (a) Schema. (b) Photographs. ................................................ 133

Figure 7-1. The sustainable 3D printing strategy of the trinity of recycling printing wastes, repairing damage parts, reducing processing defects. ......................................................... 136

# List of Appendices

**Appendix A**: The CAD models of the 3D printed parts in Figure 4-5, in turn, are (a) octopus, (b) the Eiffel Tower, (c) Tiantan and (d) Arc de Triomphe. ..................................................... 175

**Appendix B**: The CAD models of the 3D printed parts in Figure 4-7, in turn, are (a) Chinese "Fu" character, (b) butterfly and (c) honeycomb. ................................................................ 175

**Appendix C**: The CAD model of the 3D printed part in Figure 5-11 is Hanging Gardens of Babylon. ......................................................................................................................... 176

**Appendix D**: The CAD models of the 3D printed parts in Figure 5-12, in turn, are (a) Chichen Itza, (b) Taj Mahal, and (c) the Great Wall of China. .......................................................... 176

**Appendix E**: The CAD models of the 3D printed parts in Figure 6-8, in turn, are (a) honeycomb and (b) arch bridge. ............................................................................................ 177

# Glossary of Terms

| | |
|---|---|
| **CAD** | Computer-Aided Design |
| **STL.** | Standard Tessellation Language |
| **ASTM** | American Society for Testing and Materials |
| **SLA** | Stereolithography |
| **DLP** | Digital Light Processing |
| **CLIP** | Continuous Liquid Interface Production |
| **LOM** | Laminated Object Manufacturing |
| **UAM** | Ultrasonic Additive Manufacturing |
| **PSL** | Plastic Sheet Lamination |
| **PBF** | Powder Bed Fusion |
| **BJ** | Binder Jetting |
| **SLS** | Selective Laser Sintering |
| **SLM** | Selective Laser Melting |
| **EBM** | Electron Beam Melting |
| **DED** | Direct Energy Deposition |
| **MJ** | Material Jetting |
| **ME** | Material Extrusion |
| **FDM** | Fused Deposition Modeling |
| **DIW** | Direct Ink Writing |
| **FFF** | Fused Filament Fabrication |
| **CAN** | Covalent Adaptable Networks |
| **DA** | Diels-Alder |
| **MWCNTs-OH** | Hydroxylated Multi-Walled Carbon Nanotubes |
| **CADH** | Cystamine Dihydrochloride |

| | |
|---|---|
| **DTDA** | 4,4’-Dithiodianiline |
| **4-hydroxy-TEMP** | 4-Hydroxy-2,2,6,6-Tetramethylpiperidine |
| **BADGE** | Bisphenol A Diglycidyl Ether |
| **PTMEG** | Polytetrahydrofuran |
| **IPDI** | Isophorone Diisocyanate |
| **DBTDL** | Dibutyltin Dilaurate |
| **$Zn\ (Ac)_2$** | Zinc Acetate Dihydrate |
| **$S_2Cl_2$** | Sulfur Monochloride |
| **HMDS** | Hexamethyldisilazane |
| **EG** | Anhydrous Ethylene Glycol |
| **Nitro** | Nitromethane |
| **DMF** | N, N-Dimethylformamide |
| **MeOH** | Methanol |
| **NaOAc** | Sodium Acetate |
| **DCM** | Dichloromethane |
| **NaOH** | Sodium Hydroxide |
| **MgSO4** | Magnesium Sulfate |
| **Na2SO4** | Sodium Sulfate |
| **K2CO3** | Potassium Carbonate |
| **Bi-TEMPS-OH** | Bis (4-Hydroxy-2,2,6,6-Tetramethylpiperidin-1-yl) Disulfide |
| **Bi-TEMPS-OTMS** | Bis(4-Tetramethylsiloxy-2,2,6,6-Tetramethylpiperidin-1-yl) Disulfide |
| **FTIR** | Fourier-Transform Infrared |
| **TGA** | Thermogravimetric Analysis |
| **DSC** | Differential Scanning Calorimetry |
| **DMA** | Dynamic Mechanical Analysis |

|  |  |
|---|---|
| **SEM** | Scanning Electron Microscope |
| **NIR** | Near-Infrared |

# Chapter 1

## 1 Introduction

Manufacturing development is inseparable from social progress. It is an inevitable trend for the transformation from resource-consuming traditional manufacturing to resource-saving sustainable manufacturing. During this transformation process, considerable attention has been paid to 3D printing technology. The layer-by-layer manufacturing process makes 3D printing technology competitive in raw material saving, highly customized and cost-saving, which is consistent with the idea of sustainable manufacturing. However, polymers currently account for over 90% of 3D printing material market, and the improper management of disposal will cause the significant environmental burden. Dynamic covalent chemistry is a good access to realize the 3D printing material recycling issue, along with some other benefits. This chapter will review current 3D printing technologies and discuss their challenges for further sustainable development. After a brief introduction to dynamic covalent chemistry, the current state-of-the-art 3D printable dynamic covalent polymers are reviewed. Finally, the objectives and outline of this dissertation are discussed.

## 1.1 Development of Sustainable Manufacturing

Manufacturing is transforming raw materials into finished products to be used for various applications, which comprises a large number of distinct processes [1-3]. It can refer to a wide range of human activity, from handicraft works in the pre-industrial world to factory systems after the industrial revolution [4]. As the backbone of the industry, manufacturing has generated wealth and quality of life. The first industrial revolution boosted economic growth that subsequently affected the economic, societal and technological context [5]. However, the pursuit of economic growth also caused massive consumption of finite natural resources and had a negative impact on our environment [6]. In this context, the concept of sustainable development was proposed based on the prospect of further global growth. Sustainable development was defined as “development that meets the needs of the present without compromising the ability of future generations to meet their own needs” [7, 8]. The transition toward sustainable civilization is an issue of critical importance for the whole society, especially for the manufacturing industry.

The evolution toward sustainable manufacturing is a long-term process that requires improvement in reducing, reusing and recycling, while also needs to recover, redesign and remanufacture the products over multiple life cycles [9]. Different manufacturing concepts and their contribution to stakeholder value are shown in Figure 1-1 [10]. Traditional manufacturing includes subtractive manufacturing, formative manufacturing, and joining manufacturing [11]. Limited by technologies of these manufacturing processes, material and energy waste in conventional manufacturing processes is inevitable. Moreover, for the centralized system of traditional manufacturing, redesign of components and products will require the reconstruction of the whole production line, which is cost-intensive, time-consuming, and wasteful [12].

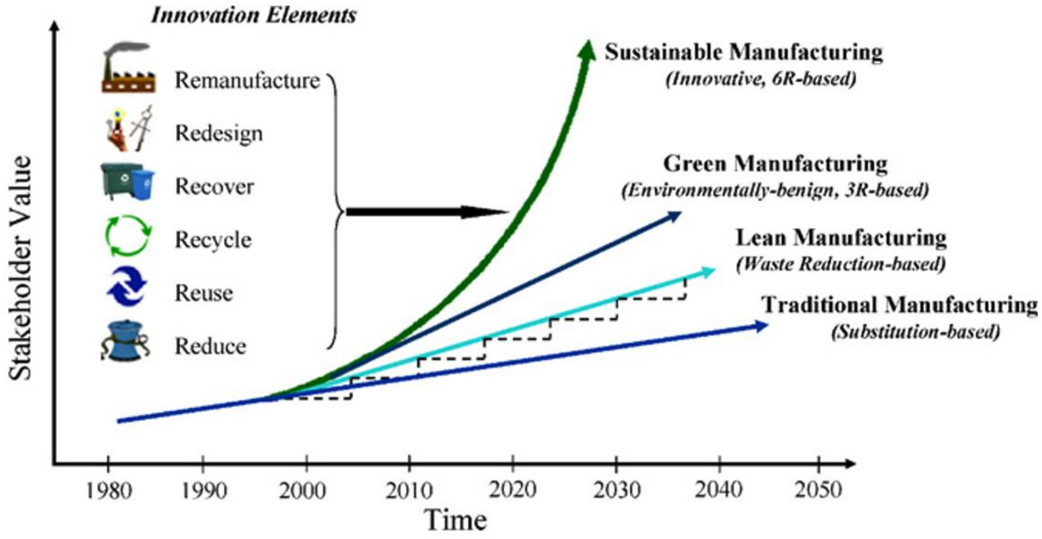

**Figure 1-1. Four different manufacturing concepts and their contributions to stakeholder value. (Reproduced with permission from ref. [10])**

Fortunately, we are currently witnessing a significant advancement and technological revolution in manufacturing, and the emergence of additive manufacturing is playing a catalytic role in this revolution [13]. Additive manufacturing, commonly known as 3D printing, mimics biological growth processes to convert raw materials into products in a layer-by-layer manner, which is different from traditional manufacturing methods [14]. Unlike conventional centralized mass production, 3D printing enables a more cost- and resource-efficient small-scale production [14, 15]. Furthermore, compared with traditional subtractive manufacturing, additive manufacturing can significantly reduce the raw material waste during the production processes due to its inherent layer-by-layer manufacturing method, which is more consistent with sustainable development. Although additive manufacturing opens the door for sustainable manufacturing development, it still faces some challenges such as poor waste management, high defective rates, and limited applications. All these issues are worth to devote much effort to develop sustainable additive manufacturing further.

## 1.2 Development of 3D Printing

### 1.2.1 Review of 3D Printing Technologies

3D Printing technology can be defined as a process of digitally controlled deposition of successive layers of material to fabricate designed three-dimensional objects [16]. Contrary to subtractive manufacturing, which manufactures products by removing materials through stamping or machining, 3D printing can directly build intricate and complex parts by adding materials layer upon layer [13]. Usually, 3D printing technology consists of three steps:

(1) A virtual 3D printing model is developed by either computer-aided design (CAD) or a three-dimensional scanner [17]. Then, it is converted into a standard 3D printing file format, such as the traditional standard tessellation language (STL.) format or the other AM file format [18].

(2) The file is transferred to a 3D printer. The corresponding setting up of process parameters is required, such as the position and orientation of printing parts, and the speed and layer thickness of the printing process.

(3) The printing file format is converted into a G-code file after the printing parameters are set up. 3D printers work under the G-code instruction to deposit materials layer-by-layer until the designed 3D object is completed.

This revolutionary manufacturing method is inherently more suitable for the manufacturing of complex structures. It also meets its promises of sustainable development by achieving mass customization, reducing material and energy consumption, and waste minimization [19, 20]. The superiority of 3D printing has attracted a great deal of interest from diverse industry fields, including architecture, automotive, aerospace, industrial design, health care, education, food, etc. [21-23]. The ever-growing demands drive the rapid development of this technology. Since the conception of 3D printing was formed in the 1980s [24], significant progress has been made in this technology. Numerous 3D printing processes exist with main distinctions arising from the methods of layer deposition, the operating principle, and the printing materials. The ASTM (American Society for Testing and Materials) classified 3D printing technology into seven main categories based on their working mechanism: binder jetting, material jetting, direct energy deposition, sheet laminations, material extrusion, powder bed fusion, and vat photopolymerization (Table 1) [16]. Each category holds distinct advantages and limitations, and is suitable for different applications [25, 26].

Vat photopolymerization is the first 3D printing process developed by Charles Hull in 1984 [27]. After 30 years of continuous development, currently most popular vat photopolymerization 3D printing techniques include Stereolithography (SLA), Digital Light Processing (DLP) [28], and Continuous Liquid Interface Production (CLIP) [29] (Figure 1-2). All these printing techniques are based on the layer-by-layer solidification of liquid photosensitive resin upon exposure to a light source [30]. High resolution with small feature size is the most significant competitive advantage of these techniques [31]. However, this popular 3D printing technology is facing challenges in expanding its applications in industrial production. For example, the printing materials of vat photopolymerization are restricted by photopolymer. Also, the sizes of printing products are determined by the volume of their printer vat [32]. The fast development of new materials and printer techniques will further make this kind of printing method more applicable.

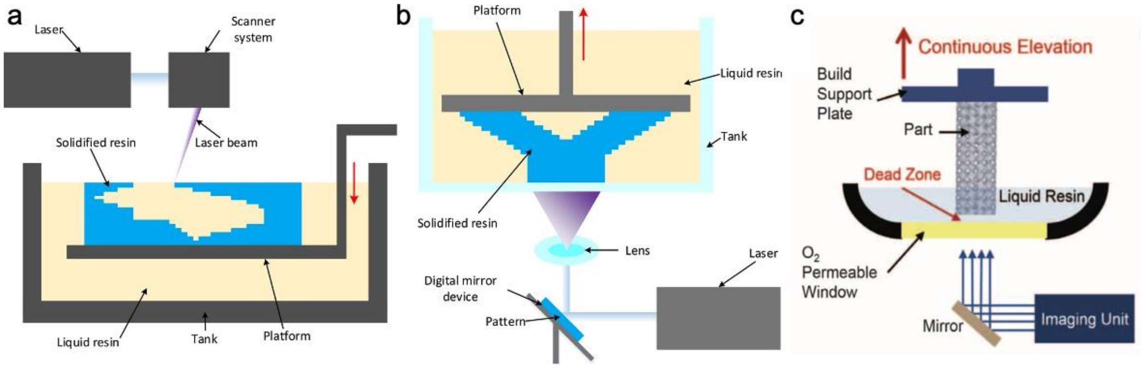
a
Laser
Scanner system
Laser beam
Solidified resin
Liquid resin
Tank
Platform
b
Platform
Liquid resin
Tank
Solidified resin
Lens
Laser
Digital mirror device
Pattern
c
Continuous Elevation
Build Support Plate
Part
Dead Zone
Liquid Resin
$O_2$ Permeable Window
Mirror
Imaging Unit

**Figure 1-2. The fundamental working process of three different types of vat polymerization 3D printing technologies (a) SLA, (b) DLP and (c) CLIP. (Reproduced with permission from ref. [28, 29] )**

## Table 1-1. Summary of 3D printing processes based on the ASTM classifications [16].

| Process categories | Definitions | Technologies | Materials |
|---|---|---|---|
| Binder Jetting | A liquid bonding agent is selectively deposited to join powder materials. | Metal Binder Jetting<br>Sand Binder Jetting | Metallic,<br>Ceramic,<br>Polymer,<br>Composite |
| Direct Energy Deposition | Material is deposited by melting, and focused thermal energy (e.g., laser, electron beam, or plasma arc) is used to fuse materials. | Direct light fabrication (DLF), Electron beam direct manufacturing (EBDM), Direct melt deposition (DMD), Direct laser deposition (DLD) | Metallic |
| Material Extrusion | Material is selectively dispensed through a nozzle or orifice. | Fused Deposition Modeling (FDM),<br>Direct Ink Writing (DIW) | Polymer |
| Material Jetting | Material is selectively deposited through droplets. | PolyJet,<br>ProJet | Polymer |
| Powder Bed Fusion | Thermal energy selectively fuses regions of a powder bed. | Selective laser sintering (SLS), Selective laser melting (SLM), Electron Beam Melting (EBM) | Ceramic<br>Metallic<br>Polymer |
| Sheet Lamination | Sheets of material are bonded together to form a part. | Laminated object manufacture (LOM) | Metallic<br>Polymer<br>Ceramic |
| Vat photopolymerization | Light energy source selectively cures liquid photopolymer in a vat. | Stereolithography (SLA), Digital Light Processing (DLP), Continuous liquid interface printing (CLIP), Two-photon polymerization (2PP) | Polymers,<br>Composite |

After the 3D printing concept was established, Laminated Object Manufacturing (LOM) became the first commercialized industrial additive manufacturing technique in 1991 [33, 34]. As shown in Figure 1-3, the working principle of LOM is applying the laser to cut layers of material supplied and utilizing a heat-activated resin to bond the layers [35]. With the development of build materials and cutting strategies, many other 3D printing processes have been developed based on LOM [36], such as Ultrasonic Additive Manufacturing (UAM) [37] and Plastic Sheet Lamination (PSL). LOM offers a faster and more low-cost 3D printing process than other AM methods, while the resolution of their printing products is much limited by the thickness of sheet materials [38]. Meanwhile, since the printing materials require complex pre-preparation processes, their material selections have some restrictions.

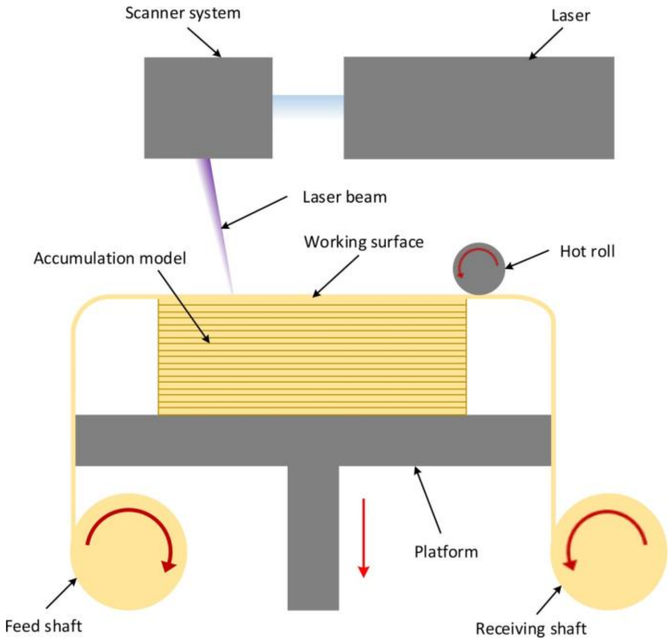
Scanner system
Laser
Laser beam
Working surface
Hot roll
Accumulation model
Platform
Feed shaft
Receiving shaft

**Figure 1-3. The fundamental working process of LOM. (Reproduced with permission from ref. [28] )**

Both vat polymerization and LOM have limitations in material options. Compared with these 3D printing technologies, powder-based 3D printing can adapt to a wide range of feedstock, like metal and ceramic. Powder Bed Fusion (PBF) and Binder Jetting (BJ) are two different types of powder-based 3D printing processes (Figure 1-4). For PBF, a thermal energy source is utilized to selectively sinter or fuse regions of the powder layer to form structures. Selective laser sintering (SLS), as one of the most important PBF methods, was invented in 1989 and became the first commercial metal additive manufacturing technique [39]. Then selective laser melting (SLM) and electron beam melting (EBM) were created to enhance the PBF systems by using a laser or a high-energy electron beam to fully melt the powder [40].

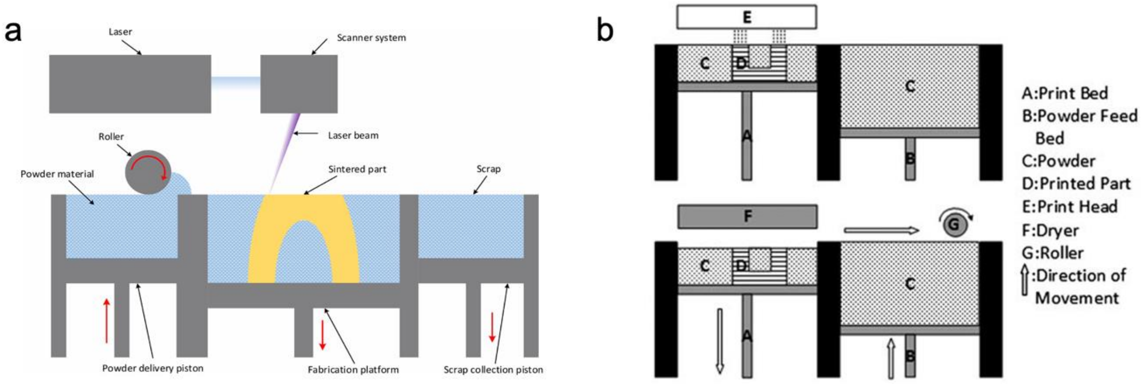
a
Laser
Scanner system
Laser beam
Roller
Powder material
Sintered part
Scrap
Powder delivery piston
Fabrication platform
Scrap collection piston
b
E
C
D
A
B
F
G
A:Print Bed
B:Powder Feed Bed
C:Powder
D:Printed Part
E:Print Head
F:Dryer
G:Roller
⇧:Direction of Movement

**Figure 1-4. Printing system of (a) PBF and (b) BJ technology. (Reproduced with permission from ref. [28, 41])**

Binder Jetting (BJ) was invented by the Massachusetts Institute of Technology in 1993 based on the inkjet technology [42]. This technology is a process in which the liquid binding agent is selectively deposited into a powder bed to fabricate complex parts using different powder materials [43]. Compared with PBF, BJ can offer relatively high throughput and large build volumes because there are no requirements for an enclosed chamber and expensive energy sources [44]. However, the main drawback of the BJ process is the degradation of mechanical performance due to the low density of the printing parts after the post-sintering [45]. Moreover, distortions caused by residual stresses and defects originated during the process are the main concerns for both techniques [46, 47]. Plenty of theoretical and experimental studies focus on these issues and look forward to the unlocking technical bottlenecks of this printing technology.

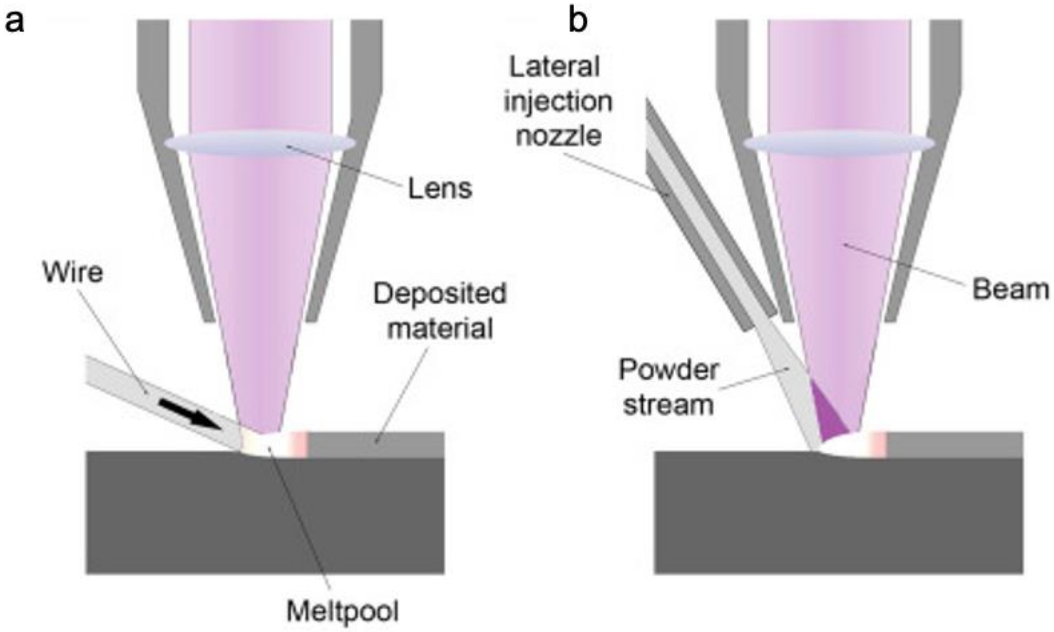

**Figure 1-5. The working process of directed energy deposition. The form of metal feedstock can be (a) a wire or (b) a powder stream. (Reproduced with permission from ref. [48])**

The Direct Energy Deposition (DED) process is another primary metal 3D printing process. As shown in Figure 1-5, DED uses a high-intensity energy source to selectively deposit metal material (powder or wire) to shape three-dimensional components [49]. It is usually used to fabricate pure metals and their alloys for various engineering and biomedical applications. Unlike other metal additive manufacturing technologies, the significant advantages of DED are no requirement of a strict seal structure and continuous operation without intervals to put a thin layer of powder [50]. Additionally, the components produced by DED have a high density and attain superior mechanical properties since the manufacturing processes include deposition, melting and solidification of powdered material [51]. Despite that, the DED process still has technical problems in shape accuracy and power efficiency due to the movement of the powder during printing processes, which can be further improved [52].

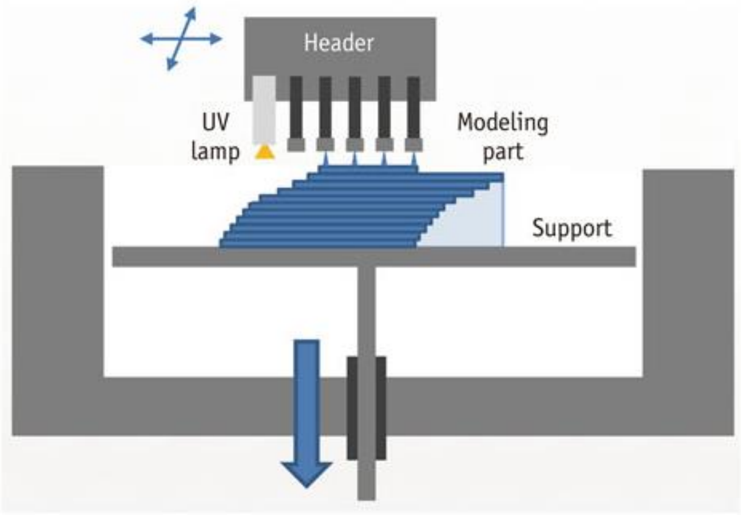

**Figure 1-6. Basic working principle of PolyJet 3D printer. (Reproduced with permission from ref. [53])**

The Material Jetting (MJ) process is also built based on inkjet printing technology. Unlike BJ using inkjet technology to deposit binder onto a powder bed, MJ creates parts by depositing photopolymers onto a building platform and then curing the resin in successive layers [54]. PolyJet from Stratesys and MultiJet from 3D Systems are the most typical representatives of this 3D printing technique [55]. Figure 1-6 shows the basic working principle of the PolyJet 3D printer. On the one hand, this printing method provides a higher throughput of products on a larger surface area and less manufacturing complexity than vat polymerization and other similar polymer additive techniques [56]. On the other hand, the printing materials have restrictions on their physical properties, particularly their viscosity and surface tension [57].

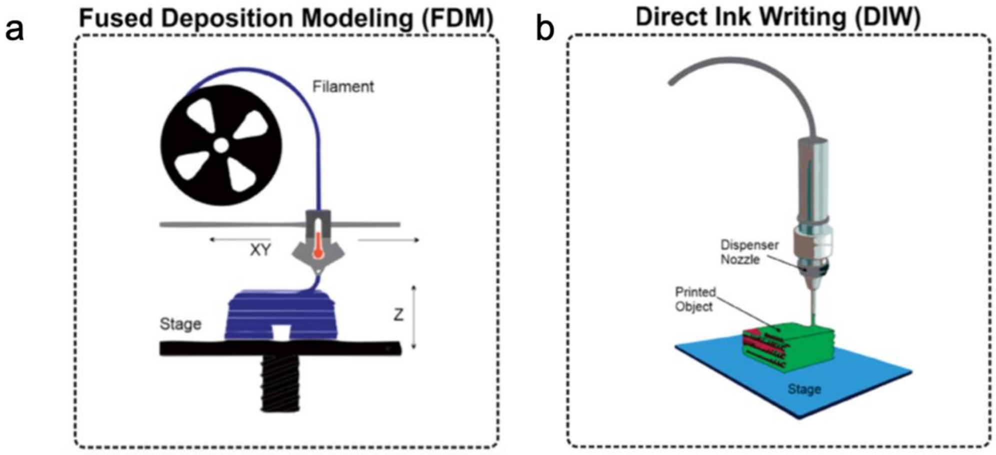

**Figure 1-7. The working process of (a) FDM and (b) DIW. (Reproduced with permission from ref. [58])**

The final category of 3D printing technology that we introduced here is Material Extrusion (ME). The working principle of ME is selectively dispensing material from the nozzle or orifice to constitute a 2D plane and then a 3D object. Fused Deposition Modeling (FDM) and Direct Ink Writing (DIW) are two of the most common printing technologies presented in Figure 1-7. Although the ME 3D printing process is not always competitive on their printing resolution and material selection, their main merit is low cost. Thanks to RepRap and Fab@Home, leading the open-source 3D-printer revolution in 2007 [59], an extrusion-based 3D printer currently only costs about 1000 dollars [28]. Open source and low-cost development have made ME 3D printers more accessible to designers, engineers, researchers, teachers and students, bringing the rapid technology development of the ME 3D printing process.

Overall, seven different types of 3D printing technologies are introduced in this section, together with their working principles and features. We can see that all these printing technologies have distinct advantages in specific working situations from the above discussions. Although they all currently face different challenges, we firmly believe that there is value in further studying and developing 3D printing technology. Furthermore, to push forward the development of 3D printing, the improvement of manufacturing processes is also inseparable from materials development.

### 1.2.2 Review of 3D Printing Materials

3D printing materials were limited in polymers at the very beginning. With the development of 3D printing technologies and research on material characteristics, various materials are currently available for additive manufacturing. 3D printing materials can be sorted by the shape of feedstocks (e.g., powders, sheets, wires and liquids) or the type of materials (e.g., metals, ceramics and polymers) [60, 61]. The shape of feedstocks still most depends on their 3D printer requirements, which is not representative of inherent material characterization. Therefore, in this section, we will review recent advancements in 3D printing materials following the classification based on their basic properties (metals, ceramics and polymers).

#### 1.2.2.1 3D Printing of Metals

Considerable attention has been paid to metal additive manufacturing because of the outstanding mechanical properties of metals in comparison with polymers. Common metallic materials for 3D printing are titanium and its alloys, aluminum alloys, nickel-based alloys and steel [62]. The feedstock forms usually are powder or wire, and the printing techniques are PBF, DED and BJ. Although the metal 3D printing has a significant advantage in freedom for manufacturing complex geometries, its printing techniques have considerable limitations in the material selection compared with traditional metal manufactured. Besides, the feedstock for these printing methods must be prepared into the corresponding form, which is time-consuming and costly. Additionally, structural and microstructural defects presented in printing processes also result in the poor mechanical performance of printing products [63].

Aiming at these problems, significant research effort has been devoted to improving metal 3D printing processes and products over the past decades. Theoretical and experimental investigations of 3D printing technologies, printing materials and post-treatment processes are comprehensive and continuously updating [64-67]. Martin et al. successfully 3D printed high-strength aluminum alloys that avoid intolerable microstructures with large columnar grains and periodic cracks by introducing nanoparticles of nucleants to control solidification [68]. These nanoparticles induced the grain refinement of the aluminum alloys 3D printing that not only contributes to the aluminum alloys 3D printing development but also provides a metallurgical tool for other metal printing processing [69].

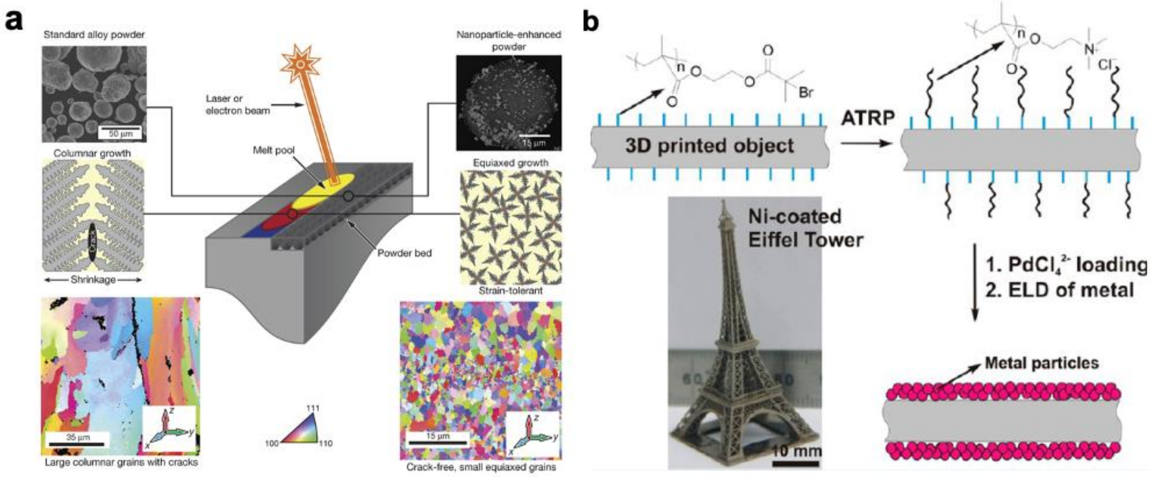
a
Standard alloy powder
50 µm
Columnar growth
Shrinkage
35 µm
Large columnar grains with cracks
Laser or electron beam
Melt pool
Powder bed
111
100
110
Nanoparticle-enhanced powder
15 µm
Equiaxed growth
Strain-tolerant
15 µm
Crack-free, small equiaxed grains
b
n
O
Br
ATRP
3D printed object
N
Cl
Ni-coated Eiffel Tower
10 mm
1. PdCl$_4^{2-}$ loading
2. ELD of metal
Metal particles

**Figure 1-8. (a) The comparison between standard alloy(left) and nanoparticle-enhanced alloy (right) solidification process during metal 3D printing. (b)The schematic of the Initiator-Integrated 3D printing process and the photo image of 3D Printed Ni-coated Eiffel tower. (Reproduced with permission from ref. [68] and [70])**

Furthermore, Yang's group creatively proposed an initiator-integrated 3D printing (i3DP) technique for complex metallic architecture fabrication [70]. The designed structures were first fabricated by stereolithography with the resin containing a Br-containing vinyl-terminated initiator. The printed components were then grown with polyelectrolyte brushes via surface initiated atomic-transfer radical polymerization (SI-ATRP) for the subsequent electroless plating of metal, such as copper and nickel. After etching the polymer matrix away, the ultralight metals architectures can be achieved (Figure 1-8). This i3DP strategy, as a cost-effective and universal approach, opens the door to following research on metal additive manufacturing [71-73].

#### 1.2.2.2 3D Printing of Ceramics

The need to fabricate ceramic products with complex shapes for tissue engineering and lightweight components has derived the development of 3D printing ceramic. PBF, BJ, LOM and direct ceramic stereolithography (CSL) as the main methods of 3D printing ceramic can effectively reduce the fabrication time and product costs of ceramic parts with complex geometry used in tissue engineering such as scaffolds for bones and teeth [74]. However, material selection limitation, surface finish, and printing accuracy are still the main challenges of 3D printing ceramic [75]. A recent work reported by Cooperstein et al. demonstrated a new approach for 3D printing transparent ceramic structures, which used to limit conventional fabrication methods [76]. The yttrium aluminum garnet 3D printing process and photos of printed parts are shown in Figure 1-9. The printing ink was synthesized based on the sol-gel process of metal salts ($AlCl_3$, $YCl_3$ and $NdCl_3$) in the presence of acrylic acid. A two-photon printing technique was used to fabricate micrometric 3D objects. The post-heating treatment removed the organic materials and obtained the transparent polycrystalline yttrium aluminum garnet. From this work, we can see the high printing resolution, the advanced function, and the innovative use of material are desirable to exploit in the 3D printing of ceramics materials.

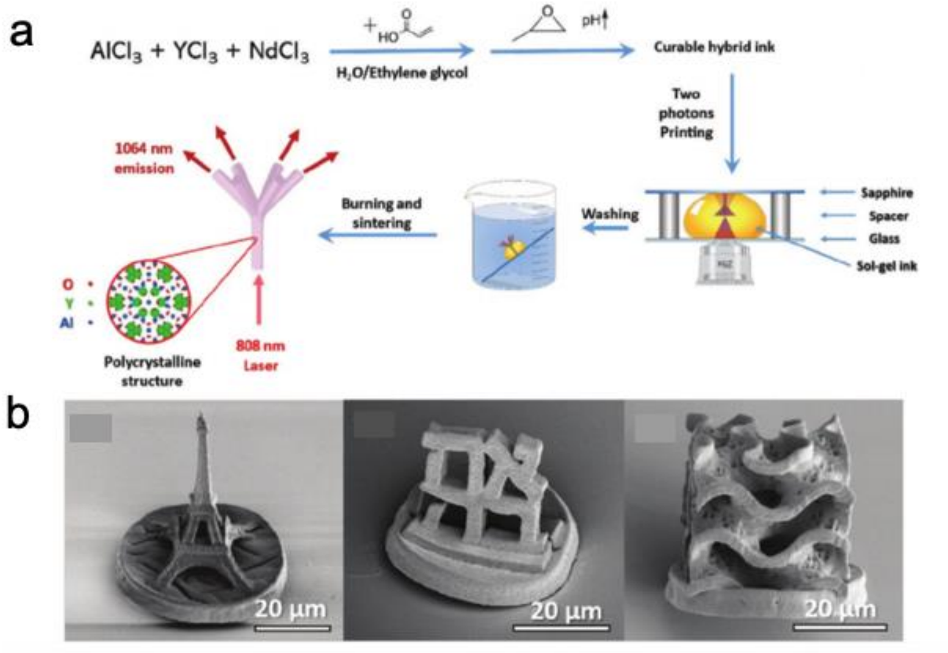
a
AlCl3 + YCl3 + NdCl3
HO
H2O/Ethylene glycol
pH
Curable hybrid ink
Two photons Printing
Sapphire
Spacer
Glass
Sol-gel ink
Washing
Burning and sintering
1064 nm emission
O
Y
Al
Polycrystalline structure
808 nm Laser
b
20 µm
20 µm
20 µm

**Figure 1-9. The 3D printing process of transparent polycrystalline yttrium aluminum garnet. (a) Scheme of the ink synthesis and printing mechanism. (b) Printed ceramic structures after post-heating treatment. (Reproduced with permission from ref. [76])**

### 1.2.2.3 3D Printing of Polymers

Polymers are the most widely used printing materials in additive manufacturing because of their diversity and adaptability to different printing processes. Both thermoplastic polymers such as acrylonitrile butadiene styrene (ABS) [77, 78] and polylactic acid (PLA) [79, 80], as well as thermosetting polymers like poly (ethylene glycol) diacrylate (PEGDA) [81, 82], urethane dimethacrylate (UDMA) [83, 84] and epoxy resin [85, 86] could be processed by 3D printing technology. Various polymeric materials offer different chemical and mechanical properties. Although commercial 3D printing materials fulfill most of the desired requirements of final products, their application areas are still very limited and short of functional development. The two main tendencies of the development for polymer 3D printing materials are (i) improving the physicochemical and mechanical properties of the 3D printing materials and (ii) the development of functional materials for 3D printing to match different applications, such as biomedical, ferroelectric, energy storage and 4D printing devices.

The major problem of polymer-based 3D printing products is their low mechanical properties compared with metal and ceramic products. Decker et al. demonstrated a dual curing photopolymer-based 3D printing system [87]. This dual cure network combined the monomer of biscycloaliphatic diepoxide for the cationic polymerization with the monomer of bisphenol A diacrylate derivative for the radical polymerization to form interpenetrating networks. By adjusting the photopolymerization rate and cross-link density, researchers can improve the molecular architecture of printing materials and enhance their mechanical properties [88].

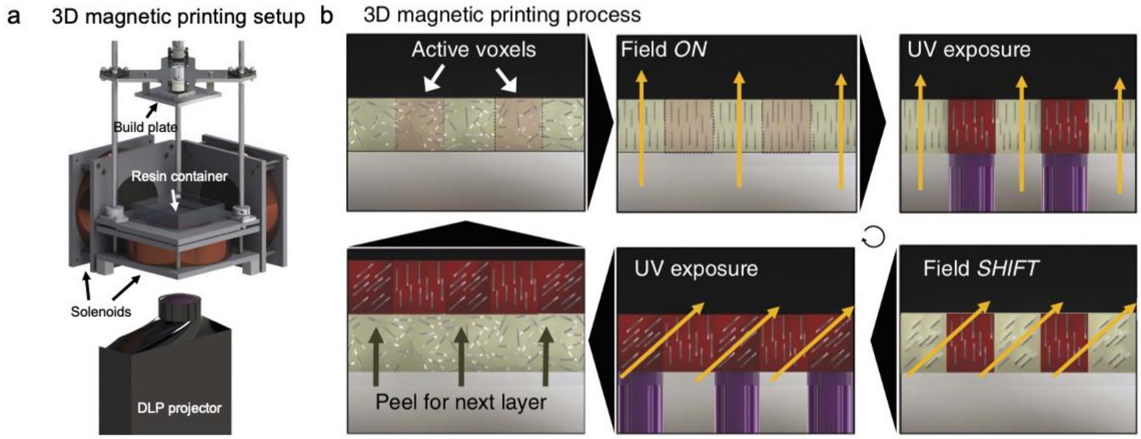
a
3D magnetic printing setup
Build plate
Resin container
Solenoids
DLP projector
b
3D magnetic printing process
Active voxels
Field *ON*
UV exposure
Field *SHIFT*
UV exposure
Peel for next layer

**Figure 1-10. The 3D magnetic printing process. (a) The 3D magnetic printing setup combined a DLP based 3D printer with a magnetic field that applied via electromagnetic solenoids. (b) The schematic of the 3D magnetic printing process. Fillers systematically align, then resin selectively polymerizes following voxels programming to have specific reinforcement orientation. (Reproduced with permission from ref. [89])**

Besides these strategies, introducing fillers into polymer systems is another effective method to improve the performance of printing parts. Inspired by mineralized natural materials, Dimas et al. used the PolyJet 3D printer to print the bio-inspired composites [90]. With complementary computational model predictions, their composite printing parts with different mesoscale topologies designs obtained considerable toughening mechanisms and stable fracture resistance. In addition, Martin et al. proposed an innovative concept of "3D magnetic printing" that can create highly programmable discontinuous fiber composites by combining a real-time colloidal assembly with DLP additive manufacturing [89]. The 3D magnetic-printer setup and printing process were schematically shown in Figure 1-10. Magnetic-labelling techniques were employed to coat traditionally nonmagnetic $Al_2O_3$

(alumina) particles. Before the photopolymerization of each layer, the magnetic field will first rotate to align the reinforcing microparticles. With this 3D magnetic printing technology, the characteristics of printing architectures, such as their stiffness, strength, toughness and multi-functionality, can be programmably tuned and enhanced.

The development of 3D printable functional polymers is also crucial for 3D printing technology to apply in various applications. Especially in bio fabrication, 3D printing has incomparable advantages in highly customization for patients suffering from organ failure or bone and tissue damage. Therefore, biocompatible, biodegradable or even regenerable 3D printing materials are highly desired. Poly (ethylene glycol) diacrylate (PEGDA), natural gelatin methacrylate (GelMA), poly (ε-caprolactone) (PCL) and poly (D, L -lactic-co-glycolic acid) (PLGA) are all attractive biomaterials for the 3D printing of biological tissue and organs [91]. Kang et al. reported a high mechanical stability 3D bioprinting system by printing cell-laden hydrogels and sacrificial hydrogels together with biodegradable PCL in designed shape (Figure 1-11) [92]. The printed ear-shaped cartilages, human-scale mandible bones and organized skeletal muscles all showed high structural integrity and promising functional characteristics *in vitro* and *vivo*.

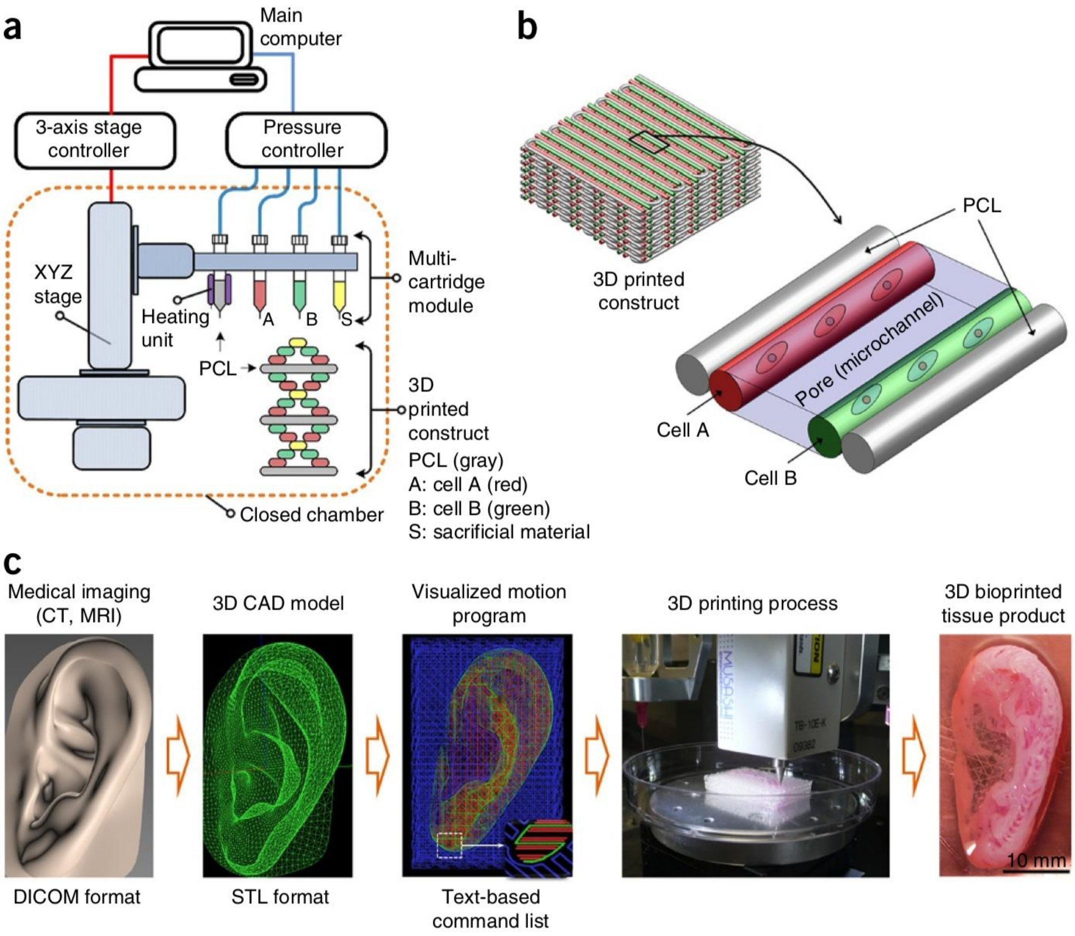
a
Main computer
3-axis stage controller
Pressure controller
XYZ stage
Heating unit
A
B
S
PCL
Multi-cartridge module
3D printed construct
PCL (gray)
A: cell A (red)
B: cell B (green)
S: sacrificial material
Closed chamber
b
3D printed construct
PCL
Pore (microchannel)
Cell A
Cell B
c
Medical imaging (CT, MRI)
3D CAD model
Visualized motion program
3D printing process
3D bioprinted tissue product
DICOM format
STL format
Text-based command list
10 mm

**Figure 1-11. The integrated tissue-organ printing system. (a) The integrated tissue-organ printer was composed of three parts: a 3-axis stage controller, a dispensing module and a closed chamber. (b) Schematic of 3D printing patterning with multiple cell-laden hydrogels and supporting PCL polymer. (c) CAD/CAM process for the integrated tissue-organ printing system. (Reproduced with permission from ref. [92])**

Tibbits' research group first initiated 4D printing at MIT [93]. It was a process that the property, the functionality or shape of 3D printing structure can change with time. This concept opens a new era for 3D printing applications such as cardiovascular and tracheal stents [94, 95], smart connectors [96], drug delivery systems [97], and actuators [98]. The stimulus-responsive polymer is one of the most critical building blocks of 4D printing processes. Zarek et al. presented a 4D printing of personalized tracheal stent based on a shape memory polymer [95]. Semicrystalline methacrylate polycaprolactone (PCLMA) was applied to this application as the shape memory polymer. The stent should be implanted in its temporary state. Once the stent is triggered, it deploys back into its permanent shape to match the geometry of the trachea (Figure 1-12).

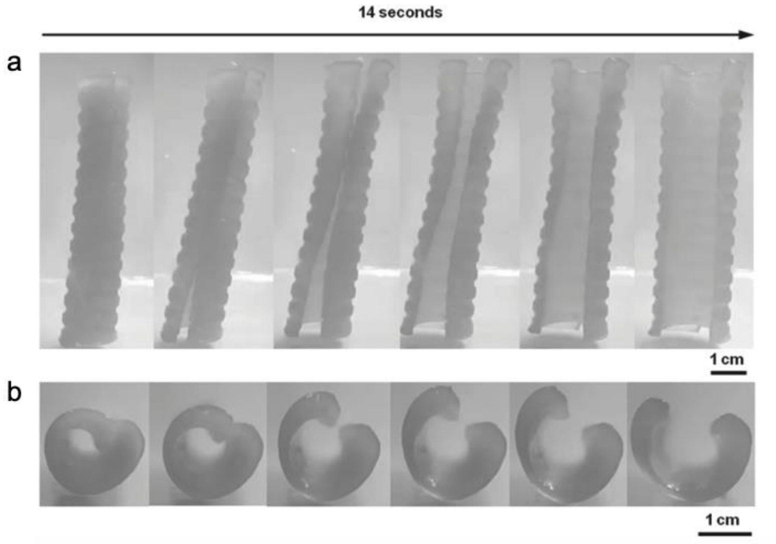

**Figure 1-12. Images of macroscopic shape memory performance of trachea stent. The time taken for the stent transiting from the temporary state to the permanent shape was 14 s. (a) Dorsal view. (b) On end view. (Reproduced with permission from ref. [95])**

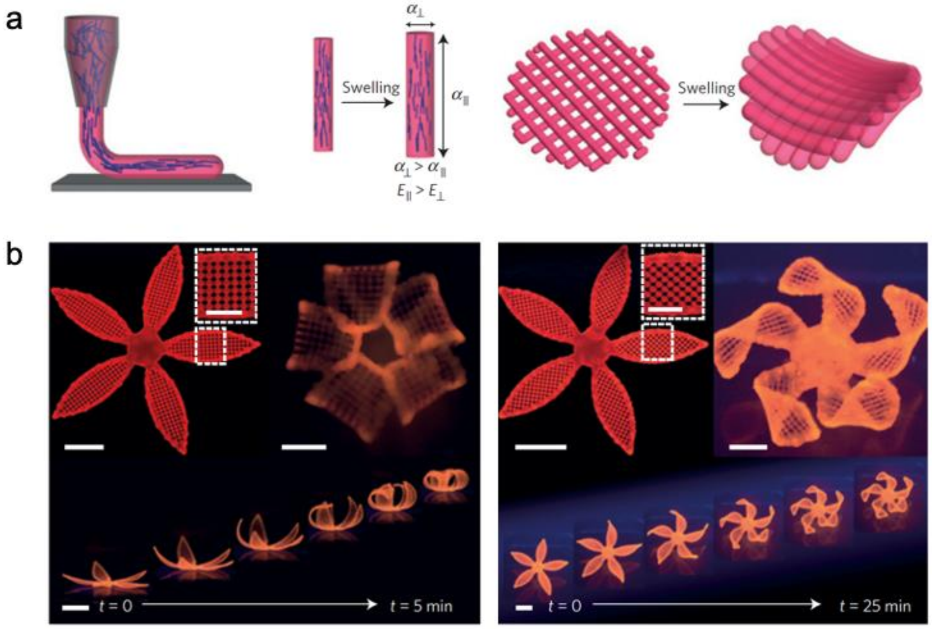

**Figure 1-13. The biomimetic 4D printing process. (a) One-step shear-induced alignment of fibrils during DIW printing of hydrogel composite ink and the influence of swelling strain $\alpha$ and anisotropic stiffness $E$. (b) Morphologies of 4D printed flowers composed of 90°/0° (left) and -45°/45° (right) bilayers during the swelling process. (Reproduced with permission from ref. [99])**

Furthermore, Gladman et al. realized a biomimetic 4D printing via a composite hydrogel with nanofibrillated cellulose [99]. This 4D printing system is inspired by nastic plant motions such as the response of leaves, flowers and bracts to environmental stimuli. Thanks to the embedding of cellulose fibrils along the prescribed printing pathway, the printed structure was encoded with localized, anisotropic swelling behavior. Figure 1-13a illustrates the one-step shear-induced alignment of fibrils due to DIW printing and the anisotropic swelling behavior of the printing parts. As shown in Figure 1-13b, the 4D printed flower architectures with two different designed configurations of bilayer lattice

(90°/0° and -45°/45°) are presented with their swelling process (closed and twisted). This novel biocompatible and flexible printing ink design paves a new way to shape-shifting 4D printing.

### 1.2.3 Perspectives and Challenges for 3D Printing

Although additive manufacturing experienced an enormous breakthrough in printing methods and printing materials in the past few decades, it remains some ongoing challenges due to its inherent working mechanism. As shown in Figure 1-14 [17], traditional subtractive manufacturing relies on material-removing machining processes, including milling, sawing, drilling and broaching. In contrast, additive manufacturing builds up objects in a layer-by-layer manner. It shows advantages in material and resource efficiency, high geometric freedom of designs and flexibility in customized small batch production. Whereas subtractive manufacturing usually costs more material waste during the process and requires designing and creating specific manufacturing tools to match the different shapes of objects. However, even though 3D printing has proven to be a successful method for rapid prototyping, only a handful of industry applications have been addressed to date. Serval challenges remain to be approached to expand the range of 3D printing industrial applications: i) the slow process of 3D printing restricts their potential for large-scale production, ii) the material limitation restricted by 3D printing technology, iii) the mechanical properties degradation caused by unavoidable printing defects and anisotropic performance.

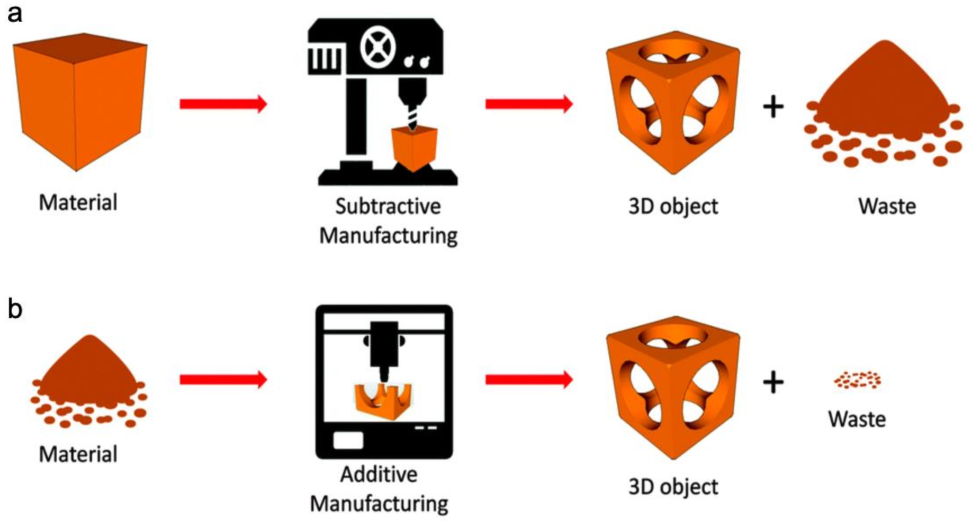

**Figure 1-14. The comparison between additive and subtractive manufacturing. (a) Subtractive manufacturing relies on material-removing machining processes (milling, sawing, drilling, etc.). (b) Additive manufacturing applies a layer-by-layer fabrication method via different 3D printing machines (SLA, DIW, FDM, SLS, etc.). (Reproduced with permission from ref. [17])**

Most importantly, 3D printing technology has been given countless expectations in the sustainable manufacturing field. The fundamental of 3D printing holds the promise to reduce material waste as well as to shorten the product development cycle. Among all types of printing materials, polymers with excellent performance at low cost, lightweight, high performance and durability are still primary working materials for most 3D printing technologies. However, the growing usage of 3D printing and the fast update of polymeric parts have resulted in tremendous polymer waste growth over the past few decades [100]. Polymer accounts for over 90% of the material feedstock for 3D printing, while their recycling process is not standardized [101]. Currently, polymer waste disposal strategies are generally landfill, incineration and mechanical recycling, resulting in either severe pollution or stringent treatment handling constraints [102]. This situation not only causes environmental problems but also will limit the application and development of 3D printing technology. The most effective method to extend the printing material lifetime and reduce polymer waste is to make printed parts repairable and recyclable. Therefore, to achieve sustainable development in additive manufacturing, it is highly desirable to devise a recycling and repairing strategy for 3D printing to reduce the waste of finite resources, minimize the negative impact on the environment, and prolong the service life of 3D printed products.

## 1.3 The Solutions with Dynamic Covalent Chemistry

### 1.3.1 Introduction to Dynamic Covalent Chemistry

Fortunately, the development of dynamic covalent chemistry offers a way to overcome the above challenges. For classical polymer materials, especially the thermosets, chemical reactivity within polymers is unexpected and needs to be avoided for their chemical resistance and stabilities in high service temperature[103]. However, these materials cannot be reprocessed and recycled, which has a significant negative impact on the environment. Recently, polymers with dynamic covalent bonds have emerged as an attractive candidate because of their functional characteristics such as shape memory, stimuli-responsiveness, self-healing and reprocessing capability [104-107]. With desirable polymer dynamics, polymer networks can flow or macroscopically reshape when the dynamic covalent bonds are activated by external stimuli, and stay stable under normal circumstances [108]. These polymer systems have also been defined as covalent adaptable networks (CANs) in a broader context [109]. The CANs enable thermosets to have versatility and recyclability that previously existed in thermoplastics, thus offering unprecedented possibilities for polymer and materials science innovation [110, 111]. To our knowledge, the earliest report about the stress relaxation behavior of covalent bonds was in the 1940s [112]. Tobolsky's research group observed the stress relaxation behavior of polysulfide rubbers during studying the viscoelastic behavior of polymers [113], which has become a recognized characterization method for identifying the interchange behavior of dynamic covalent bonds. After that, the ionic interchange of the Si-O bond also attracted interest and was utilized for healing properties in 2012 [114, 115]. The great demand for 'shape memory' and 'self-healing' functional polymers enables the scope of dynamic covalent chemistry to be rapidly expanded.

Currently, there are various dynamic covalent reactions including Diels-Alder bond [116, 117], boronic acid condensation [118, 119], and transesterification [120, 121], disulfide bond [122, 123], and others. These dynamic covalent bonds can be generally divided into two groups: i) asymmetrical and directional dynamic covalent bonds that require the combination of two different components (e.g., C=N, B-O and C-O bonds); ii) symmetrical bonds that allow self-exchange (e.g., C=C, C≡C and S-S bonds) and can self-react to form dimer or oligomers [109]. The fundamental understanding of these bonds has been built based on numerous studies, while their applications in different fields are still desirable to exploit. For an overview of these dynamic covalent reactions, some important progress on the development of CANs is summarized on aspects of some typical and common dynamic covalent reactions.

#### 1.3.1.1 Diels-Alder Reaction

Dynamic C-C bonds can exist in many reactions including Aldol reaction [124], Diels-Alder reaction [116, 117], phenol/aldehyde condensation [125], olefin metathesis [126], alkyne metathesis [127], [2+1] cycloaddition [128], etc. Among them, the Diels-Alder (DA) reaction is the most widely applied reaction because of its mild condition and efficient reversibility at elevated temperatures. The DA reaction was first reported in 1928 by Otto Diels and Kurt Alder [129]. As shown in Figure 1-15, the [4+2] cycloaddition reaction between furan and maleimide can produce cyclohexene adduct and is reversible at elevated temperatures. The discovery of this reaction led them to receive the Nobel Prize in Chemistry in 1950.

DA chemistry is possibly considered as the earliest chemistry to construct the dynamic covalent network. In 2002, Chen et al. creatively developed a thermally re-mendable polymeric material [130]. This work is remarkable and inspires the following numerous studies surrounding the concept of self-healing materials. In recent years, the polymer networks adopted DA bonds extended to polyurethanes [131], epoxy resins [106], polyamides [132] and rubbers [133]. Further exploration of accelerating reactions at room temperature and controlling the on and off of bond exchange processes is anticipated to broaden their application potential.

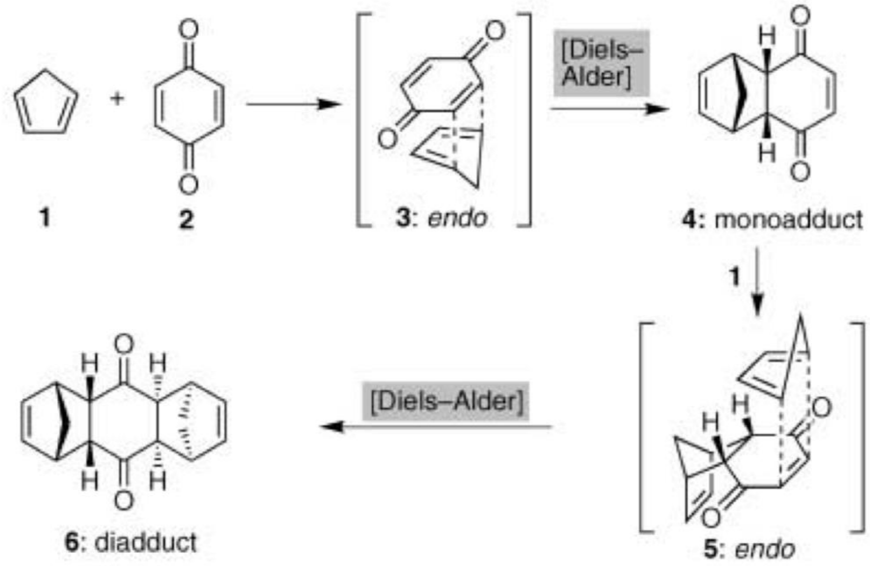

**Figure 1-15. The process of Diels-Alder reaction. (Reproduced with permission from ref. [129])**

### 1.3.1.2 Transesterification

Transesterification is one of the most classic reactions that have been commonly used in material chemistry and organic synthesis. In 2011, Libeler's research group adopted the transesterification reaction into epoxy polymer networks to achieve recyclable and reprocessable thermosets [120]. Under the high temperature, the ester exchange can be triggered with zinc acetate as the catalyst, and the network topology can be rearranged following external mechanical force guidance. Figure 1-16 schematically presents the transesterification reaction in dynamic covalent networks. It is interesting to note that the epoxy network shown Arrhenius-like gradual viscosity variations like inorganic glasses. These network systems were named as vitrimer in the following studies that were not limited to an epoxy network. Hillmyer et al. synthesized a polyesterurethane network with high-density esters by crosslinking the star-shaped polylactide precursor with 4,4'-diphenylmethane diisocyanate [134]. With higher density esters than the epoxy network, this vitrimer showed impressive short characteristic relaxation times of less than 50 s at 140 °C. The essential catalyst or high temperature is the major challenge of the transesterification application faced and still requires further research.

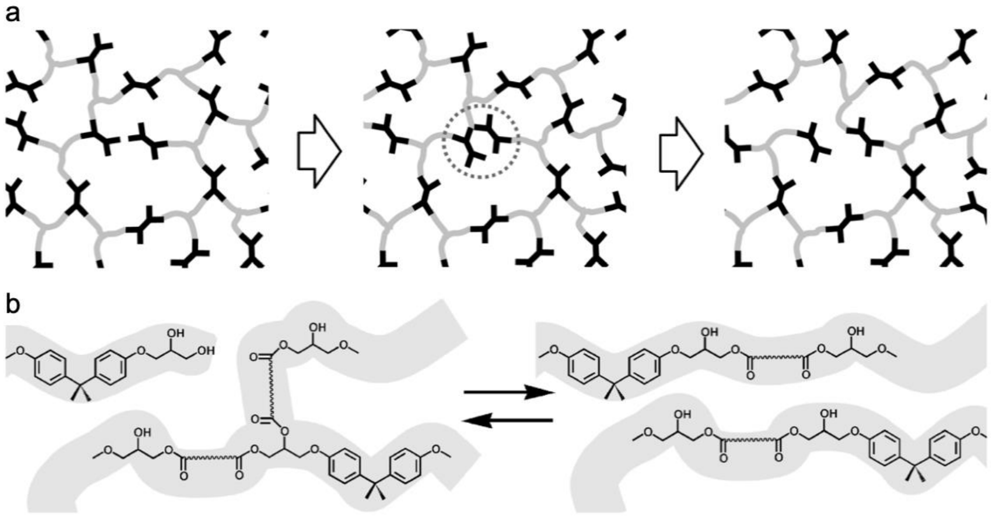

**Figure 1-16. Topographical rearrangement mechanism via transesterification. (Reproduced with permission from ref. [120])**

### 1.3.1.3 Disulfide Exchange Chemistry

As the earliest reaction studied in dynamic covalent chemistry, the disulfide exchange reaction has been thoroughly studied in dynamic materials. Disulfide bonds are a favourite choice because their reversible formation and breaking reaction can be triggered under mild temperature and catalyst-free conditions [135, 136]. Together with their low cost and low toxicity, disulfide monomers are suitable for self-healing or recyclable networks. The mechanisms of disulfide exchange reactions can be generally grouped into two categories: anionic exchange or radical exchange [137]. Figure 1-17a presents the anion exchange mechanism that requires a thiolate anion to nucleophilic attack the sulfur atom of disulfide bond. The thiolate anion attacks result in new thiolate anions generation from the cleavages of original S-S bonds and the formations of new disulfide bonds [138]. Radical pathways have more variants, such as light response radical transfers and crossover reactions (Figure 1-17b) [139], or the additional radical initiator triggered disulfide exchange reaction (Figure 1-17c) [140]. Furthermore, as shown in Figure 1-17d, studies of the aromatic disulfide metathesis at room temperature also have attracted extensive interest [135].

In 2014, Odriozola's research group reported a catalyst-free self-healing polyurethane based on aromatic disulfide metathesis under room-temperature [135]. With excess thiols and quadruple hydrogen bonds presenting, self-healing performance can be guaranteed. In Figure 1-18a, the cut sample could be repaired by keeping contact at room temperature for over 2 h, and the healing efficiency was about 80%. Light inducing dynamic disulfide chemistry is also worth to be studied because of the spatiotemporal controllability of light energy [141]. Rowan et al. synthesized a semicrystalline polydisulfide with the inherent thermal/light-responsive shape memory and healing properties [142]. As shown in Figure 1-18b, this polydisulfide film can be reprogrammable or healable through elevated temperature (80 °C) or ultraviolet light (UV) irradiation. Thanks to relatively rapid interchange reaction, disulfide exchange reaction is one of the most extensively used dynamic covalent chemistry. However, the spontaneous oxidation of thiol in the air as the drawback of this reaction should be considered when it applied [137].

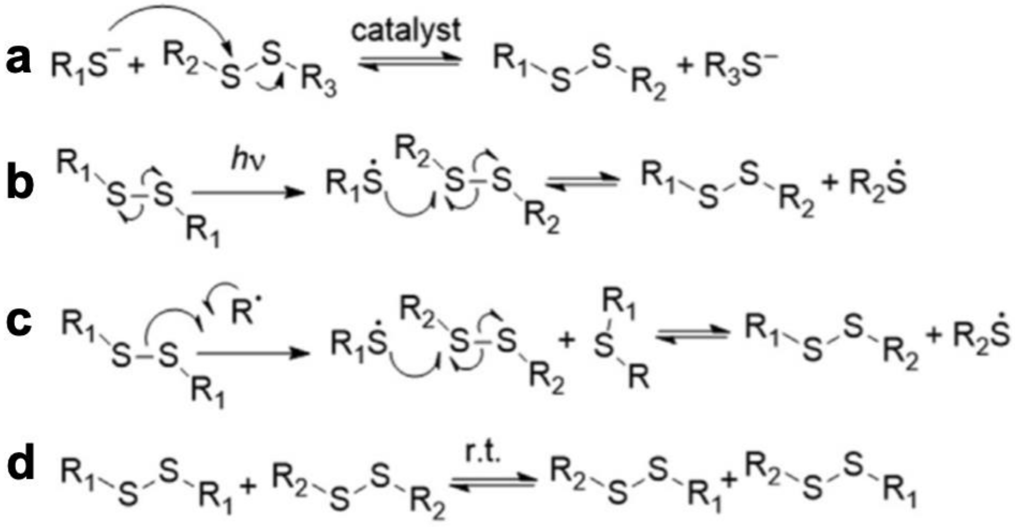

**Figure 1-17. Different mechanistic pathways for dynamic disulfide exchange. (Reproduced with permission from ref. [137])**

In conclusion, the above three dynamic covalent chemistries have historically played an essential role in CANs studies. There are also other dynamic covalent reactions widespread, such as imine chemistry, boronic esters, siloxane exchange, etc. As space is limited, we are not able to provide details of all these mechanisms. In recent 20 years round, the studies surrounding dynamic covalent chemistry have provided insight into the next generation of advanced materials applications. At the fundamental and practical level, much work has yet to be done to understand the material better and impact society beyond the academic niche broadly.

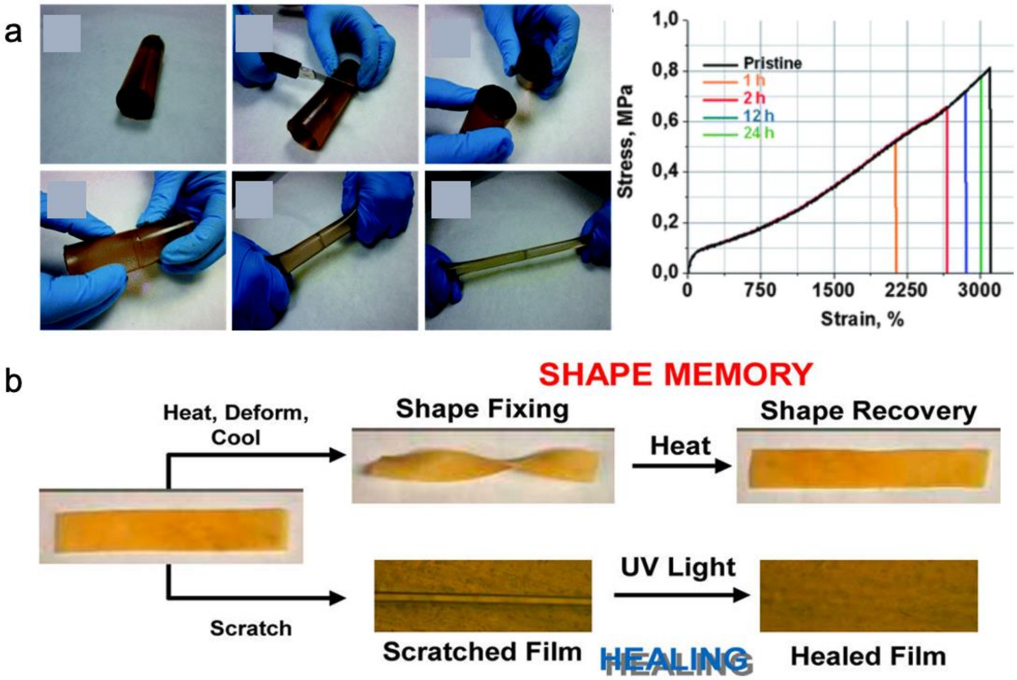

**Figure 1-18. Materials based on dynamic disulfide chemistry. (a) A pristine sample cut in half then healed by staying in contact for 2 h. (b) Shape memory and self-healing behavior of polysulfide materials. (Reproduced with permission from ref. [135] and [142])**

### 1.3.2 Development of 3D printing Technology Based on Dynamic Covalent Chemistry

To the best of our knowledge, the idea that integrated dynamic chemistry with 3D printing technology was first mentioned in the research from Burdick's group in 2015 [143]. Although some previous studies have discussed the possibility of 3D printing dynamic covalent networks from theoretical studies [144], Burdick et al. first utilized the self-healing hydrogels as the support to print shear-thinning hydrogels directly. The hydrogels are based on dynamic noncovalent guest-host bonds to achieve supramolecular assembly. The dynamic nature of this new 3D printing technology has opened up many opportunities in 3D printing technology and paved a new way to solve the challenges of 3D printing.

In 2016, Voit and Smaldone made an interesting attempt to improve the mechanical properties of printed parts via dynamic covalent chemistry [145]. Commercially fused filament fabrication (FFF) printable PLA was blended with furan-maleimide DA adducts. The thermally reversible dynamic covalent reaction can significantly improve the inter-filament adhesion of printed parts along the z-axis and therefore reduce their anisotropic (Figure 1-19a). After this attempt, their impressive work about the first generation of printable DA reversible thermoset resins was published [146]. Unlike the simply blended DA adduct in a commercial thermoplastic resin, new furan-maleimide DA crosslinked polymers were synthesized. The printable resin featured thermoset properties at service temperatures as well as ultra-low melt viscosity at print temperatures. During the printing process between 90 and 150 °C, the reversible DA reaction further contributed to the smooth surface finish and as-printed isotropic mechanical properties of printed components.

As shown in Figure 1-19b, compared with the commonly 3D printed thermoplastic, the cross-sectional pictures of DA thermoset printed parts have no visible layer structure. The toughness of the printed DA thermoset in different printing directions was not significantly different.

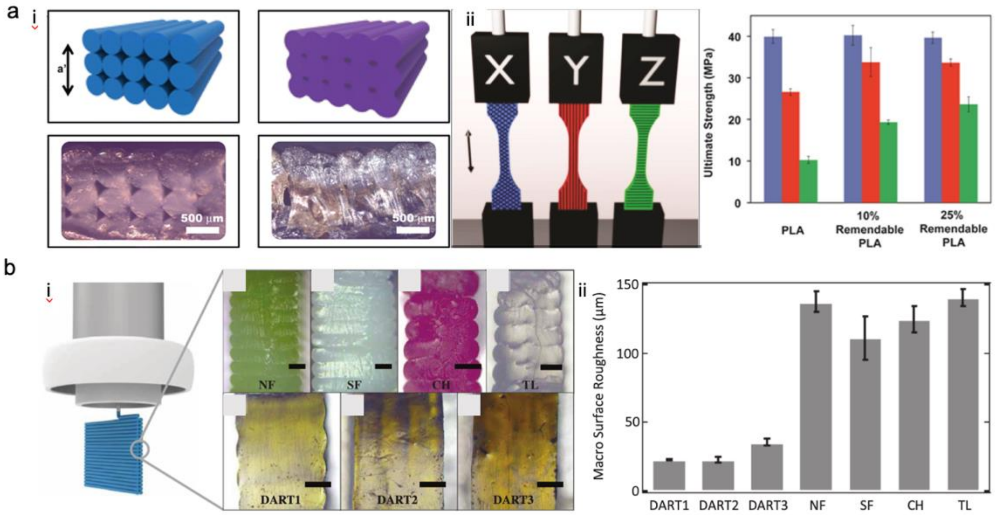

**Figure 1-19. 3D printing materials based on the DA reaction. (a) DA enhanced PLA based 3D printing material. (i) Illustration and photographs of pure PLA and PLA with DA adducts. (ii) Ultimate strength results of pure PLA and PLA with 10% and 20% DA adducts in X/Y/Z printing directions. (b) DA reversible thermoset printing material. Comparison of microscope pictures (i) and macro surface roughness (ii) of the cross-section of printed parts from different materials. (Reproduced with permission from ref. [145] and [146])**

More and more 3D printing related studies have started to explore the utilization of dynamic covalent chemistry in recent years. Zheng et al. employed the siloxane bond exchange reaction in 3D printing ceramics technology [147]. In Figure 1-20a, their mechano-plastic pyrolysis (MPP) printing strategy required two steps: i) mechano-plastic shaping and ii) pyrolysis. The poly(dimethylsiloxane) (PDMS) was first printed into a 2D shape. The MPP process can thermally trigger the dynamic bond exchange reaction of siloxane bonds in PDMS and permanently deform the printed 2D shape into a 3D structure. Huang's group work focused on the self-healing function of 3D printed parts [148]. A polyurethane acrylate containing disulfide bonds is synthesized and applied as a photopolymer resin with photoinitiators and a reactive diluent. With the excellent fluidity and high curing rate, the photopolymer resin can be fabricated by the DLP 3D printer. The printed parts exhibited high tensile strength and elongation and outstanding healing efficiency (Figure 1-20b). The broken sample can be repeatedly healed at 80 °C for 12 h, and the healing efficiency is about 95%.

Besides functional 3D printing development, dynamic covalent chemistry can also benefit the sustainable development of 3D printing. As we mentioned, the growing usage of 3D printing has brought concerns about the environmental impact. The recent growth in dynamic covalent chemistry provides a promising solution to develop fully recyclable 3D printing ink. Qi's group has studied the transesterification based vitrimer behavior since 2016. Based on the comprehensive understanding of the transesterification reaction, their group developed a recyclable vitrimer epoxy 3D printing ink based on solvent-assisted transesterification [149]. Figure 1-21a shows that the fatty acid-epoxy mixture with nanoclay additives was required pre-crosslinking and then applied as the DIW based printing ink. The printed sample also required two steps of post-curing processes before use. The 3D printed waste can be fully dissolved in an ethylene glycol solvent at 180 °C to achieve fully recyclable 3D printing. The solution can be reformed into a printable ink through solvent evaporation and partially repolymerization.

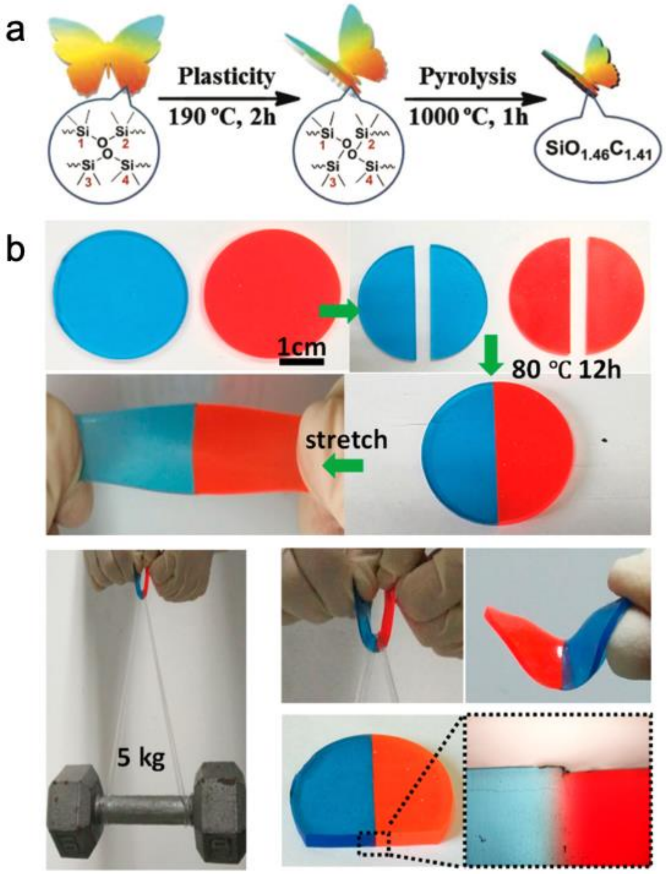
a
Plasticity
190 °C, 2h
Pyrolysis
1000 °C, 1h
Si
O
1
2
3
4
$SiO_{1.46}C_{1.41}$
b
1cm
80 °C 12h
stretch
5 kg

**Figure 1-20. Examples of the 3D printing process utilized dynamic covalent bonds. (a) Schematic illustration of the plastic deformation and pyrolysis in the mechano-plastic pyrolysis process. (b) The colored disulfide based polyurethane acrylate samples were cut into two pieces and healed. Images of sample deformation under manual stretching and 5 kg weightlifting. (Reproduced with permission from ref. [147] and [148])**

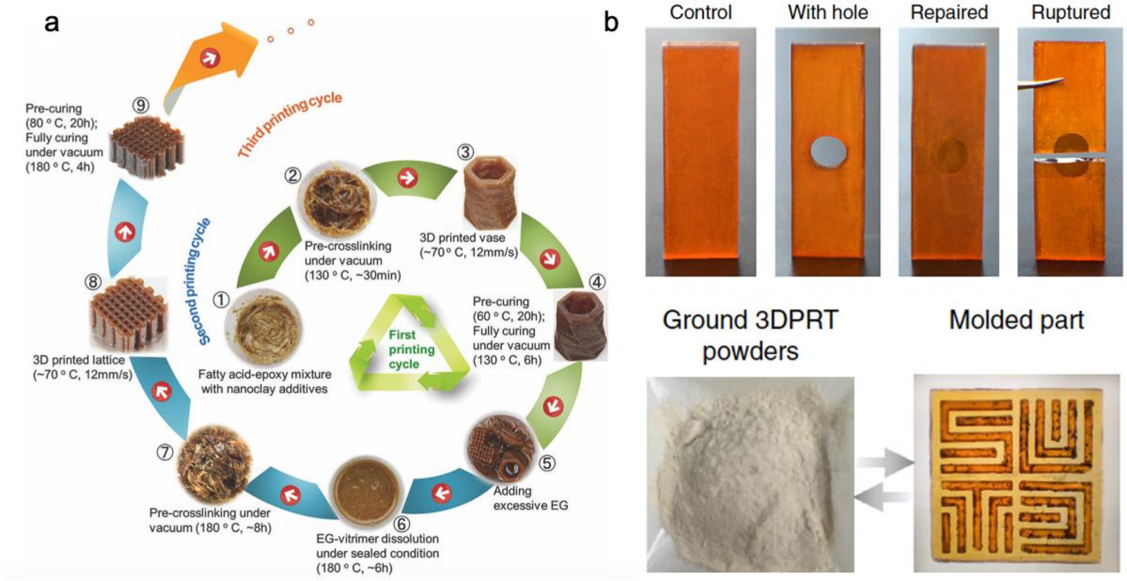
a
Third printing cycle
Pre-curing
(80 ° C, 20h);
Fully curing
under vacuum
(180 ° C, 4h)
⑨
Second printing cycle
②
Pre-crosslinking
under vacuum
(130 ° C, ~30min)
③
3D printed vase
(~70° C, 12mm/s)
④
Pre-curing
(60 ° C, 20h);
Fully curing
under vacuum
(130 ° C, 6h)
⑧
3D printed lattice
(~70 ° C, 12mm/s)
①
Fatty acid-epoxy mixture
with nanoclay additives
First
printing
cycle
⑤
Adding
excessive EG
⑦
Pre-crosslinking under
vacuum (180 ° C, ~8h)
⑥
EG-vitrimer dissolution
under sealed condition
(180 ° C, ~6h)
b
Control
With hole
Repaired
Ruptured
Ground 3DPRT
powders
Molded part

**Figure 1-21. (a) The crosslinking-dissolution-recrosslinking cycle of recyclable DIW 3D printing of nanoclay-reinforced vitrimer epoxy. (b) The repairability and recyclability of photopolymerization-based printing material. (Reproduced with permission from ref. [149] and [150])**

Replacing the re-printability, Zhang et al. reported a new type of reprocessable transesterification-based CAN for photopolymerization-based recyclable 3D printing [150]. Their printing process is more straightforward compared with the previous DIW printing process. In the photopolymer solution, zinc acetylacetone hydrate was added as the catalyst to accelerate the transesterification reaction. With the transesterification reaction, the broken parts can be repaired by filling the hole with the photopolymer solution followed by applying UV irradiation and heating to 180 °C for 4 hours. The printed waste can also be recycled by molding the ground powder at 220 °C for 2 hours (Figure 1-21b). Although both Qi's and Zhang's works offered a solution for 3D printed parts fully recycling, the following manufacturing processes of recycling materials either require a number of processing steps before reprinting or limit in the high-temperature hot-pressing method. The complicated preparation and restricted recycling procedure may limit their practical applications.

### 1.3.3 Thesis Objectives

3D printing has attracted considerable attention due to its rapid responsiveness, convenient operation, and personalization. However, the constantly increasing waste of printed polymers imposes a heavy burden on the environment, which contradicts the circular economy concept. To achieve sustainable manufacturing, the ultimate objective of this thesis is to develop a sustainable 3D printing strategy based on dynamic covalent chemistry. We are looking forward to an omnidirectional solution, including waste recycling and resource conservation.

Our group first attempted work is about DA reaction-based thermoreversible 3D printable polyurethane. Besides printing material recyclability, this project focuses more on the targeted shape memory and self-healing properties as well as their applications as next-generation intelligent devices [151]. In this thesis, we leverage existing works and results to find the optimal solution for sustainable 3D printing development. A series of practical strategies of sustainable 3D printing has been developed from studying recyclable and repairable 3D printing materials and exploring 3D printing manufacturing methods. There are typically three main challenges: 1) the ease and precision of 3D printing processing, 2) the need for identical properties of fully recycled polymers with original materials, and 3) the precisely controlling in-situ repair and simplified post-process.

We selected the transesterification and disulfide metathesis to build the recyclable and repairable 3D printing material among the various dynamic covalent chemistries. Four different dynamic covalent materials were synthesized and discussed: reprocessable epoxy based on transesterification (FA-Epoxy), thermoreversible epoxy based on aliphatic disulfide bonds (CADH-Epoxy), polyurethane-based on heterocyclic disulfide bonds (TEMPS-PU) and polyurethane-based on aromatic disulfide bonds (DTDA-PU). After comparing the mechanical properties of synthesized materials and their requirements of recycling condition, two polyurethane materials with different disulfide monomers were selected to study their 3D printing behavior and recyclability. To further enhance the mechanical property and printability, the aromatic disulfide bonds-based polyurethanes incorporating hydroxylated multi-walled carbon nanotubes (DTDA-PU/MWCNTs-OH) were prepared. Furthermore, after a comprehensive study about photothermal properties of DTDA-PU/MWCNTs-OH composites, a precisely in-situ repair process and simple support structure removal method were demonstrated to prolong the lifespan of printing parts, reduce printing waste and make better use of resources.

The highlights and the main contributions of this thesis are as following:

i. Propose a recyclable printing mode based on a dynamic covalent bond system, which has universal applicability and greatly reduces the cost of material recycling.

ii. Introduce photothermal conversion materials, MWCNTs-OH, into the dynamic covalent bond printing system to change the response stimulus source from thermal energy to light energy. Through the temporal and spatial controllability of the stimulus source, accurate in-situ defect repair can be achieved.

iii. Propose a new method of non-contact light control to remove the printing support structure, improve the post-processing efficiency of 3D printing, and reduce the defective rate of printed products.

## 1.4 Thesis Outline

This thesis follows the monograph-article format outlined in the Thesis Regulation Guide by the School of Graduate and Postdoctoral Studies (SGPS) of The University of Western Ontario. Following is a road map that briefly outlines the contents of an entire dissertation.

In the current chapter, we review background information relevant to this thesis work and overall project objectives. After reviewing the importance of sustainable manufacturing and its development, we notice that 3D printing technology plays a leading role in this revolution path. The state-of-the-art 3D printing technology and 3D printing materials are summarized. Based on the discussion of existing challenges in the sustainable development of 3D printing, dynamic covalent chemistry is targeted as the approach of 3D printing sustainability. The systematic introduction of dynamic covalent chemistry and its recent application in 3D printing are also reviewed. Finally, our overall project objectives and the thesis outline are also identified.

Chapter 2 first introduces the materials and chemicals that are used for printing materials manufacturing. The synthetic procedure of polymer and composite, and 3D printing technology for material fabricating are demonstrated. After that, this chapter also introduces the instruments employed for materials characterizations and the procedures for testing.

Chapter 3 demonstrates the synthesis of four different dynamic covalent polymers for recyclable and repairable 3D printing. The polymer structure and the type of dynamic covalent bonds of these polymers are different, which is convenient for us to make a comprehensive comparison. Their physical and chemical properties are evaluated and discussed. After comparison, the polyurethane-based disulfide polymers (TEMPS-PU and DTDA-PU) with better mechanical performance and mild recycling conditions are chosen for follow-up experimental research.

The printability of these two materials is further studied in Chapter 4. Their viscoelastic and rheological behavior is evaluated to provide a reference for their printing conditions. From the images of reprinted samples and the tensile test results, the spontaneous oxidation of thiol significantly affects the TEMPS-PU recycling performance. At the same time, the DTDA-PU exhibits excellent recycling performance.

In Chapter 5, we further step towards the mechanical enhancement of 3D printing materials using MWCNTs. Hydroxy-functionalized MWCNTs (MWCNTs-OH) are introduced to the DTDA-PU network for better dispersion. The incorporation of the MWCNTs dramatically improves the solvent-resistance and mechanical properties of printing materials. The assessments of their printability and recyclability are also evaluated.

In Chapter 6, the photothermal effect of MWCNTs composites is studied. Aiming at the damage of 3D printed complex structures, this chapter presents an unconventional approach to achieving the precisely in-situ repair by utilizing photothermal conversion to trigger the disulfide bonds reaction. Furthermore, support structures are often required for 3D printing of parts with overhangs, but the removal of mechanical support risks the damage of printed parts. A new solution for precise and rapid removal of the support is also discussed to effectively reduce printing waste.

Finally, Chapter 7 provides a conclusion and summary of the results and important findings in this project. It also gives perspectives on future research in this area.

# Chapter 2

## 2 Experimental and Characterization Techniques

This chapter introduces the chemicals and methods used for 3D printable dynamic covalent polymers synthesis and characterization. The chemicals and synthetic routes applied on FA-Epoxy, CADH-Epoxy, TEMPS-PU and DTDA-PU fabrication are first demonstrated. Then, the advantages of DIW 3D printing technology and the printing parameters of the following experiments are discussed. The experimental methodologies of preliminary investigations are also included in this chapter. Finally, the instruction of instruments and test settings are presented.

### 2.1 Introduction

Epoxy and polyurethane are two of the essential components of polymer networks. They have long been widely used in various daily applications due to their distinctive mechanical performance and durability. Therefore, our printing material candidates were also aiming at these two types of materials. We prepared four different types of dynamic covalent polymer, FA-Epoxy, CADH-Epoxy, TEMPS-PU and DTDA-PU. They are various in polymer networks and dynamic covalent bonds, which represents most typical scenarios in the materials categories. The DTDA-PU composites with different content of MWCNTs-OH was also prepared to study their mechanical enhancement performance and photothermal property. DIW 3D printing has advantages in highly flexible and adjustable [152]. Therefore, it was chosen as the manufactory technology in our instant recyclable and repairable 3D printing strategy.

Furthermore, the chemical structures and physical properties of materials are probed and measured in many ways. To comprehensively understand the reactants and the reaction process, Fourier transform infrared spectroscopy (FTIR) was carried out to identify the chemical structures of intermediate products and synthesized materials. The thermal stability, glass transition temperature and other thermo-mechanical properties were investigated by combining the results from thermogravimetric analysis (TGA), differential scanning calorimetry (DSC), dynamic mechanical analysis (DMA) and rheometer. All these thermal physical properties can help us to understand their stabilities and printability. In addition, solvent resistance property test was also evaluated to explore their chemical stability and crosslinking degree. The applications of printed products may very well depend on the mechanical performance of printing materials. For the evaluations of mechanical performance of as-synthesized materials, tensile tests were conducted on these specimens.

The objective of this thesis is to develop recyclable and repairable 3D printing materials for sustainable 3D printing development. Therefore, the recyclability and repairability were evaluated by comparing the mechanical properties of printed parts before and after recycling or repairing. The scanning electron microscope (SEM) and optical microscopy were also employed to analyze the corresponding topography of printed, recycled and repaired samples. The photothermal properties of MWCNT composites were investigated by a thermal imager (FILR) to explore their applications in NIR light-triggered repair and support removal.

## 2.2 Materials and Chemicals

Bisphenol A diglycidyl ether (BADGE), polytetrahydrofuran (PTMEG, average Mn ~1000 g/mol), isophorone diisocyanate (IPDI, 98%) and dibutyltin dilaurate (DBTDL, 95%), zinc acetate dihydrate (Zn $(Ac)_2$, ACS reagent), sulfur monochloride ($S_2Cl_2$, > 98%), hexamethyldisilazane (HMDS, ≥ 99%), anhydrous ethylene glycol (EG, 99.8%), nitromethane (Nitro, ≥ 95%) were purchased from Sigma-Aldrich, Inc. Cystamine dihydrochloride (CADH, > 97%), 4,4'-dithiodianiline (DTDA, > 98%), 4-hydroxy-2,2,6,6-tetramethylpiperidine (4-hydroxy-TEMP, > 98.0%) was purchased from TCI America, Inc. All these chemicals were used without further purification. Sodium hydroxide (NaOH, ACS reagent), magnesium sulfate ($MgSO_4$, ACS reagent), sodium acetate (NaOAc, ACS reagent), sodium sulfate ($Na_2SO_4$, ACS reagent), potassium carbonate ($K_2CO_3$, ACS reagent), dichloromethane (DCM, ACS reagent), methanol (MeOH, ACS reagent), N, N-dimethylformamide (DMF, ACS reagent) and toluene (ACS reagent) provided by Caledon Laboratories Ltd. Hydroxylated multi-walled carbon nanotubes (MWCNTs-OH) were obtained from Suzhou Tanfeng Co., Ltd. (purity > 95%, outer diameter < 8 nm, as-produced length 10-30 μm) and used without further treatment. The fatty acid (Pripol 1040, 296 g/$mol_{COOH}$) was kindly provided by Croda International PLC. It is a mixture of $C_{18}$ fatty acids derivatives with up to 25 wt% dimmers and more than 75 wt% trimers. All chemicals were used as received, except DMF and toluene used after drying over 4 Å molecular sieves and CADH neutralized before used.

## 2.3 Materials Synthesis and Fabrication

### 2.3.1 Synthesis of FA-Epoxy

The FA-Epoxy is the typical transesterification based dynamic covalent polymer. The FA-Epoxy is the typical transesterification based dynamic covalent polymer. The synthetic route was following the previous literature with minor modifications[120, 153]. 14.8 g fatty acid (50.0 mmol COOH) and about 0.055 g Zn $(Ac)_2$ (5 mol% to the COOH groups) were first added to the PTFE beaker and gradually heated from 100 °C to 180 °C with mechanical stirring for 3 h to fully solve Zn $(Ac)_2$. Then, 8.5 g BADGE (50.0 mmol epoxy) was added to the previous PTFE beaker with fatty acid and Zn $(Ac)_2$ mixture and was manually stirred to phase miscibility at 130 °C. The reaction was continued to proceed at 130 °C for 6 h until fully reacted.

### 2.3.2 Synthesis of CADH-Epoxy

The synthesis of CADH-Epoxy in this project is based on the epoxy resin cured with the amine hardener. The neutralization of CADH was performed as described in the literature with minor modifications [153]. Briefly, 13.5 g CADH (60.0 mmol) was first dissolved in 20 ml NaOH solution (6 M) with 1 h stirring at room temperature. The resulting mixture was then removed the water under a vacuum. The solid product was redissolved in 40 ml DCM. After removing the precipitate, the liquid was then dried over magnesium sulfate and filtered. The cystamine was obtained by further concentrating the filtrate in a vacuum overnight.

Stoichiometric amounts of BADGE (8.51 g, 25.0 mmol) and cystamine (3.81 g, 25.0 mmol) were mixed directly with a magnetic stirrer at room temperature for 30 min. The mixture was then gradually heated to 125 °C in 0.5 h and kept for another 1.5 h under magnetic stirring. The CADH-Epoxy was obtained as a dark viscous state. After pouring into a mold and cooling to room temperature, the as-prepared sample resulted in an opaque, brittle polymer.

### 2.3.3 Synthesis of TEMPS-PU

#### 2.3.3.1 Synthesis of Bis (4-Hydroxy-2,2,6,6-tetramethylpiperidin-1-yl) Disulfide (Bi-TEMPS-OH)

HMDS (20.8 g, 129 mmol) and 4-hydroxy-TEMP (20.2 g, 129 mmol) were added to a 250 mL two-neck round-bottom flask containing 130 mL nitromethane. The reaction was allowed to proceed at 50 °C for 12 h under mechanical stirring. Then, the resulting solvent was removed by vacuum at room temperature for 8 h. The resulting crude product of 4-tetramethylsiloxy-2,2,6,6-tetramethylpiperidine was used in the next step without purification.

DMF (60 mL) and sodium acetate (10.5 g, 129 mmol) were added to the flask with the above product. The flask was immersed in an ice-water bath. When the solution was cooled to 0 °C, disulfur dichloride (6.95 g, 51.4 mmol) in 50 mL DMF was added dropwise at a speed of ~ 30 drops per min under nitrogen atmosphere. The resulting mixture was stirred for an additional 15 min, then poured into cold water. The resulting precipitate was collected by filtration and washed with water three times, then redissolved in hexane and dried over sodium sulfate. After filtering, the solution was placed under reduced pressure to obtain the crude product of Bis(4-tetramethylsiloxy-2,2,6,6-tetramethylpiperidin-1-yl) disulfide (Bi-TEMPS-OTMS).

Bi-TEMPS-OTMS (6.78g, 13.0 mmol) was dissolved in 85 mL MeOH. Then, 1.80 g potassium carbonate (13.0 mmol) was added to the above solvent. The mixture was stirred for 4 h at room temperature and then poured into water. The precipitate was collected by suction filtration and then washed with water. After being dried under the vacuum, the crude product was recrystallized from methanol to obtain Bi-TEMPS-OH.

#### 2.3.3.2 Synthesis of TEMPS-PU Polymer

TEMPS-PU was prepared in two steps. The bis-isocyanate-terminated polyurethane as prepolymer was first prepared via the reaction between IPDI and PTMEG. PTMEG (29 g, 29 mmol) was first heated at 120 °C under vacuum for 2 h to remove moisture and then cooled to 50 °C. Then, IPDI (13.54 g, 60.9 mmol) with 20 mL of dried DMF was dropwise added into the mixture of PTMEG with one drop of DBTDL. The resulting mixture was stirred at 70 °C for 2 h under the nitrogen atmosphere to obtain the prepolymer. After the prepolymer solution was cooled down to room temperature, Bi-TEMPS-OH (10.91g, 29 mmol) in 10 mL DMF was slowly added. The mixture was heated to 50 °C and kept for 2 h under stirring. Then the resulting product was moved into a PTFE dish. The solvent was removed by vacuum drying at 60 °C for three days. After the mold was gradually heated from 40 °C to 150 °C for over 24 h, the final TEMPS-PU product was obtained.

### 2.3.4 Synthesis of DTDA-PU

The synthetic route was following the previous literature with minor modifications[186]. The prepolymer synthesis was carried out in a 250 mL three-necked round bottom flask equipped with a mechanical stirrer, a reflux condenser, and a funnel. The flask was immersed in an oil bath. PTMEG (29 g, 29 mmol) was first heated at 120 °C under vacuum for 2 h to remove moisture and then cooled to 50 °C. Then, IPDI (13.54 g, 60.9 mmol) and DBTDL (0.05 g) with 20 mL of dried DMF were added dropwise into the mixture of PTMEG. The well-mixed solution continued to react at 70 °C for 2 h under the nitrogen atmosphere. The mixture was cooled down to room temperature, and a resolution of DTDA (7.26 g, 29 mmol) in DMF (20 mL) was added. The mixture was further stirred for another 2 h at 50 °C. The homogeneous solution was poured into a PTFE dish, and then the solvent was removed by vacuum drying at 60 °C for three days until no bubbles were observed inside the resin samples. Consequently, the as-prepared samples were heated from 40 °C to 150 °C at a rate of 10 °C/hour to release internal stress.

### 2.3.5 Synthesis of DTDA-PU/MWCNTs-OH

After PTMEG (29 g, 29 mmol) removed moisture according to the above, the desired amount of MWCNTs-OH (1 wt%, 2 wt% and 3 wt%) was added to PTMEG. PTMEG and MWCNTs-OH were then mixed directly with a magnetic stirrer for 30 min. Then, IPDI (14.0 g, 63.0 mmol) and DBTDL (0.05 g) with 20 mL of dried DMF were added dropwise into the mixture of PTMEG and MWCNTs-OH and then stirred for 2 h at 70 °C under the nitrogen atmosphere. After the reactor was cooled to room temperature, a solution of DTDA (7.26 g, 29 mmol) in DMF (20 mL) was added as a chain extender. The mixture was heated to 50 °C and stirred for another 2 h. The resulting solution was loaded into a PTFE mold. After the residual solvent was removed by vacuum drying at 60 °C for three days, the mold was gradually heated from 40 °C to 150 °C for over 24 h. The final DTDA-PU composites are denoted as *x* wt% DTDA-PU, where x is the weight ratio of MWCNTs-OH to DTDA-PU matrix.

## 2.4 DIW 3D Printing Technology

The flexible and adjustable DIW 3D printing technique was applied as the 3D printing method, which provides the significant advantages of low equipment and maintenance cost, modifiable energy sources and the potential for large-scale production [154]. The advantages of DIW 3D printing technology can effectively combine with the synthesized recyclable and repairable print material to develop the highly customized and cost-efficient sustainable 3D printing strategy.

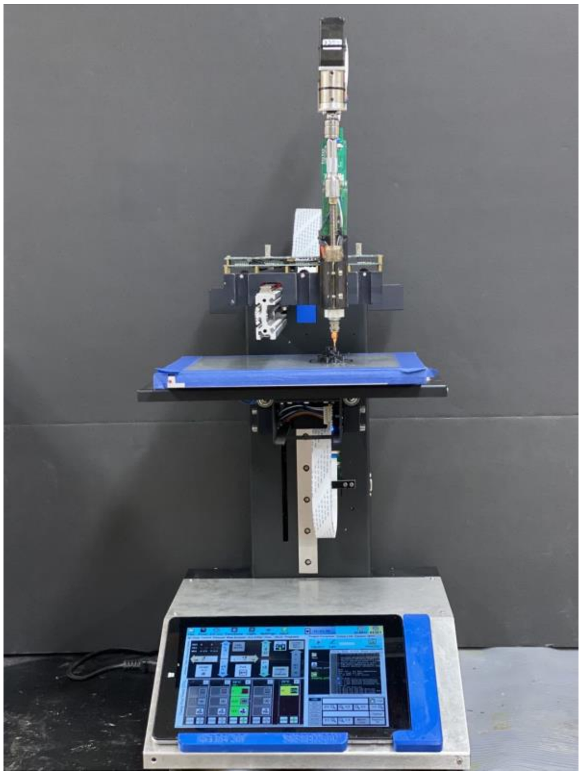

**Figure 2-1 A picture of Engine SR 3D printer with KR2 15 modular printing heads from Hyrel 3D.**

In this work, 3D printing was carried out by a customizable commercial 3D printer (Engine SR, from Hyrel 3D company) shown in Figure 2-1. A needle with an inner diameter of 600 μm was used as the printing nozzle, and the printing speed was adjusted based on the preliminary tests results of different materials. The printing temperature for different materials will be adjusted according to the experiment. For example, the printhead temperature and the build platform temperature of 2 wt% DTDA-PU were set at 145 °C and 25 °C, respectively. Before 3D printing, the as-prepared materials were crushed and loaded into a Luer-lock syringe, followed by melting at 120 °C for 15 min to remove any residual air bubble. Then, the syringe was mounted onto the 3D printer. In a typical printing process, the material was extruded and printed on a glass substrate as filaments parallel to the X-axis. The substrate was moved to the programmed center-to-center filament spacing in the Y direction to form the desired structure. All the 3D printed samples were allowed to stand for 12 h before further testing.

## 2.5 Instruments and Characterization

All the instruments used in this project are listed in Table 2-1. Fourier-transform infrared spectroscopy (FTIR) is a widely used technique to quickly estimate the structure of organic or polymer compounds. The FTIR instrument sends infrared radiation through the testing sample. The detector under the sample can respond to the intensity of radiation falling on them varies. Therefore, it can report an infrared spectrum of absorption or emission of samples, representing the stretching vibration of different chemical bonds [155]. Each molecule or chemical structure corresponds to a unique infrared spectrum, which is also known as the molecular fingerprint. The FTIR spectroscopy of chemicals and samples in this work was performed by a TGA-FTIR coupled system (TG-IR, Perkin-Elmer). The analysis was performed between 650 cm$^{-}$1and 4000 cm$^{-1}$. The resolution was set at 2 cm$^{-1}$, and the number of scans was 32.

The thermogravimetric analysis (TGA) and differential scanning calorimetry (DSC) are both used to study and characterize the physical and chemical changes of materials over temperature changes. Here, TGA was used to verify the synthesized material thermal stability by monitoring the weight change when the sample is heated at a constant rate [156]. The unstable samples with solvent or readily oxidizable or decomposable compounds will directly be reflected in significant weight loss by the precision balance in the furnace. TGA was performed on a TA Instruments TGA-Q600. The heating rate was 5 °C/min from 30 °C to 600 °C under a nitrogen atmosphere.

Additionally, DSC was employed to identify the phase changes of materials. Its principle is measuring the amount of heat required to increase the temperature of a sample. This result reflects the energy transferred to or from a sample experiencing a physical or chemical change[157]. DSC was carried out with a DSC-Q200 instrument (TA Instruments). The temperature ranges were verified based on different situations, and heating rate was 10 °C/min under a steady flow of nitrogen purge.

The dynamic mechanical analysis (DMA) is used to study the viscoelastic behavior of polymers. With a fixed frequency of the stress and gradually evaluated temperature, the property variations of materials can reflect the transitions corresponding to molecular motions. DMA was performed using a DMA-Q800 (TA Instruments). Testing samples with dimensions of $3.0 \times 1.0 \times 0.5$ $cm^3$ were measured at a heating and cooling rate of 3 ℃ $min^{-1}$ from -60 to 60 ℃ with 1 Hz fixed frequency in a liquid $N_2$ atmosphere.

A universal mechanical testing machine (eXpert 7603 eP2, ADMET) is employed to test the mechanical properties of materials. Tensile tests on the samples were performed according to the ASTM D638 test method. Tests were carried out at room temperature, and the crosshead speed was 1 mm/min for epoxy-based material and 100 mm/min for polyurethane-based material. The Young’s modulus was calculated from the slope of the initial section (up to 0.02% strain for epoxy and up to 0.5% strain for polyurethane) of the stress-strain curve.

The printing materials of DIW 3D printers need to present a low viscosity under extrusion conditions, while shearing-thinning behavior is also looking forward. Therefore, the investigations of the rheological behavior are necessary. The rheological properties of the samples were measured using a strain-controlled rotational shear rheometer (MCR 302, Anton Paar GmbH). The rheometer was fitted with a cone and plate tool with a 50 mm diameter and a 1° cone angle (CP50-1, Anton Paar). The viscosity was measured as a function of temperature at a fixed shear rate and a function of shear rate at a fixed temperature. For the temperature-dependent viscosity measurements, the shear rate was set at 1 $s^{-1}$ while the temperature was continuously increased from 120 °C to 150 °C, then cooled back to 120 °C at a rate of 1 °C/min. For the shear rate-dependent measurements, the temperature was fixed at 145 °C, and the shear rate was increased linearly from 1 $s^{-1}$ to 10 $s^{-1}$ in steps. The system was allowed to equilibrate for 3 min at each shear rate before measurements were taken.

The solvent resistance of the samples was studied by measuring the weight changes with respect to the time of immersing composites and pure material in toluene at room temperature. The solvent resistance test is a reasonably accurate and practical method to adverse deduce the polymer crosslinking degree. The swelling ratios of the materials were calculated as $W/W_0 \times 100\%$, where $W_0$ and W are the weight of samples before and after immersion without drying.

The distribution of MWCNTs-OH in the DTDA-PU matrix and repaired sample images were recorded by a scanning electron microscope (SEM 1540XB, Zeiss). The detailed structures of printing samples were observed by an optical microscopy (VHX-6000, Keyence). To observe the photothermal behavior of the specimens, the surface temperature of materials was measured with a thermal camera (T530sc, FILR) as a function of time as NIR laser illumination was turned on and off. Both NIR lasers had a wavelength of 808 nm, with powers of 1 W (referred to as the H-laser) and 0.5 W (the L-laser). The distance between the sample and the laser head was 30 cm. Each measurement was repeated five times.

**Table 2-1. Summary of instruments used in experiments.**

| Instrument | Model | Manufacturer |
|---|---|---|
| Fourier-transform infrared (FTIR) Spectrometer | TG-IR | Perkin-Elmer, Inc. |
| Thermogravimetric Analyzer (TGA) | TGA-Q600 | TA Instruments, Inc. |
| Differential Scanning Calorimeter (DSC) | DSC-Q200 | TA Instruments, Inc. |
| Rheometer | MCR 302 | Anton Paar GmbH |
| Universal Testing Machine | eXpert 7603 eP2 | ADMET, Inc. |
| Dynamic Mechanical Analyzer (DMA) | DMA-Q800 | TA Instruments, Inc. |
| Scanning Electron Microscope (SEM) | SEM 1540XB | Carl Zeiss AG |
| Optical Microscopy | VHX-6000 | Keyence, Corp. |
| Scientific Thermal Imager | T530sc | FILR |

# Chapter 3

## 3 Synthesis and Characterization of 3D Printable Dynamic Covalent Polymers

Polyurethane and epoxy are two of the most classical and broadly used polymers for the industry. They have the distinctly different mechanical performance that can be applied to various products. However, they are both notoriously difficult to reprocess and recycle due to their strong chemical bonds between the polymer molecules. Instead of landfilling and mechanical recycling, chemical recycling with dynamic covalent chemistry has emerged as an interesting candidate that is more environmentally friendly and resource efficient. In this chapter, two epoxy-based polymers and two polyurethane-based polymers with different dynamic covalent polymers were synthesized. They are reprocessable epoxy based on transesterification (FA-Epoxy), thermoreversible epoxy based on aliphatic disulfide bonds (CADH-Epoxy), polyurethane based on heterocyclic disulfide bonds (TEMPS-PU) and polyurethane based on aromatic disulfide bonds (DTDA-PU). All these materials are different in their polymer network structure, dynamic covalent chemistry, and the molecular structures of dynamic covalent monomers. The polymer synthesis reactions were investigated by the characteristic peaks of their FTIR results. Both the recycling procedure and their mechanical performance are carried out to explore their feasibility for the following applications in 3D printing.

## 3.1 Introduction

The traditional extrusion-based 3D printing materials are usually limited to thermoplastic, such as polylactic acid (PLA), acrylonitrile butadiene styrene (ABS) and polyethylene terephthalate (PET). However, these printable thermoplastics are usually susceptible to creep, temperature, and chemicals [158]. There are some studies about DIW 3D printing of thermoset by extruding the liquid photopolymer then curing via UV light for solidification [152, 159]. Thermosets, unlike previously discussed thermoplastics, offer an enhanced high-performance combination of structural integrity, thermal stability and chemical resistance [160], while their chemical stability is not amenable to reprocessing or recycling once cured [102]. Their property is neither feasible for extrusion-based 3D printing manufacturing nor our concept of sustainable manufacturing. To overcome this challenge, dynamic covalent chemistry actually offers an unconventional but effective approach.

Dynamic covalent polymers are a rapidly developing class of materials and have been firmly integrated into broad research areas in the last two decades [161, 162]. The dynamic features of these polymers are contributed by the reversible chemical reaction under equilibrium control [163]. For traditional organic compounds, the irreversible formation and efficient production is looking forward. Therefore, these organic compounds are synthesized by kinetically controlled reactions, and their product distribution is decided by the relative magnitude of the energy barrier. As shown in Figure 3-1, A goes C rather than B due to the lower activation energy $\Delta G_C^{\ddagger}$ than $\Delta G_B^{\ddagger}$. However, for dynamic covalent polymers, their bond formation and breaking are reversible and sufficiently fast. Thus, reactions go to the relatively stable resulting products under thermodynamic control [109]. In Figure 3-1, due to the lower change of Gibbs free energy $\Delta G_B$ than $\Delta G_C$, A goes to B rather than C [161, 164]. If we want the dynamic reaction to proceed, the change in free energy during the reaction should be favourable, which means Gibbs free energy $\Delta G^0$ in the following equation should be negative [161, 165].

$$\Delta G^0 = \Delta H^0 - T\Delta S^0 = -RTln\,K$$

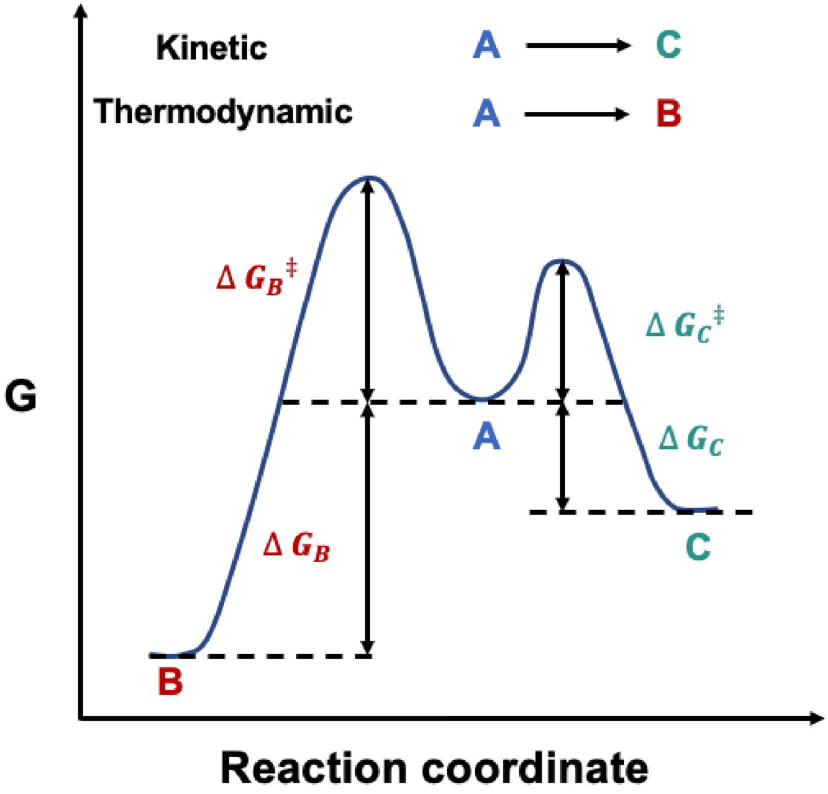
Kinetic
A → C
Thermodynamic
A → B
G
$\Delta G_B^{\ddagger}$
$\Delta G_C^{\ddagger}$
A
$\Delta G_C$
$\Delta G_B$
C
B
Reaction coordinate

**Figure 3-1. Free energy profile illustrating kinetically (A to C) and thermodynamically (A to B) controlled reaction.**

Therefore, the equilibrium of the reaction and proportions of the products are dramatically influenced by the starting material inherent features and conditions, and external factors during reaction, such as, temperature and pressure. Polymers consisting of dynamic covalent bonds have attracted extensive interest because of their remarkable reactivity and properties. The studies of their tunable and reversible dynamic covalent chemistry have opened a window for thermosets reprocessing, repairing and recycling. Therefore, they have been considered as the crucial access to our sustainable 3D printing development.

When designing the repairable and recyclable 3D printing polymers based on dynamic covalent bonds, there are two aspects that need to be considered. One is what dynamic covalent bonds we will use, and the other one is what polymer networks we should choose. There is a range of different dynamic covalent bonds. Transesterification and disulfide exchange are two of the most widely studied dynamic covalent reactions that are amenable for our desired printing materials design. For polymer networks, we have chosen epoxy and polyurethane as the basic compounds of polymer networks because of their distinctive mechanical performance and durability.

Four different types of polymers were designed and synthesized from the selected dynamic covalent bonds and polymer networks. For dynamic covalent polyepoxides, FA-Epoxy was first prepared as the classic reprocessable dynamic covalent epoxy based on transesterifications. The other recyclable epoxy based on dynamic disulfide bonds were also synthesized and named CADH-Epoxy. Since the transesterification is the exchange reaction before ester and alcohol, the hydroxy-ester structure of polyurethane usually embeds in branch chains, which should improve the difficulty for long polyurethane chain movement during the printing process. Therefore, for dynamic covalent polyurethane, only TEMPS-PU and DTDA-PU based on disulfide bonds were synthesized by introducing the disulfide compounds as the hard segments to polymer main chain. All these four materials were successfully synthesized and verified by FTIR analysis. Basic material characterizations, including the TGA, DSC, DMA and tensile tests, were carried out to evaluate their thermal and mechanical performance and provide references for selecting suitable materials for the following studies about recyclable and repairable printing materials.

## 3.2 Result and Discussion

### 3.2.1 Materials Synthesis

#### 3.2.1.1 FA-Epoxy Synthesis

Epoxy thermosets are one of the most classical and broadly used polymers for a number of diverse applications, including adhesive, structural materials, coating, and electrical insulation [166]. However, the nondegradable waste from this thermosetting resins has caused severe environmental pollution [167]. To address this issue, recent research and development in epoxy based on transesterification reactions provide a promising solution. The topologies of epoxy-acid networks can be rearranged by transesterification reactions with proper catalysis and external conditions, and therefore, polymer recycling can further achieve [121]. BADGE epoxy-fatty acid (FA-Epoxy), as one of the most well-explored dynamic covalent systems, was first investigated.

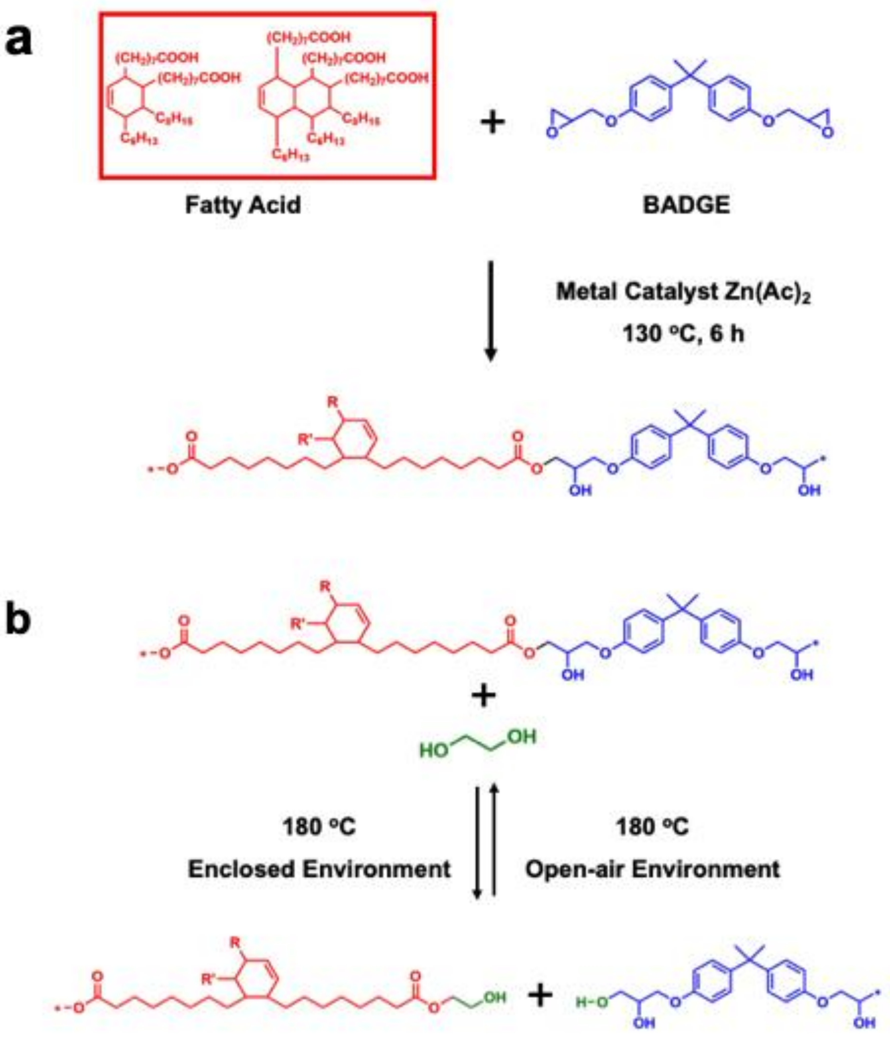
a
(CH2)7COOH
(CH2)7COOH
C8H15
C6H13
Fatty Acid
BADGE
Metal Catalyst Zn(Ac)2
130 °C, 6 h
R
R'
O
OH
b
HO
OH
180 °C
Enclosed Environment
180 °C
Open-air Environment
H-O

**Figure 3-2. Scheme graphs showing the polymerization and repolymerization mechanisms. (a) Synthetic scheme for FA-Epoxy. (b) The dissolution and repolymerization process of FA-Epoxy with EG aiding.**

The FA-Epoxy was synthesized by utilizing commercially available monomers, crosslinkers and catalyst: BADGE, fatty acid, and metal catalyst Zn $(Ac)_2$ (Figure 3-2a). About 50.0 mmol epoxy groups of BADGE reacted with equivalent COOH groups of fatty acid in the presence of 5 mol% Zn $(Ac)_2$ under 130 °C for 3 h. As shown in Figure 3-3a, the resulting sample was a transparent light brown material. The reaction between BADGE and fatty acid can be observed using FTIR spectroscopy in Figure 3-3b. The characteristic peaks range of carbonyl correlative is from 1690 cm$^{-1}$ to 1760 cm$^{-1}$. In the fatty acid spectrum, the strong absorption peaks of carboxylic acid groups can be observed at 1710 cm$^{-1}$. The decrease of the absorption peak of acid groups and the increase of the C=O stretching peak of ester groups at 1735 cm$^{-1}$ show in FA-Epoxy [168]. The broad peak of hydroxyl groups at around 3300 cm$^{-1}$ overlaps with methyl and methylene double peaks around 2920 and 2860 cm$^{-1}$ in spectrum of FA-Epoxy. Also, the epoxy characteristic peak at 918 cm$^{-1}$ disappears in the result of FA-Epoxy [169]. All these results indicate the reaction between COOH and epoxy groups and the successful synthesis of materials.

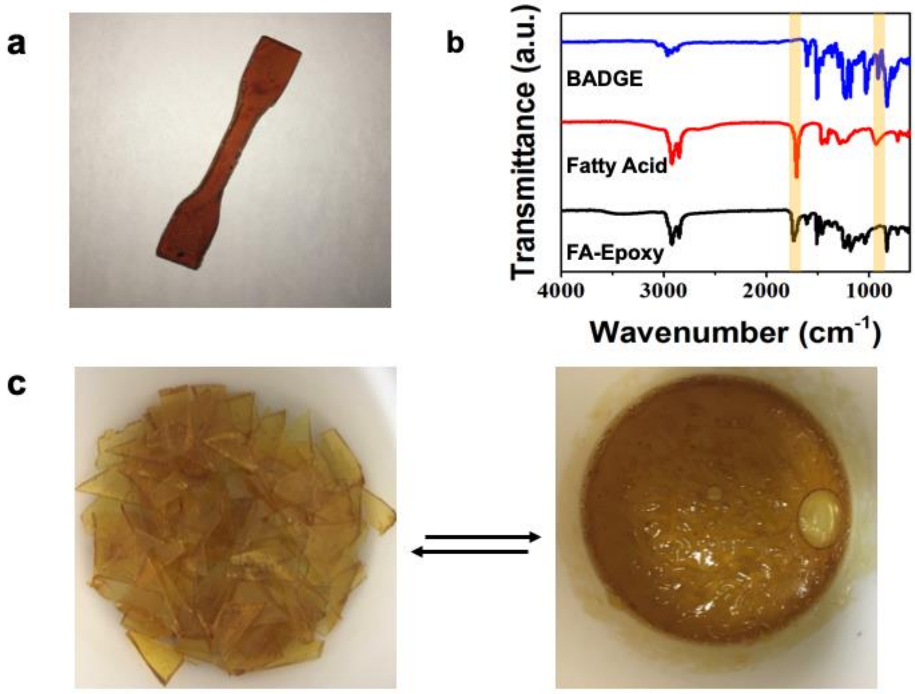

**Figure 3-3. (a) Image of the as-prepared FA-Epoxy sample. (b) The FTIR spectra diagram of BADGE, fatty acid and FA-Epoxy. (c) The recycling process of FA-Epoxy.**

The resulting sample can be hot pressed in a brass mold under 240 °C and reprocessed into the desired shape. Another way to reprocess materials is by dissolving in EG and repolymerizing while solvent evaporating. With the assistant of solvent, the reprocess temperature can dramatically reduce to 180 °C and realize pressure-free [170]. The schematic graph in Figure 3-2b illustrates how EG participates in the exchange reaction with the ester groups. The photographs of material dissolution and repolymerization processes are shown in Figure 3-3c.

#### 3.2.1.2 CADH-Epoxy Synthesis

Other than transesterification, the disulfide exchange reaction is another reaction among the earliest reactions that have been used in dynamic covalent chemistry [137]. Relatively rapid disulfide exchange in the network provides more feasibility to apply its relevant polymers in recyclable DIW 3D printing than transesterification. Also, material recycling and repairing can be achieved under mild environmental conditions. In this part, we directly integrated disulfide bonds to the epoxy network by introducing the disulfide monomers, cystamine, as the crosslinker. The cystamine with low molecular mass was selected as the aliphatic disulfide crosslinker to ensure the flowability of dynamic covalent epoxy at high temperature with enough disulfide bonds participated in the exchange reaction.

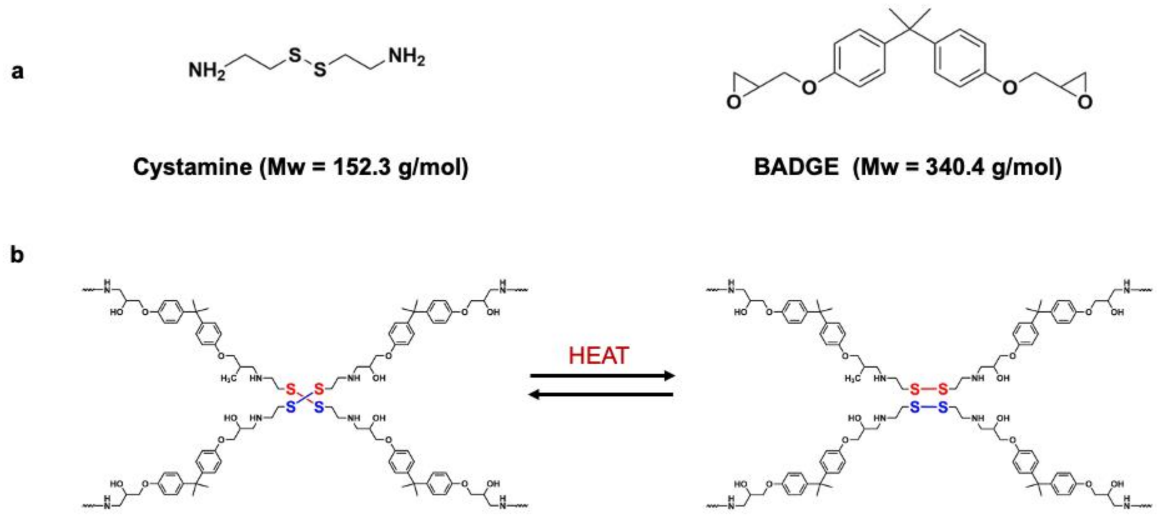

**Figure 3-4. (a) Compounds that have been used in CADH-Epoxy synthesized. (b) Network formation of CADH-Epoxy during the disulfide bond metathesis.**

The synthesis of CADH-Epoxy material was carried out based on the reaction between epoxy groups and primary amines (Figure 3-4). Figure 3-4a shows the monomers used in this work, including their chemical structures and molecular weights. The molar ratio of cystamine and BADGE was 1:1. The monomers reacted under high temperature (125 °C, ~2 h) without catalyst participating. The chemical structure of the synthesized CADH-Epoxy and the disulfide metathesis under heating were schematically shown in Figure 3-4b. The resulting product was dark viscous liquid. After cooling to room temperature, it resulted in a brittle material (Figure 3-5a).

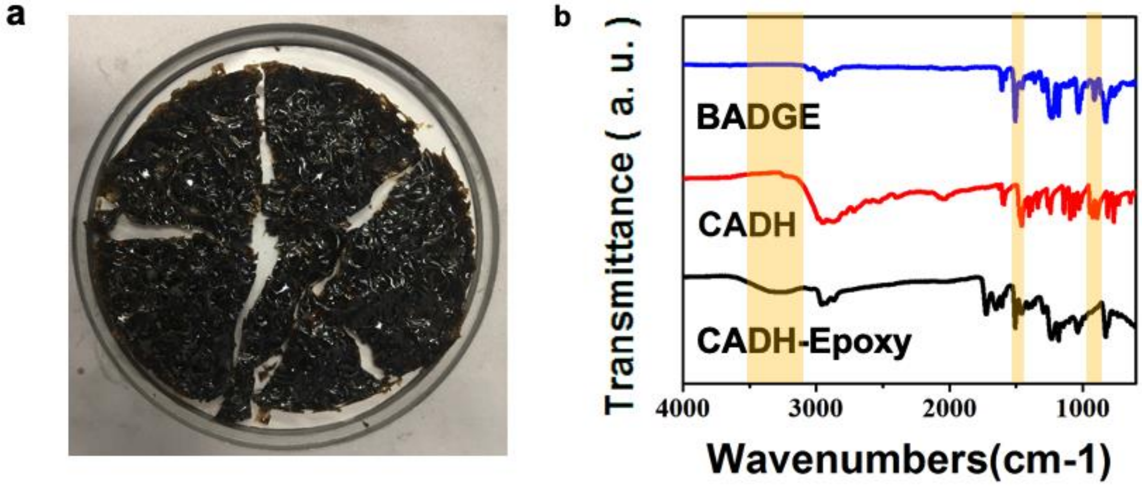

**Figure 3-5. (a) The photograph of a synthesized CADH-Epoxy sample. (b) The FTIR spectra diagram of BADGE, CADH and CADH-Epoxy.**

The FTIR spectrums of BADGE, CADH and CADH-Epoxy were recorded and compared to demonstrate the synthesized material in Figure 3-5b. The absorption peak at approximately 917 cm$^{-1}$ of the BADGE, assigned to the C-O deformation band, disappeared in the CADH-Epoxy, corresponding to the epoxy rings complete reaction [171]. The broad band located at around 3500 cm$^{-1}$ in CADH-Epoxy, which was attributed to the O-H stretching of hydroxyl groups and weak N-H stretching, also indicates the ring open reaction and polymer synthesized. Meanwhile, the absorption peak located at 1510 cm$^{-1}$ in CADH assigned to the N-H deformation of the primary amines, which was shifted towards lower wavenumber (1490 cm$^{-1}$) in CADH-Epoxy as the secondary amines, and was weak and followed by the C=C stretching on 1600 cm$^{-1}$ [172]. The comparison of the FTIR spectrums between monomers and the resulting product indicated that CADH-Epoxy had been successfully synthesized.

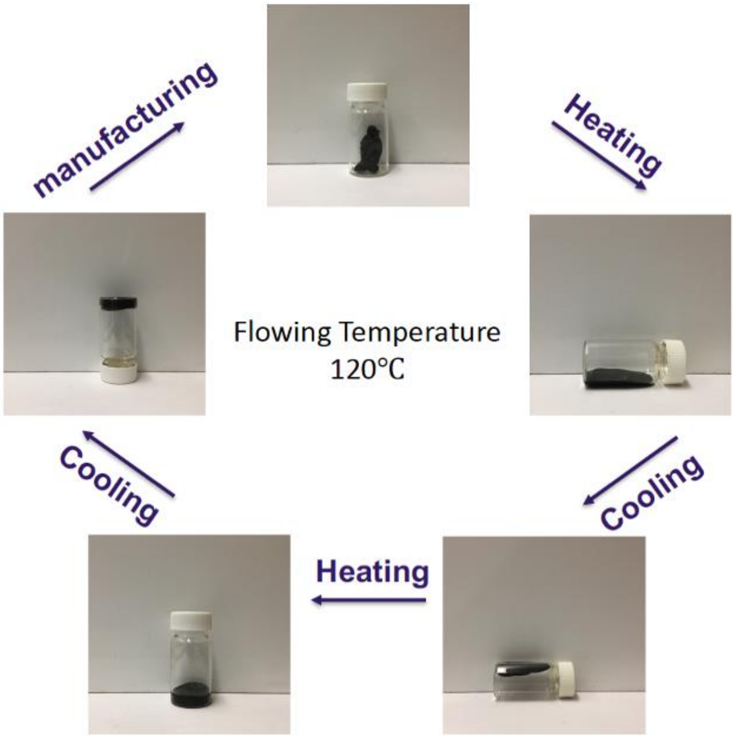

Figure 3-6. The illustration of the recycling cycle of CADH-Epoxy.

Unlike FA-Epoxy based on transesterification, their recycling process requires a hot press or the solvent assistant. The CADH-Epoxy, based on disulfide exchange reaction, can present a flow state under high temperature. Their recycling process shows in Figure 3-6. At room temperature, the CADH-Epoxy piece was in solid-state. When the temperature rose to 120 °C, the CADH-Epoxy sample presented as viscosity liquid. With the temperature cooling back to room temperature, the viscosity liquid solidified again and remained in the shape. This recycling process is repeatable and shows the potential to apply in the 3D printing process.

#### 3.2.1.3 TEMPS-PU Synthesis

Polyurethanes with unique mechanical properties and considerably modifiable network structures are widely used in various applications [135], such as foam products [136], electrical compounds [173], soft tissue [174], and soft robotics [175, 176]. 3D printing polyurethanes, as a new research hotspot recently, were considered as another choice for our recyclable and repairable 3D printing polymer networks [177]. In this part, we present TEMPS-PU synthesis and characterizations. The reason why the Bi-TEMPS-based polyurethane network was first studied is because the low bond dissociation energy of the S-S bond in Bi-TEMPS. The bond dissociation energy of the S-S bond in Bi-TEMPS (26-31 kcal mol$^{-1}$) is about half of that in dialkyldisulfides (60-70 kcal mol$^{-1}$) [178]. Therefore, the thermal dissociation of the Bi-TEMPS is intrinsically more accessible to achieve than dialkyldisulfides.

Before the TEMPS-PU preparation, the Bi-TEMPS-OH was synthesized in three steps from commercially available chemicals (Figure 3-7a). The hydroxyl groups of 4-hydroxy-TEMP were first protected with HMDS. Then this nitroxide mediated radical reacted with $S_2Cl_2$ to gain the Bi-TEMPS-OTMS [179]. Finally, the resulted Bi-TEMPS-OH was collected after washing the Bi-TEMPS-OTMS in MeOH and $K_2CO_3$ to deprotect hydroxyl groups [180]. The as-prepared Bi-TEMPS-OH was employed as a functional component in polyurethane networks. As shown in Figure 3-7b, the bis-isocyanate-terminated prepolymer was first synthesized from one equivalent of PTMEG with two equivalent IPDI, using DBTDL as the catalyst. Then, the Bi-TEMPS-OH was reacted with the prepolymer to obtain the TEMPS-PU. The photograph of the as-prepared sample is presented in Figure 3-8a with a light-yellow transparent appearance.

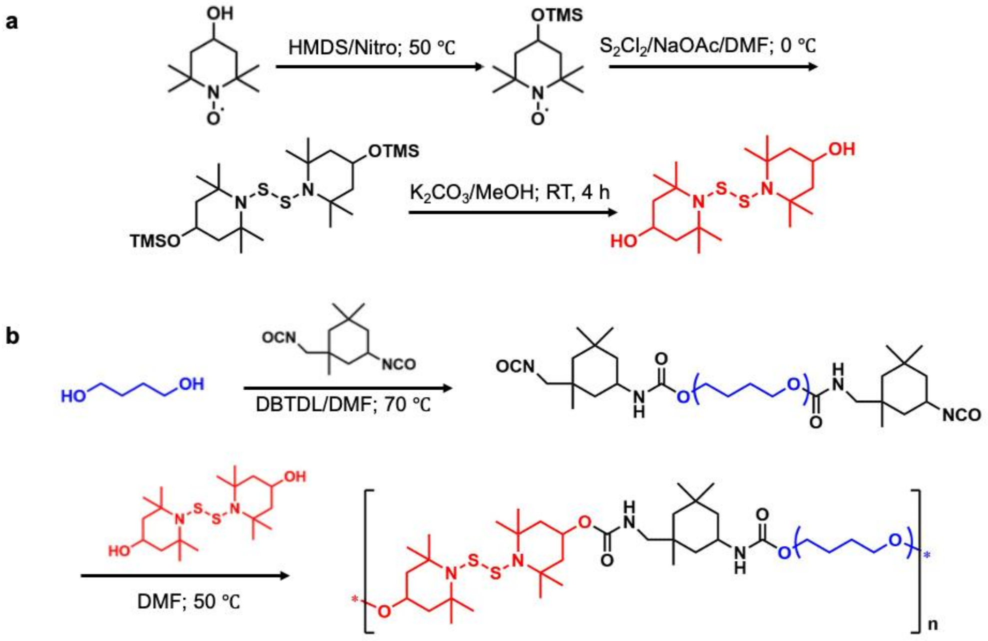
a
OH
HMDS/Nitro; 50 ℃
OTMS
S2Cl2/NaOAc/DMF; 0 ℃
N
O·
TMSO
OTMS
K2CO3/MeOH; RT, 4 h
HO
OH
N
S
S
N
b
HO
OH
OCN
NCO
DBTDL/DMF; 70 ℃
O
H
N
DMF; 50 ℃
n

**Figure 3-7. Synthesised route of (a) Bi-TEMPS-OH and (b) Bi-TEMPS-OH incorporated polyurethane.**

The FTIR spectrums of PTMEG, IPDI and Bi-TEMPS-OH were recorded and compared with that of TEMPS-PU to illustrate the reaction (Figure 3-8b). The peak at 2250 cm$^{-1}$ in the FTIR spectrum of IPDI corresponded to the -NCO groups was absent in the spectrum of TEMPS-PU, which indicated the complete synthesis of the polymer [106]. Moreover, the absorption peak at 3450 cm$^{-1}$ of the PTMEG and broad peak at 3250 cm$^{-1}$ of the Bi-TEMPS-OH, which were the characteristic absorption peak standing for O-H stretching, was replaced by the absorption peak of N-H stretching at 3310 cm$^{-1}$ in the FTIR spectrum of TEMPS-PU [181]. In addition, the peaks at around 1709 cm$^{-1}$ and 1530 cm$^{-1}$, corresponded to the C=O stretching and N-H bending, can also prove the polyurethane synthesized.

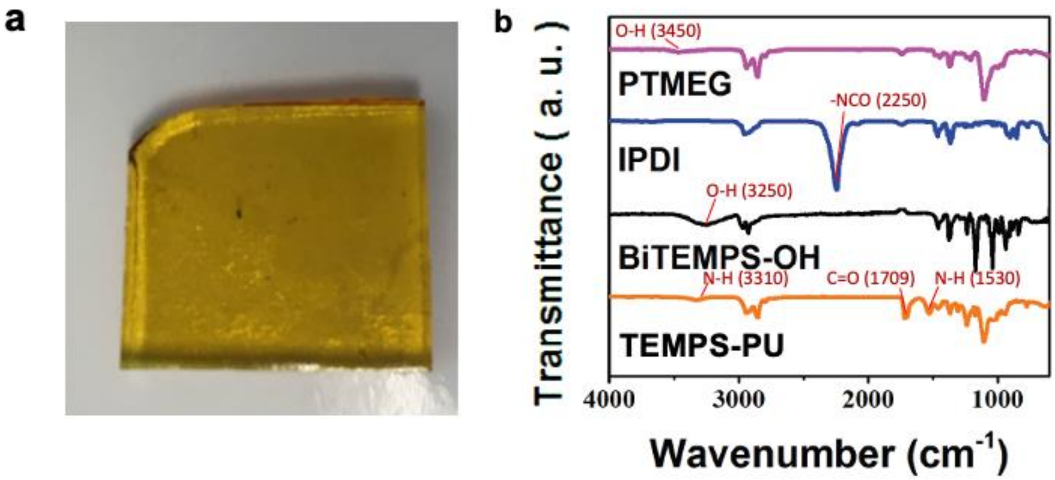

**Figure 3-8. (a) The photograph of the synthesized TEMPS-PU sample. (b) The FTIR spectra of monomers and TEMPS-PU.**

### 3.2.1.4 DTDA-PU Synthesis

In the fourth group of recyclable and repairable material study, aromatic disulfide bonds are introduced to the polyurethane network. Unlike the aliphatic disulfide, which need extra stimulations to trigger the exchange reaction, aromatic disulfide exchange can work under room temperature and catalyst free conditions [135]. Also, the commercially available aromatic disulfide monomers can easily be introduced into various polymer networks [182]. The synthesis route of DTDA-PU is shown in Figure 3-9a. Firstly, PTMEG reacted with IPDI in the presence of DBTDL as the catalyst to obtain a bis-isocyanate-terminated prepolymer. Then, the prepolymer completely reacted with DTDA to acquire the DTDA-

PU polymers. The molar stoichiometric balance between -NCO and total -OH groups was equivalent for all samples, and the molar stoichiometric ratio of DTDA and PTMEG was also one to one in here.

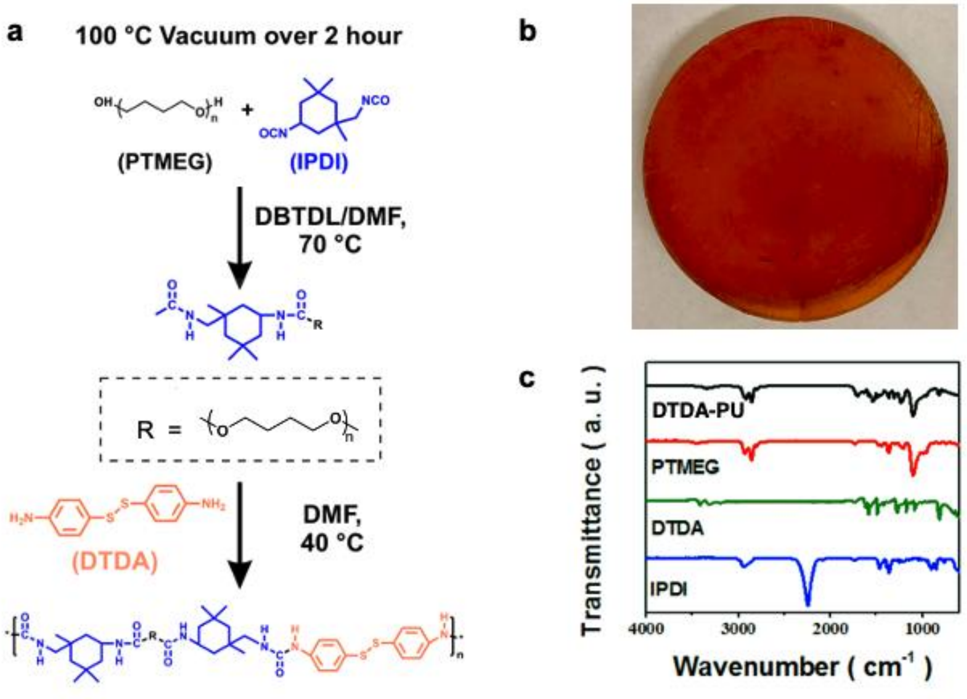
a
100 °C Vacuum over 2 hour
(PTMEG)
(IPDI)
NCO
OCN
DBTDL/DMF, 70 °C
R =
(DTDA)
DMF, 40 °C
b
c
DTDA-PU
PTMEG
DTDA
IPDI
Transmittance ( a. u. )
4000
3000
2000
1000
Wavenumber ( cm$^{-1}$ )

**Figure 3-9. (a) Synthetic scheme for DTDA-PU. (b) Image of the as-prepared DTDA-PU sample. (c) FTIR spectra of PTMEG, DTDA, IPDI and synthesized DTDA-PU.**

The resulting sample was presented as a dark orange transparent elastomer (Figure 3-9b). The complete synthesis of DTDA-PU was confirmed by the corresponding FTIR spectra results, which were shown in Figure 3-9c. The absence of a characteristic peak at around 2270 cm$^{-1}$ indicated that all of -NCO groups were fully reacted [106]. The absorption peak at about 3350 cm$^{-1}$ (O-H stretching) from PTMEG also disappeared, which indicates the complete end-capping reaction of the polymer by -OH groups [123, 183]. The peaks at around 2940 $cm^{-1}$ and 2850 $cm^{-1}$ corresponded to the C-H stretching vibration, and the peak at about 2790 $cm^{-1}$ was attributed to the $O\text{-}CH_2$ stretching vibration. Meanwhile, the characteristic absorption peak of the C=O stretching vibration at around 1670 $cm^{-1}$, and the peaks at around 3320 $cm^{-1}$ and 1533 $cm^{-1}$, which were attributed to the N-H stretching and N-H deformation, commonly indicated the synthesis of polyurethane polymers [181]. Results from FTIR spectrums illustrated the DTDA-PU was fully synthesized.

### 3.2.2 Thermal Properties of FA-Epoxy, CADH-Epoxy, TEMPS-PU and DTDA-PU

The work mechanism of DIW printing technology is extruding material at low viscosity and quick solidifying to set. As we mentioned above, all of the bond exchange reactions of these dynamic covalent polymers are triggered by heat. Therefore, their printing, repairing and recycling processing is highly dependent on their thermal behavior. For the heat-controlled printing and recycling processes, it is crucial to study the temperature-dependent stability, properties transitions and viscoelastic behavior of these materials.

TGA was first carried out to investigate the decomposition process of synthesized materials to survey their thermal stability during heat-controlled printing and recycling processes. Figure 3-10 shows the TGA curves of four samples under a nitrogen atmosphere between 40 and 600 °C. The relative thermal stability data of the materials, including the temperatures at 5% weight loss ($T_{d5}$), the temperature at 10% weight loss ($T_{d10}$), the temperature of the maximum rate of weight loss ($T_{max}$) and final decomposition temperature (FDT), are summarised in Table 3-1.

As shown in Figure 3-10c, there is an ambiguous weight loss that happened after 100 °C for TEMPS-PU. This slightly weight loss may be caused by thermal degradation or the residual solvent evaporation during the heating process. It is also interesting to note that two steps of thermal decomposition were observed in both polyurethane samples in Figure 3-10c and Figure 3-10d. The hard segments of polyurethane are usually more prone to thermal decomposition than soft segments [184, 185]. Both the TEMPS-PU and DTDA-PU used the PTMEG as soft segments structure in their polyurethane networks. Their different hard segments, Bi-TEMPS and DTDA, are the critical factors influence the material initial thermal decomposition. Therefore, the $T_{d5}$ and $T_{d10}$ have noticeable differences for these two polyurethanes while their $T_{max}$ are similar.

**Table 3-1. Thermogravimetric analysis data of synthesized materials.**

| | $T_{d5}$ (°C) | $T_{d10}$ (°C) | $T_{max}$ | FDT |
|---|---|---|---|---|
| FA-Epoxy | 310 | 352 | 435 | 564 |
| CADH-Epoxy | 230 | 272 | 308 | 412 |
| TEMPS-PU | 271 | 286 | 384 | 445 |
| DTDA-PU | 283 | 294 | 386 | 446 |

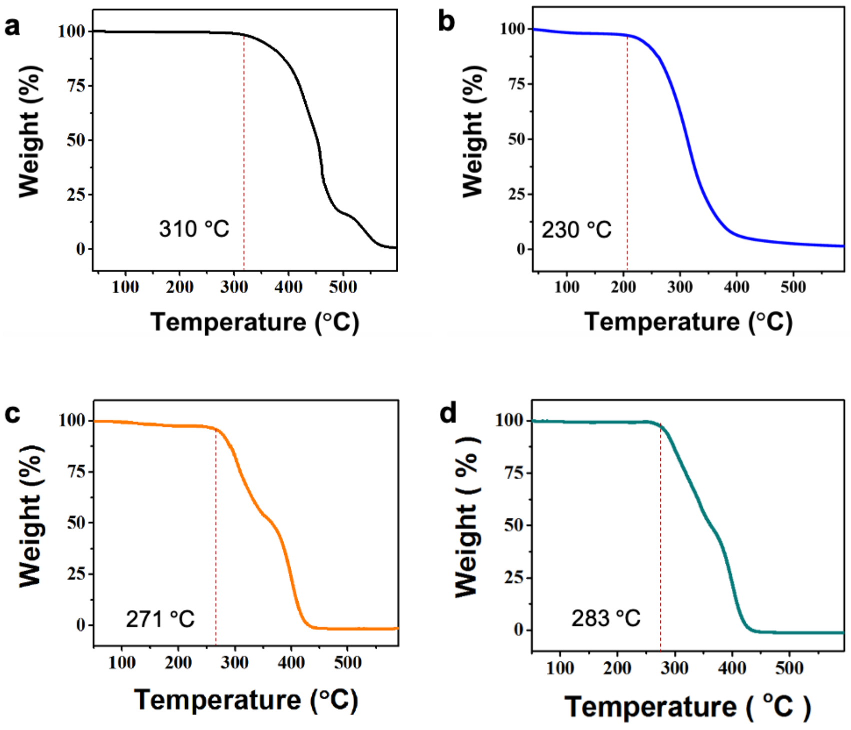

**Figure 3-10. TGA curves of (a) FA-Epoxy, (b) CADH-Epoxy, (c) TEMPS-PU and (d) DTDA-PU. Their temperatures at 5% weight loss ($T_{d5}$) are labelled out in the diagrams.**

The initial decomposition temperature, $T_{d5}$, of FA-Epoxy, CADH-Epoxy, TEMPS-PU and DTDA-PU were around 310 °C, 230 °C, 271 °C and 283 °C, respectively, which are all higher than their dynamic reaction trigger temperature. Comparing all these four materials, FA-Epoxy presents better thermal stability than other materials. This result indicates that this transesterification-based material is more stable than disulfide-based materials. Furthermore, the molecular mass of disulfide monomers from large to small in proper order are: DTDA, Bi-TEMPS-OH and cystamine, which corresponds to their $T_{d5}$ order from low to high. The smaller the molecular mass of the disulfide monomer is, the larger the disulfide bonds percentage in the polymer network is. Therefore, we speculate that although the disulfide bonds in the polymer networks can endow polymers with recyclability and repairability, while their participation may reduce the thermal stability of polymers.

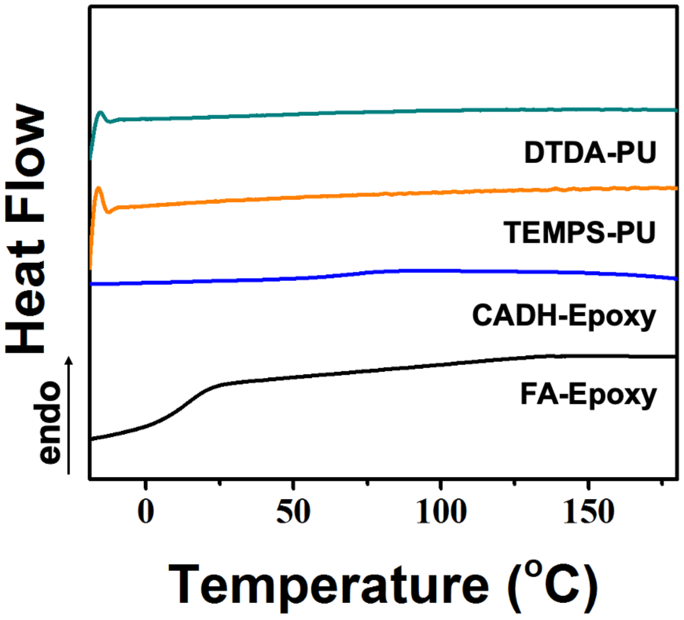

**Figure 3-11. The thermogram of as-prepared samples via differential scanning calorimetry.**

The results of the DSC measurement shown in Figure 3-11 reveal the thermal properties transition of the materials. Based on their TGA results, the DSC measurement temperature range is from -20 to 180 °C. Each sample has run three cycles for heating and cooling to assess stability. We present the third cooling run of four samples in Figure 3-11. Since the glass transition temperatures ($T_g$) stage of TEMPS-PU and DTDA-PU cannot observe in the DSC result from -20 to 180 °C, which may occur due to their low packing density of hard segments [186]. The additional DMA test for these two samples was carried out and presented in Figure 3-12. $T_g$ is a critical feature that relates to the mobility of polymer chains within the polymer structure. The substance transforms from a glassy state to a rubbery state are happened at this temperature. The measuring principles of DSC and DMA are different. DSC measures the heat flows associated with transitions in materials, while DMA measures the modulus and energy dissipation properties of materials [187]. Since the change of the mechanical behavior in DMA results is larger than the change in thermal properties on $T_g$ in DSC results, $T_g$ of TEMPS-PU and DTDA-PU can clearly observe in their DMA results.

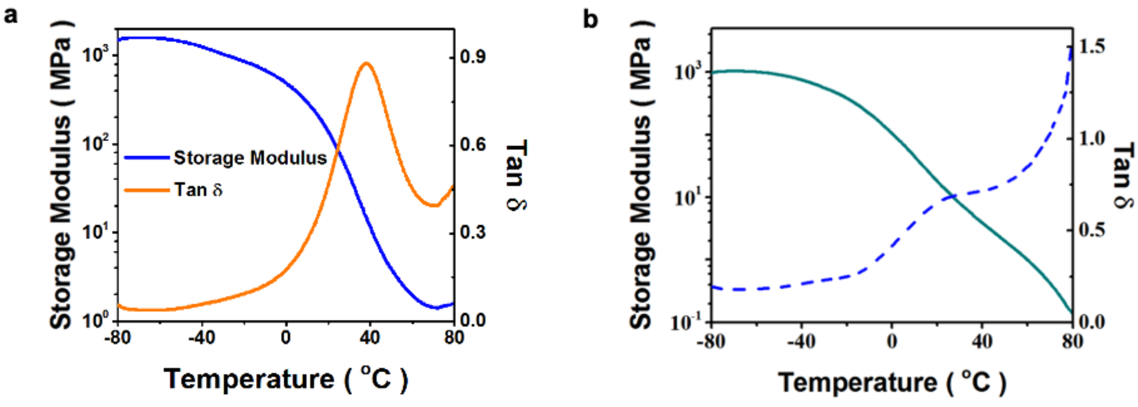

**Figure 3-12. Loss tangent and storage modulus data depending on the temperature of (a) TEMPS-PU and (b) DTDA-PU measured using a dynamic mechanical analysis machine.**

According to their DSC and DMA curves, the $T_g$ of FA-Epoxy, CADH-Epoxy, TEMPS-PU, and DTDA-PU are about 20.5 °C, 70.8 °C, 39.7 °C and 21.5 °C, respectively. In fact, the various test settings of DSC and DMA results in the different thermal histories of samples. Therefore, the comparison between $T_g$ from different methods is not valid [188]. As shown in Figure 3-11, the $T_g$ of CADH-Epoxy from DSC result is higher than room temperature, corresponding to its hard and brittle behavior. On the contrary, the $T_g$ of FA-

Epoxy from DSC result is around the room temperature that matches its relatively ductile behavior than CADH-Epoxy [189]. For the DMA results, the $T_g$ of two polyurethane samples were determined as the peak of loss tangent delta (tan $\delta$) curves and are all around room temperature. The similar storage modulus above $T_g$ indicates the similar cross-link density of these two materials [190]. Furthermore, the absence of any peak in the DSC results from 80 °C to 180 °C revealed amorphous thermoset structures for both four samples [191].

### 3.2.3 Mechanical Properties of FA-Epoxy, CADH-Epoxy, TEMPS-PU and DTDA-PU

The mechanical performance of printing materials will directly affect their practical applications of the printed products. The rigid and hard materials (epoxy) are appropriate for structural 3D printed product fabrication. In contrast, flexible and ductile materials (polyurethane) are suitable to be utilized in functional 3D printed products, such as actuators and wearable devices. Tensile tests were determined at room temperature according to the ASTM D638 standard to evaluate the mechanical properties of synthesized materials. The selected tensile stress-strain curves of each sample are shown in Figure 3-13. The characteristic data of each material are listed in Table 3-2. CADH-Epoxy exhibited the highest Young's modulus. Simultaneously, the ultimate elongation is only about 0.29%, and the ultimate tensile strength is about 0.916 MPa. The brittle behavior of CADH-Epoxy is attributed to the rigid main chain structure of the epoxy network [192]. With the long-chain fatty acid increasing the polymer chain flexibility, the ultimate tensile strength and the ultimate elongation of FA-Epoxy show significant enhancement.

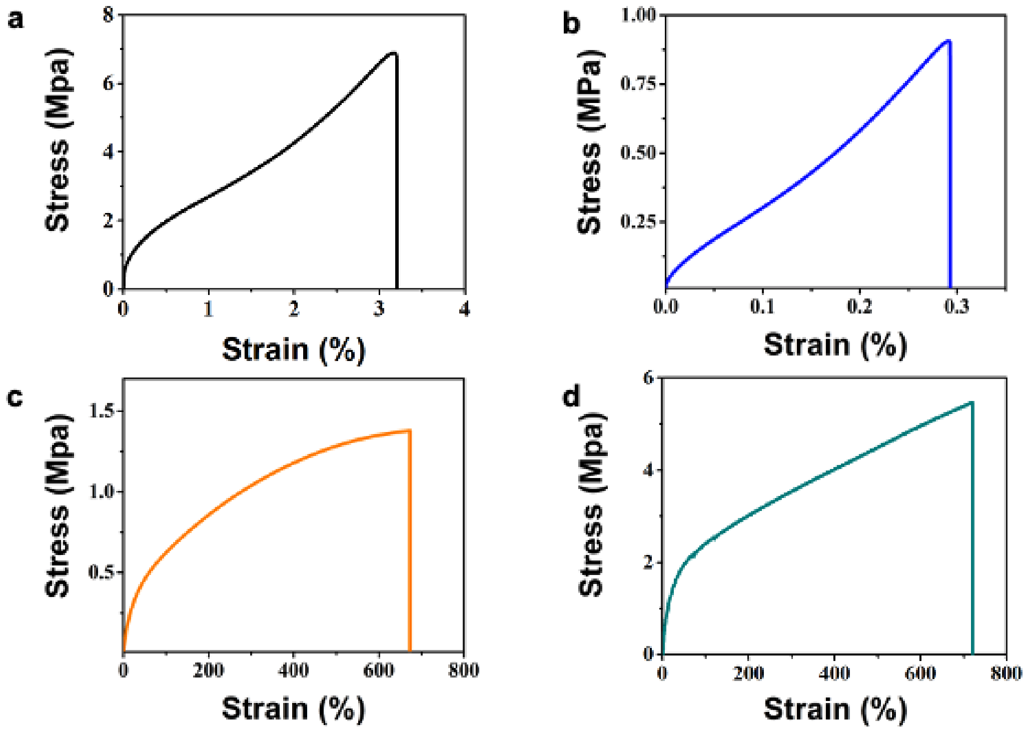

**Figure 3-13. The mechanical properties of synthesized materials. The stress-strain curves of (a) FA-Epoxy, (b) CADH-Epoxy, (c) TEMPS-PU and (d) DTDA-PU.**

For polyurethane materials, both TEMPS-PU and DTDA-PU show high flexibility and acceptable ultimate strength. The elongations of these two polyurethane samples were all over 650%, which can be classified as typical elastomers. Considering the following applications of these materials in 3D printing, polyurethane elastomers with their unique mechanical performance will be more useful in various fields [193]. Although the ultimate strength of DTDA-PU was slightly lower than FA-Epoxy, the critical requirement for FA-Epoxy printing and recycling thwarts its further applications in 3D printing. Therefore, TEMPS-PU and DTDA-PU were chosen for the following 3D printing study.

**Table 3-2. Tensile properties of FA-Epoxy, CADH-Epoxy, TEMPS-PU and DTDA-PU.**

| | Young's Modulus (MPa) | Tensile Strength at Break (MPa) | Elongation at Break (%) |
|---|---|---|---|
| FA-Epoxy | 19.9 ± 0.51 | 6.90 ± 0.37 | 3.21 ± 0.25 |
| CADH-Epoxy | 144 ± 29 | 0.916 ± 0.032 | 0.292 ± 0.031 |
| TEMPS-PU | 2.22 ± 0.16 | 1.38 ± 0.13 | 673 ± 17 |
| DTDA-PU | 6.30 ± 0.53 | 5.52 ± 0.41 | 720 ± 22 |

## 3.3 Summary

Four different kinds of recyclable epoxy and polyurethane based materials were successfully synthesized based on disulfide bonds or transesterification. Two different recycling procedures of FA-Epoxy and CADH-Epoxy are displayed, representing the transesterification reaction and the disulfide exchange reaction. FTIR spectroscopy was used to identify the chemical structure of synthesized polymers. The TGA results show that all materials present good thermal stability. Further thermal properties of epoxies and polyurethanes were investigated by DSC and DMA results, respectively.

Tensile tests of four synthesized materials were carried out to evaluate their mechanical properties. The stress-strain curves of FA-Epoxy and CADH-Epoxy are following the classical epoxy behavior. The FA-Epoxy with long-chain fatty acid as the crosslinker presents higher strength than the CADH-Epoxy with short-chain cystamine as the crosslinker. Conversely, TEMPS-PU and DTDA-PU perform like elastomers with good flexibility and considerable ultimate strength.

The critical recycling requirements of FA-Epoxy include solvent evaporation and high operation temperature. Therefore, the special processes and printer modifications are demanded for their 3D printing processes. For CADH-Epoxy, TEMPS-PU and DTDA-PU, their mild flowing conditions are more feasible for our existing printing process and more suitable for further popularization. For CADH-Epoxy, its high rigid mechanical performance is more applicable for some micro-scale structural 3D printing products, which may not be compatible with DIW printing technology. TEMPS-PU and DTDA-PU with their flexible and ductile properties can be widely used in various functional 3D printing applications, such as wearable devices, actuators and components on vehicle. Therefore, the follow-up study about recycling 3D printing will choose TEMPS-PU and DTDA-PU as the printing materials. The printability and recyclability of these two polyurethanes will be studied in the next chapter.

# Chapter 4

## 4 Recyclable 3D Printing of Polyurethanes based on Heterocyclic Disulfide Bonds and Aromatic Disulfide Bonds

This chapter steps further to investigate the printability and recyclability of previous synthesized materials, TEMPS-PU and DTDA-PU. Although their printing and recycling feasibility have been proved in the last chapter, their practical processing parameters still need to be evaluated according to the relationship between viscosity and temperature. Therefore, the investigations of their temperature-dependence rheology behavior were carried out. Based on these preliminary experiment results, both materials have been successfully printed according to the CAD models. Furthermore, each of the printed sample has been reprinted three times to evaluate the performance stability of these two materials during recycling. The optical images of their reprinted parts can intuitively perform the stability of materials after multiple rounds of recycling. The tensile tests of reprinted samples were also carried out to evaluate their recyclability. From these results, we can see that DTDA-PU presents reliable printability and recyclability compared to TEMPS-PU, which can be utilized as our recyclable 3D printing material for the following development of sustainable 3D printing strategy.

## 4.1 Introduction

As an important class of polymers, elastomers have been ubiquitously applied in many fields such as wearable devices, healthcare, vehicles and aerospace. However, the development of 3D printing elastomers remains an ongoing challenge due to their inherent rheological properties [193]. For the 3D printing of traditional thermoplastic elastomer, additional pre-curing processing or support baths are often indispensable [194, 195]. In an effort to overcome this challenge, we are looking forward to a recyclable and repairable 3D printing strategy that bases on the combination with the high customization of DIW technique and the reversible disulfide bonds of synthesized polyurethanes. The process of DIW 3D printing schematically shows in Figure 4-1 to illustrate the concept of this sustainable 3D printing elastomer strategy.

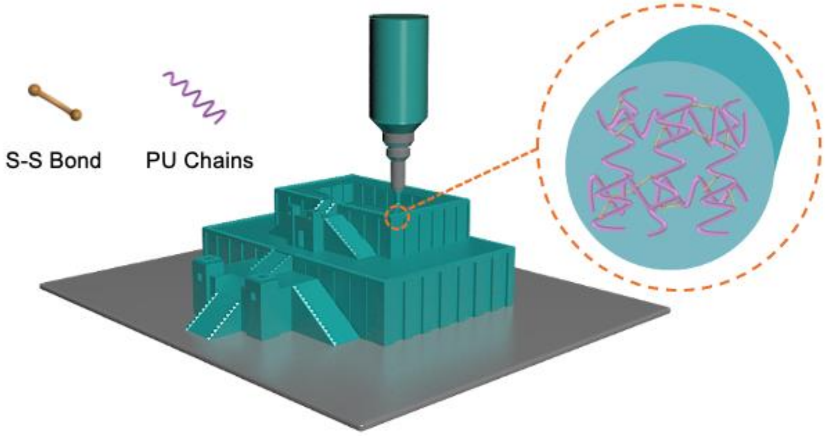

**Figure 4-1. Schema of polymer printing via a DIW extrusion printer.**

DIW 3D printing technology has been widely applied in various applications, such as electronics [196], biomedicine [197], artificial organs and tissue [198], and soft robotics [199]. Although DIW offers a significant cost advantage due to its designability and flexibility, it has high demands on the printing materials properties [152]. For standard DIW printing processes, the viscoelastic inks are formed into fibers by extrusion from nozzles under external pressure and deposited into patterns via the prescribed motion of nozzles [200]. Different designs of ink compositions leads to different solidification approaches, such as traditional thermoplastic melting, solvent evaporation [149], gelation [201], and photopolymerization [202]. For the rheological behavior of printing inks, we are looking forward to low viscosity during extrusion and rapidly increased viscosity after extrusion to solidify and resist deformation [203]. The printing parameters are also essential, since it is usually constant during the whole printing process. The nozzle's diameter, layer height, print density, and print speed are all adopted through trials and errors, and closely related to the final printing resolution [204]. Therefore, the ink compositions, rheological behavior, and printing parameters need to be carefully controlled to achieve the ink smooth extrusion and instant solidification.

As mentioned in Chapter 3, two disulfide polyurethanes were synthesized as DIW inks based on the utility of different disulfide functional monomers. The temperature-induced dynamic covalent reaction contributed to the printability of materials. Consequently, the temperature dependence of viscosity for TEMPS-PU and DTDA-PU were studied to evaluate their printability preliminarily. Their estimated printing parameters were confirmed and adjusted on the basis of the following practice printing experiments. Moreover, the recyclability of printing inks is also demonstrated in this chapter. The photographs of printed and recycled samples are shown, and the mechanical performance of recycled materials is also investigated to do a comparative study. Both TEMPS-PU and DTDA-PU can be recycled for three successive cycles. The recycled DTDA-PU exhibits more stable printing performance and consistent mechanical properties compared with TEMPS-PU. The direct ink writing of dynamic covalent polymers in this study paves a new way to highly customized and simple method for 3D printing waste recycling. Further research about printing material enhancement and printing technology improvement can be looking forward to a universal solution for sustainable 3D printing development.

## 4.2 Result and Discussion

### 4.2.1 Rheological Behavior of TEMPS-PU and DTDA-PU

Before the 3D printing of as-synthesized materials, the preliminary experiment about the rheological behavior of TEMPS-PU and DTDA-PU was carried out (Figure 4-2 and Figure 4-3). Disulfide bond exchange reaction is highly time- and temperature-dependent [205]. In order to control the variable, the temperature-dependent rheological behavior of two materials was measured under the same temperature rate to simulate their actual behavior during the heating and cool-down process. Since the low bond energy of both aromatic disulfide bonds and heterocyclic disulfide bonds, their bond metathesis starts at mild temperature and accelerates with temperature elevation. Therefore, unlike the Diels-Alder or other common dynamic covalent bond-based materials that have significant viscosity dropping at specific bond open temperature, the viscosity of disulfide-based polyurethanes gradually decreases with the increasing of the temperature.

As shown in Figure 4-2, the viscosity of TEMPS-PU and DTDA-PU at 120 °C was initially 189 Pa·s and 114 Pa·s, respectively. As temperature rise, the viscosity of TEMPS-PU and

DTDA-PU at 150 °C gradually dropped to 31.7 Pa·s and 20.1 Pa·s. The similar polymer structures of these two disulfide-based polyurethanes lead to similar rheological behavior in the heating process. Different structures of disulfide-based hard segments may influence the rigidity and mobility of the polyurethane backbone and cause a slight difference in their viscosity under the same condition [206]. For most commercial 3D printing materials, their viscosities under extrusion conditions usually vary from 102 to 105 Pa·s [146]. Accordingly, the extrusion temperature of TEMPS-PU and DTDA-PU for the subsequent printing test will be set as 129 °C and 122 °C, respectively.

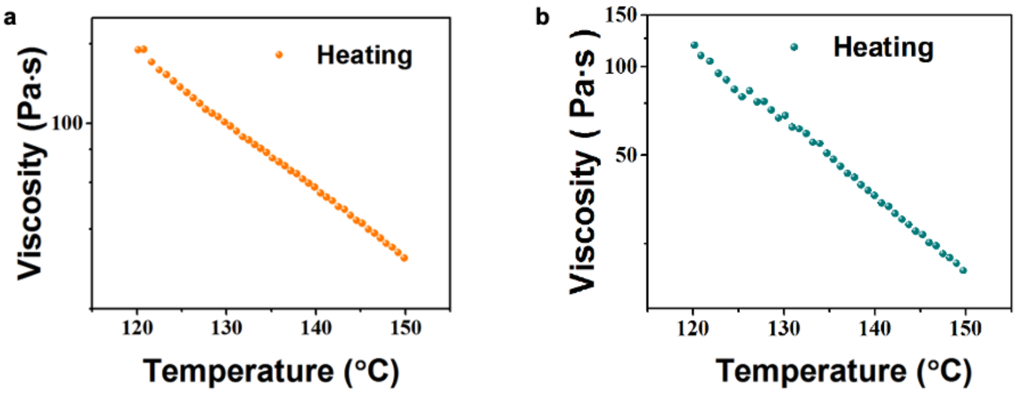

**Figure 4-2. Temperature-dependent viscosity curves of (a) TEMPS-PU and (b) DTDA-PU with a fixed share rate (share rate=1 $s^{-1}$) in heating process from 120 to 150 °C.**

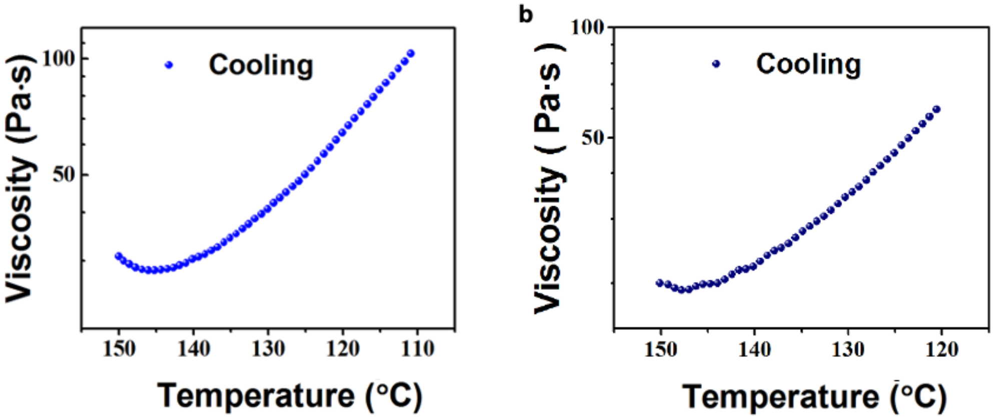

**Figure 4-3. Temperature-dependent viscosity curves of (a) TEMPS-PU and (b) DTDA-PU with a fixed share rate (share rate=1 s$^{-1}$) in cooling process from 150 to 120 °C.**

Their rheological behavior during the cooling process was also investigated to assess their solidification performance after extrusion. An apparent viscosity increasing with hysteresis presents in both TEMPS-PU and DTDA-PU results in Figure 4-3. For TEMPS-PU, the viscosity kept falling until the temperature drops to 145 °C. Then, with the temperature drop to 110 °C, the viscosity increased from 27.8 Pa·s to 102 Pa·s. For DTDA-PU, the viscosity continued dropping ended at 148 °C. When the temperature descends to 110 °C, the viscosity increased from 19.3 Pa·s to 63.1 Pa·s. Disulfide metathesis begins to decelerate once the temperature decreases; therefore, the disulfide polyurethanes trends to increase viscosity. The hysteresis of their rheological performance is due to the time needed for disconnected network reconstructing during metathesis [122]. Rapid viscosity rising during the cooling process is suitable for quick solidification of ink and high accuracy and resolution of the printed products. Still, it may also cause the layer separation problem during printing [193, 203]. The appropriate hysteresis may contribute to the interlayer adhesion and surface finishing in the subsequent printing test. Also, the additional gas cooling system for the printing bed and the printing speed adjustment may require preventing ink overflow and allowing solidification of printed samples.

### 4.2.2 3D Printability of TEMPS-PU and DTDA-PU

After confirming the rheological behavior of TEMPS-PU and DTDA-PU, they were employed as inks for DIW 3D printing. The extrusion nozzle diameter and print layer height are the crucial factors in the spatial resolution of the printed parts. Therefore, the preprinting test with different extrusion nozzles was first carried out and presented in Figure 4-4. When material viscosity around 105 Pa·s, it can be extruded continuously and smoothly via nozzles with an inner diameter of 1.55mm to 0.60 mm. The width and height of printed lines are basically consistent with the diameters of nozzles. The detailed printing parameters of TEMPS-PU and DTDA-PU during actual printing processes are listed in Table 4-1. Based on the above rheological behavior and practical printing performance, the printing speed of TEMPS-PU was higher than DTDA-PU, and an additional cooling fan on the printing bed was applied to prevent ink overflow.

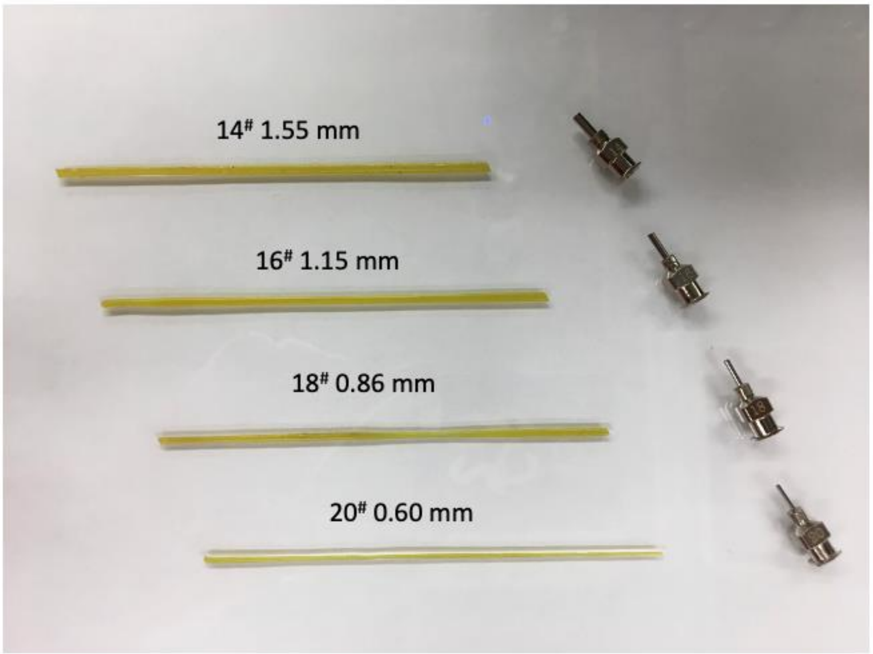

**Figure 4-4. The ink filaments extruded from the DIW printer with different nozzle diameters. The ink filament diameters are approximately equal to the nozzle size.**

**Table 4-1. Printing parameters of DIW 3D printing processes for TEMPS-PU and DTDA-PU.**

| Printing Materials | Printing Temperature (°C) | Printing Speed (mm/s) | Extrusion nozzle diameter (μm) | Cooling system for Printing bed |
|---|---|---|---|---|
| TEMPS-PU | 129 | 3 | 600 | Yes |
| DTDA-PU | 122 | 2 | 600 | No |

As shown in Figure 4-5, we have successfully printed TEMPS-PU and DTDA-PU in various structures. The printing resolution of printed parts is affected by many complex factors, such as the printer nozzle size, the precision of the 3D printer, and the inherent properties of the polymer. Comparing the printed samples from two materials, the models printed from DTDA-PU show higher printing resolution. The details of printed structures like the convex shape of the Arc de Triomphe demos and the eaves of Tiantan are accurate, corresponding to their CAD models (Appendix A). In contrast to that, the TEMPS-PU printed parts feature a superior surface finish. At the same time, the structural details in CAD models, such as the terraces of Eiffel tower demos, did not reflect in the printed result. It is interesting to note that the color of TEMPS-PU printed sample looks darker than the as-synthesized TEMPS-PU sample in Figure 3-4. This phenomenon may be due to the thermal degradation, as shown in the TGA result in Figure 3-10. TEMPS-PU radical oxidization may also happen under the sustained high temperature during printing processes [207]. According to this speculation, the recycling performance of TEMPS-PU may also be affected.

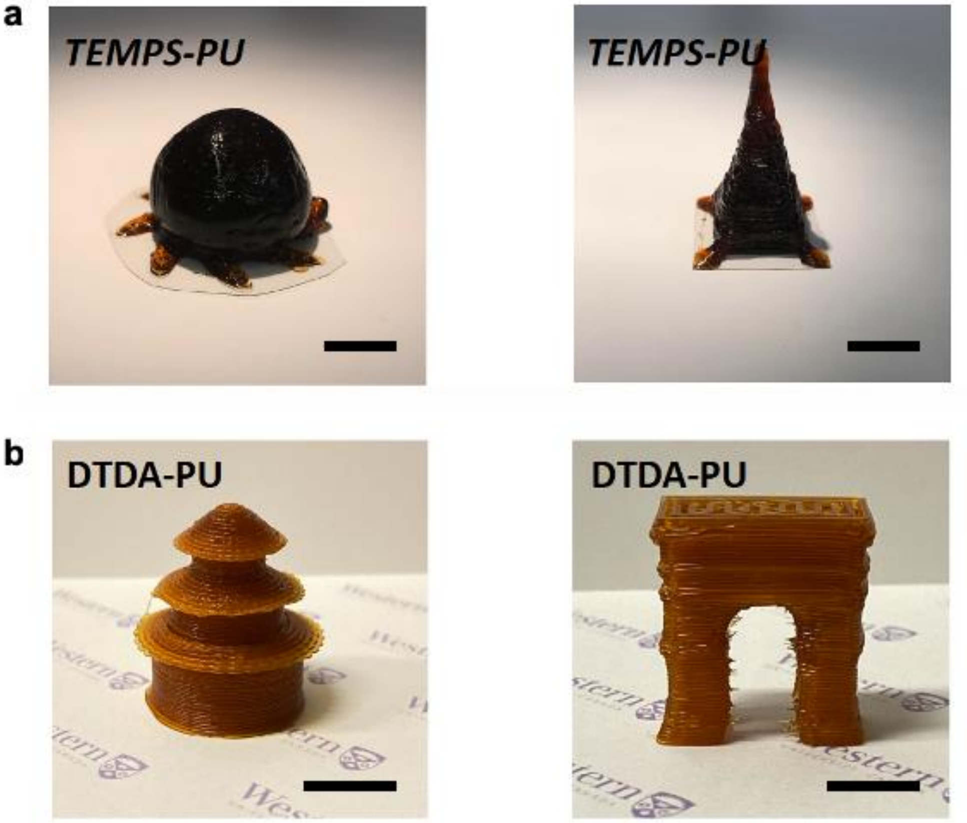

**Figure 4-5. (a) Photographs of 3D printed octopus and Eiffel tower demos from TEMPS-PU. Scale bars: 10 mm. (b) Photographs of 3D printed Tiantan and the Arc de Triomphe demos from DTDA-PU. Scale bars: 10 mm.**

### 4.2.3 Recyclability of TEMPS-PU and DTDA-PU

The recycling of 3D printed parts is our fundamental strategy to reduce the amount of polymer waste and achieve the sustainable development of 3D printing. Our goal is to provide a highly customized and simple recycling approach for 3D printing waste. This recycling approach is built on the existing DIW 3D printing technology and our reversible disulfide polyurethane. In the recycling procedure, as shown in Figure 4-6, the printed parts or printing waste only need to be crushed into small pieces and reloaded into the syringe of DIW printer. These crushed particles following pre-melting and removing residual air bubbles can then be employed as ink to form new parts. This easy and fully re-printable recycling process can be achieved with no need for additional additives or reagents.

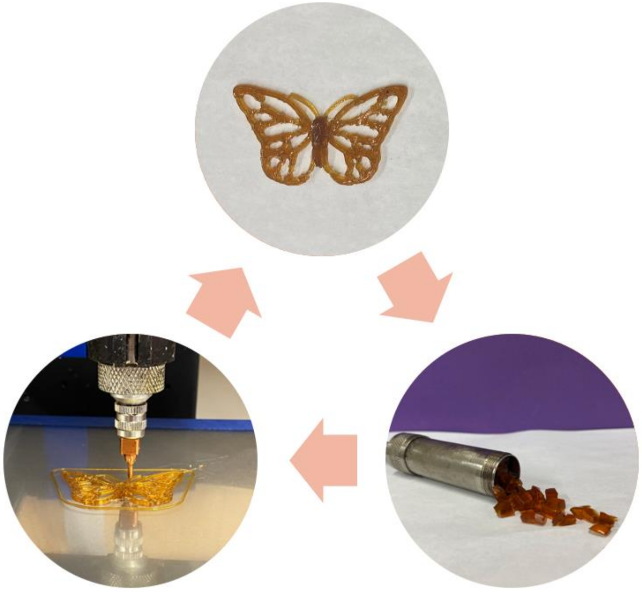

**Figure 4-6. An illustration of the reprinting process of disulfide-based 3D printing materials.**

Both TEMPS-PU and DTDA-PU were circularly printed in a variety of new models, as shown in Figure 4-7. 2D architectures with complex structures were selected to directly review the printing accuracy and avoid ink oxidation due to the long time heating in the printer syringe. Compared with TEMPS-PU, DTDA-PU printed samples show better cycling stability. In the first printing cycle, both the printed character Fu from TEMPS-PU and DTDA-PU shows clear and detailed structures. The printed butterfly from TEMPS-PU in the second cycle also presents the accuracy pattern of wings, while the sample colour is slightly darker than before.

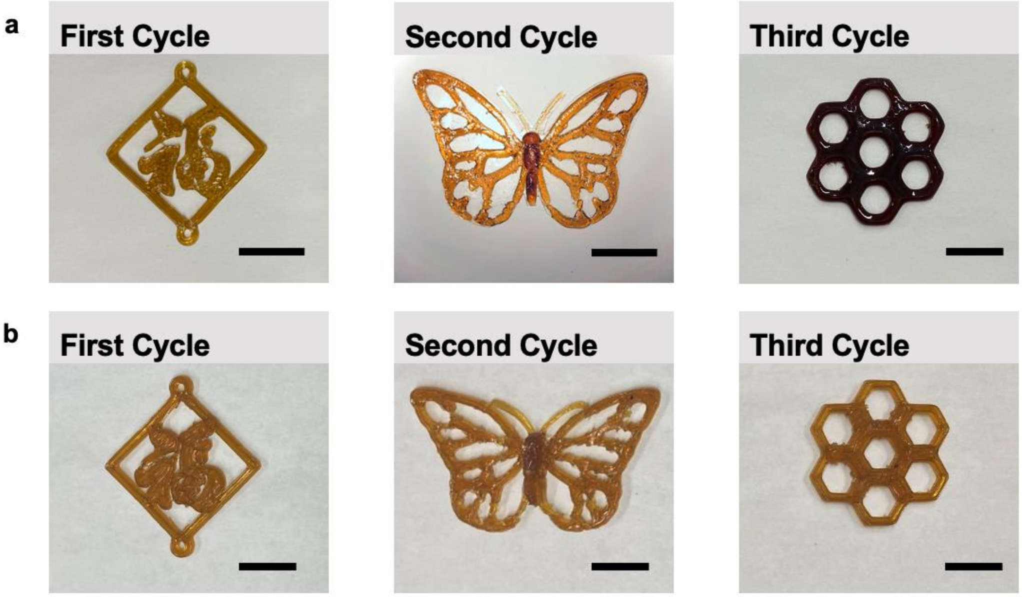

**Figure 4-7. Photographs showing the re-printability of TEMPS-PU and DTDA-PU. (a) Three cycles of printed parts from TEMPS-PU. Scale bars: 10 mm. (b) Three cycles of printed parts from DTDA-PU. Scale bars: 10 mm.**

However, in the third cycle, the printed results of the two materials are obviously different. The appearance of printed honeycomb demo from DTDA-PU is constant with the first cycle printed product. In contrast, the third cycle printed demo from TEMPS-PU is turning to reddish-brown color, and the individually printed layers are less prominent. Although the high interlayer adhesion may enhance the mechanical properties of printed samples, the color change also reveals the chemical properties change of TEMPS-PU. Therefore, the recyclability of these two materials needs to be analyzed in combination with the tensile testing results of their recycling samples.

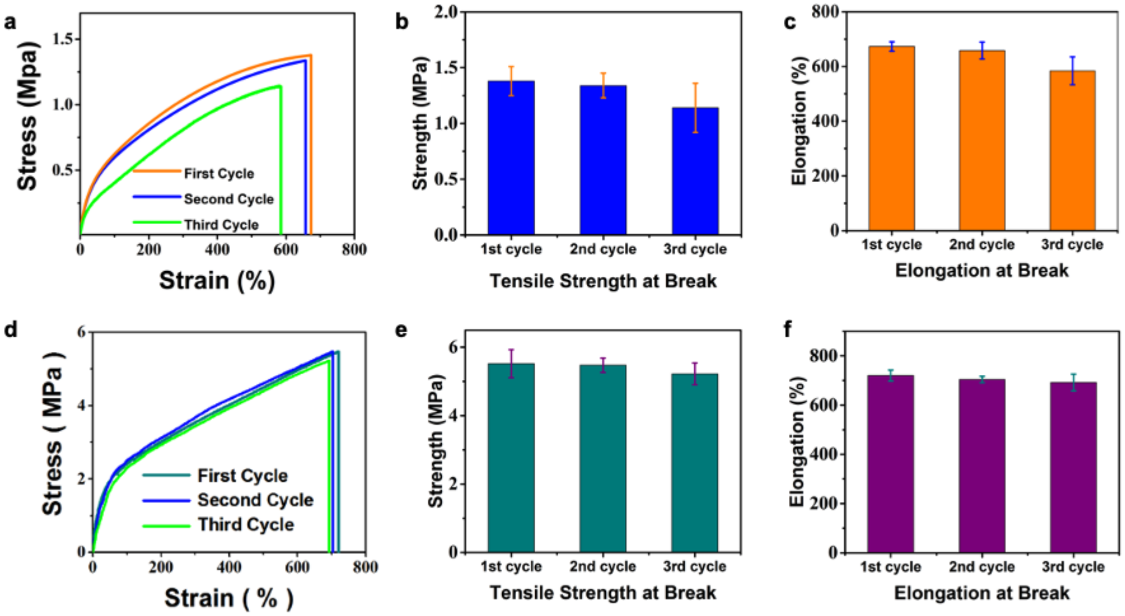

**Figure 4-8. The experiment results of uniaxial tensile tests for multiple times recycled. (a) Typical stress-strain curves for TEMPS-PU samples of three recycled cycles, and their corresponding values of (b) tensile strength at break and (c) elongation at break. (d) Typical stress-strain curves for DTDA-PU, and their corresponding values of their (e) tensile strength at break and (f) elongation at break.**

Tensile tests were carried out at room temperature to investigate the mechanical performance of TEMPS-PU and DTDA-PU in three recycling cycles. Their stress-strain curves and experimental results are shown in Figure 4-8. Although for the first and second cycles recycled samples, their mechanical performance has no obvious degeneration. In the third recycled cycle, the ultimate tensile strength of TEMPS-PU sample is significantly reduced from ~1.38 MPa to ~1.14 MPa. Also, the elongation at break was deceased from ~673% to ~584%. On the other hand, the stress-strain curves of DTDA-PU recycled samples are almost reduplicated with slight differences in the maximum elongation. This result illustrated the constant mechanical properties of DTDA-PU before and after recycling. All the above results together indicate that DTDA-PU possesses excellent printability and stable recyclability compared with TEMPS-PU. Therefore, we selected DTDA-PU as the study candidate for the following research of sustainable 3D printing development.

## 4.3 Summary

In this chapter, based on the previous material analysis, TEMPS-PU and DTDA-PU have been chosen to investigate their printability and recyclability. In the preliminary experiment, we studied the rheological behavior of these two materials in heating and cooling processes to predict their printing performance. At an elevated temperature, we observed that the viscosities of both materials significantly decreased, which allows the fluent extrusion process during printing. Meanwhile, their viscosities were able to rise again with temperature drop to ensure the solidification of printed part. According to the rheology test results, the extrusion temperatures of TEMPS-PU and DTDA-PU printing are set at 129 °C and 122 °C, respectively.

The practical printing tests were carried out to evaluate the material printability. The printed demos from DTDA-PU presents better resolution and stability than that of TEMPS-

PU. The following recycled printing results also confirm our suspicions that prolonged heating of the printer syringe during printing will cause TEMPS-PU oxidation. This behavior further affected the printing performance and mechanical properties of TEMPS-PU. Their tensile test results for multiple times recycled indicates that DTDA-PU presents consistent material properties while the performance degradation happens on TEMPS-PU. In view of the above results and discussions, DTDA-PU offers excellent printability and stable recyclability, and therefore, will be employed as the material for our sustainable 3D printing strategy study. Although TEMPS-PU is unadoptable to the current DIW 3D printer due to the continuous heating applied on the material during printing, it could be fabricated by other 3D printing technology with proper adjustments. For example, the FDM printing technology only applies heat to the extrusion nozzle area that may avoid material oxidization and degeneration due to overheated. We will discuss printing material modification and enhancement in the following chapters.

# Chapter 5

## 5 Recyclable 3D Printing of MWCNTs-OH Reinforced Polyurethane Composites Based on Dynamic Disulfide Bonds

The applications of 3D printed pure polymer parts are intrinsically limited by their mechanical properties and functionalities compared with metal or ceramic 3D printing. It is an effective method to enhance the performance of 3D printed polymer parts by developing their printable composites. The super high strength and large aspect ratio of carbon nanotubes (CNT) make it a strong reinforcement additive candidate for composites. In this chapter, we discuss the properties and printability of reinforced DTDA-PU with various multi-walled carbon nanotubes (MWCNTs) concentrations. A comprehensive investigation was carried out based on their thermal stability, solvent resistance, mechanical properties, rheological behavior and the practical printing tests. From the results, we can see the maximum strength of composites and their stability has significantly improved, while their printability may also be affected. After comparison, 2 wt% DTDA-PU/MWCNTs-OH presents good printability and better mechanical performance than others and can be utilized as the printing material for our study.

## 5.1 Introduction

Polymer materials have superiority over metal and ceramic in the lightweight, corrosion-resistance, flexibility and cost efficiency [208]. Combining the advantages of polymers with the rapid prototyping, 3D printing polymers has been used far and wide throughout the research, medical, art and education fields. Although the 3D printed polymer products are widely applied in conceptual prototypes, their utilization in industrial applications is limited due to their uncompetitive strength behavior as load-bearing functional components [209]. 3D printing of polymer composites provides a way to solve this problem. Polymer composite, also known as polymer matrix composite, is a composite material that employs the polymer matrix to integrally bind the reinforcement together. The matrix provides the shape, surface appearance, environmental tolerance and overall durability to the composite, while the reinforcement plays a major role in carrying most of the structural loads [210]. Therefore, 3D printed polymer composite products can effectively combine the advantages of polymer and reinforcement and perform relevantly higher macroscopic stiffness and strength compared with 3D printed pure polymer products [209].

As the primary load-bearing constituent, the reinforcement is crucial and determines the macroscopic performance of the composite. Carbon nanotube (CNT) is a comparatively common selection in polymer matrix composites. If we talk about the most exciting new materials in the last 30 years, CNT must be one of them. Sumio Iijma first observed the tubular carbon structures via high-resolution transmission electron microscopy and published this work in Nature in 1991 [211]. As one of the ultra-strong and extreme small-sized materials in the world, CNT is one of the ideal reinforcements to enhance lightweight and soft materials [212]. In 1999, a systematic study of the mechanical properties of CNT/PVA was published by Shaffer and Windle [213]. This pioneering work has opened the door to the research on the mechanical enhancement of CNT-related polymer composites and led to the explosion of interest in CNT composites. By taking advantage of these mature research results, we introduced the multi-walled carbon nanotubes (MWCNTs) to our previously studied DTDA-PU to improve the performance of printed products and expand the applications.

In this chapter, we demonstrated the synthesis and characterization of DTDA-PU/MWCNTs-OH composites. Hydroxy functionalized MWCNTs have chosen to achieve well dispersion in polyurethane matrix via -OH participating in the reaction with -NCO groups. Due to the incorporation of MWCNTs-OH involved in the synthesis reaction, the polymer chains entanglement and crosslinking degree of DTDA-PU composites should be affected. Therefore, we studied the thermal and mechanical performance, solvent resistance behavior and rheological behavior of DTDA-PU composites. After these comprehensive studies, the 2 wt% DTDA-PU/MWCNTs-OH presented a significant improvement in mechanical performance, and desirable printability was chosen as the recyclable printing material. The recycling printed samples showed high resolution and high consistency, which proved their feasibility of utilization in sustainable 3D printing.

## 5.2 Result and Discussion

### 5.2.1 DTDA-PU/MWCNTs-OH Composite Synthesis

The physical properties of printing material directly affect their printability and the practical applications of their 3D printed products. DTDA-PU has been chosen as the printing material for our sustainable 3D printing strategy study. However, comparing with the commercial elastomeric polyurethane-based 3D printing materials (tensile strength range from 2.4 to 11 MPa) [214], the mechanical properties of DTDA-PU do not show obvious advantages. Therefore, we introduced MWCNTs into the DTDA-PU network to improve the mechanical performance and printability of the printing materials.

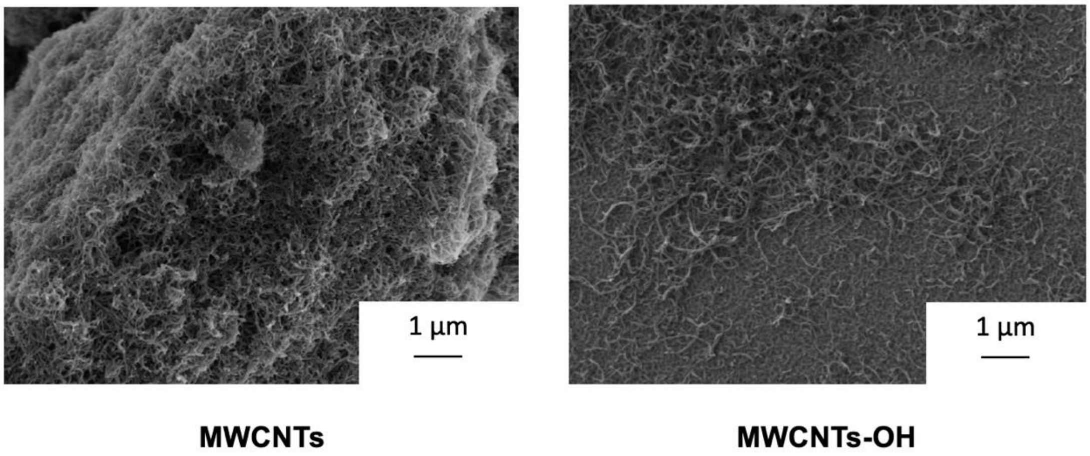

**Figure 5-1. SEM images of the distribution of MWCNTs without (left) and with (right) hydroxy functionalization in DMF (imaged after drying). Scale bars: 1 µm.**

The uniform distribution of MWCNTs in the DTDA-PU matrix is a prerequisite for stable and consistent performance of their mechanical properties, rheological properties and photothermal behavior [209]. However, MWCNTs easily form aggregates and can be unevenly distributed due to the influence of Van der Waals forces and π-π electron interactions [215, 216]. MWCNTs-OH were used in this work to address the aggregation issue. Figure 5-1 shows the initial MWCNTs and hydroxy functionalized MWCNTs distribution in the solvent. These two types of MWCNTs were all mixed in DMF and thinly coated on silicon wafers. After drying in a vacuum oven to evaporate the solvent, samples were observed via SEM. The MWCNTs-OH sample showed excellent dispersibility in DMF and avoided aggregation. Therefore, MWCNTs-OH can mix well during the sample synthesis process.

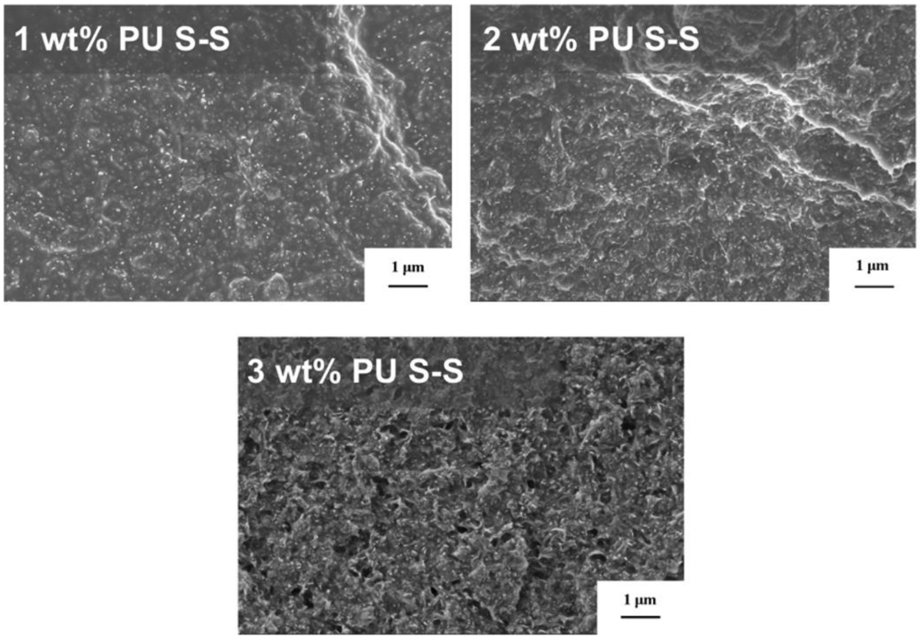

**Figure 5-2. SEM images of DTDA-PU composites with different contents of MWCNTs-OH. Scale bars: 1 μm.**

Besides, the -OH groups over the surface of MWCNTs-OH also can react with -NCO groups of IPDI during the synthesis to achieve MWCNTs-OH uniformly distributed in the DTDA-PU matrix [217]. In order to verify this, SEM was used to observe the MWCNTs distribution on fracture surfaces of DTDA-PU/MWCNTs-OH. The fracture surfaces of the DTDA-PU/MWCNTs-OH composites with 1 wt%, 2 wt% and 3 wt% MWCNTs are shown in Figure 5-2. The MWCNTs appear the uniformly distribution in the matrix of DTDA-PU, and no aggregation is observed. Some MWCNTs were pulled out of the fracture surface of all the DTDA-PU/MWCNTs-OH samples, but the amount was small compared to the number embedded in the matrix. This outcome suggests an interfacial adhesion between the MWCNTs-OH and DTDA-PU matrix [218, 219]. These results reveal that chemical interactions between MWCNTs-OH and DTDA-PU matrix contributed to the even distribution of MWCNTs within the matrix.

### 5.2.2 Physical Properties of DTDA-PU/MWCNTs-OH Composites

Since the MWCNTs-OH was participating in the reaction with IPDI, the cross-link density of synthetic composites should be affected. The Van de Waals and the π-π reaction of MWCNTs-OH in the composites should also impact the polymer chain entanglement [220]. These factors will certainly bring changes in the thermal performance, mechanical properties and rheology behavior of composites compared to pure DTDA-PU. Therefore, before we apply the composites as the DIW printing material, the relative physical properties of DTDA-PU/MWCNTs-OH composites were investigated.

TGA was carried out to study the effect of MWCNTs-OH incorporation on the thermal stability of the DTDA-PU composites. Figure 5-4 presents the TGA curves of pure DTDA-PU and its composites. It can be seen that all samples experience a two-step degradation as a traditional two-step polyurethane decomposition process. The $T_{d5}$ of all samples is around

283 °C, since it mainly decides by the decomposition process of hard segments [184]. The second step decomposition result of composites shows a gradient variation, as shown in the inset of Figure 5-4, which is associated with the degradation of soft segments. The lower weight loss of the composites with high MWCNTs content indicates the higher thermal stability [221]. We also noticed that pure DTDA-PU has no residue left at 500 °C, while charred residue was observed in composites. The char residue amount increased with MWCNTs-OH contents increase, which may be caused by the limited recombination between reactive degrading species and impurity of MWCNTs to a thermally stable charred material during decomposition [222].

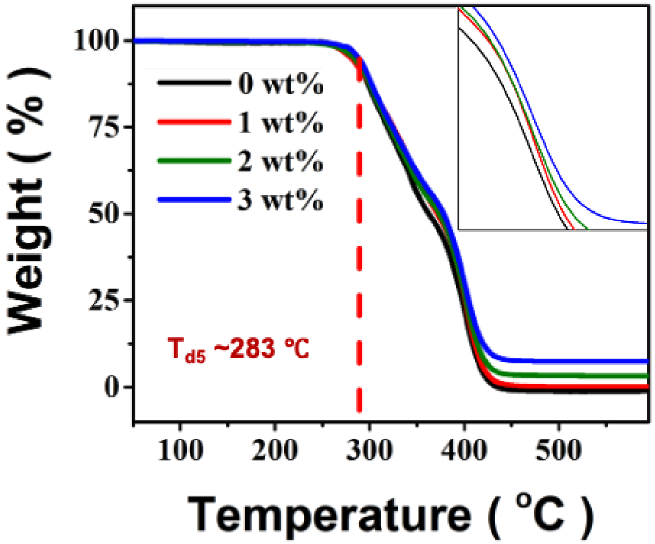

**Figure 5-3. TGA curves of DTDA-PU/MWCNTs-OH composites at a heating rate of 5 °C/min from 30 °C to 600 °C under $N_2$ environment. Inset on the top right is the detailed curves from 375 to 425 °C.**

DSC exothermic curves in Figure 5-4 depict the thermal behavior of DTDA-PU composites. Since the glass transit behavior is not observed in previous DSC testing (Figure 3-4), we lowered the initial testing temperature to -70 °C. As shown in the DSC results, the thermal behavior of DTDA-PU and their composites is following the amorphous polymers. During heating processes, their glass transitions can be observed as the stages in the curves labelled in Figure 5-4, while no peak corresponds to the melting temperature. In addition, the $T_g$ changed with MWCNTs-OH concentration and shifted toward higher temperatures with increased nanotube contents. This result indicates the restriction of molecular motion due to polymer chain entanglement increased by MWCNTs-OH incorporation. The similar storage modulus above $T_g$ indicate the similar cross-link densities of these two materials [190].

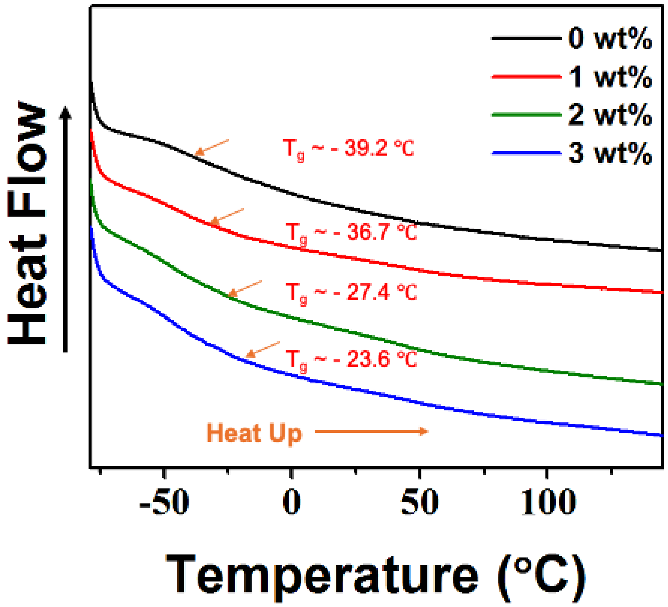

**Figure 5-4. DSC curves of DTDA-PU/MWCNTs-OH composites at a heat rate of 10 °C/min from -70 °C to 180 °C.**

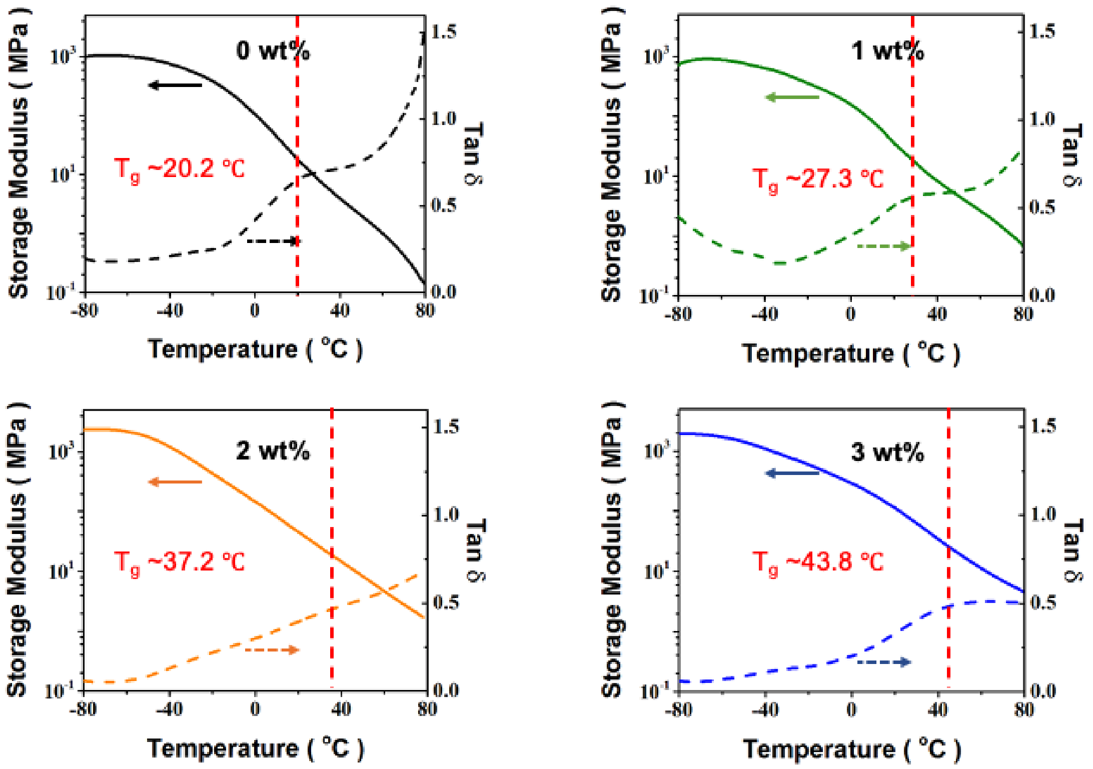

**Figure 5-5. DMA analysis of DTDA-PU/MWCNTs-OH composites from -80 °C to 80 °C. Solid lines represent storage modulus, and dashed lines represent loss tangent delta.**

Loss tangent delta (Tan δ) and storage modulus over the temperature range of -80 to 80 °C of DTDA-PU/MWCNTs-OH composites were obtained using DMA. As we mentioned before, the soft segments of DTDA-PU and their composites are not well localized due to the poorly packed hard segments, which resulted in the indistinct glass transition behavior. Only ambiguous peaks in tan δ patterns are assigned to their $T_g$. Since the DSC tests run following the calorimetric method, while the DMA follows the dynamic mechanical method, $T_g$ derived from DSC and DMA are different [188]. Despite that, their tendencies of $T_g$ shift are same that increased MWCNTs-OH concentration of composites leads to the higher $T_g$. This behavior again proves the polymer chain mobility was limited by

MWCNTs incorporation. Furthermore, the storage modulus above $T_g$ increased with increasing contents of MWCNTs, which indicates the cross-link density increased of composites [190].

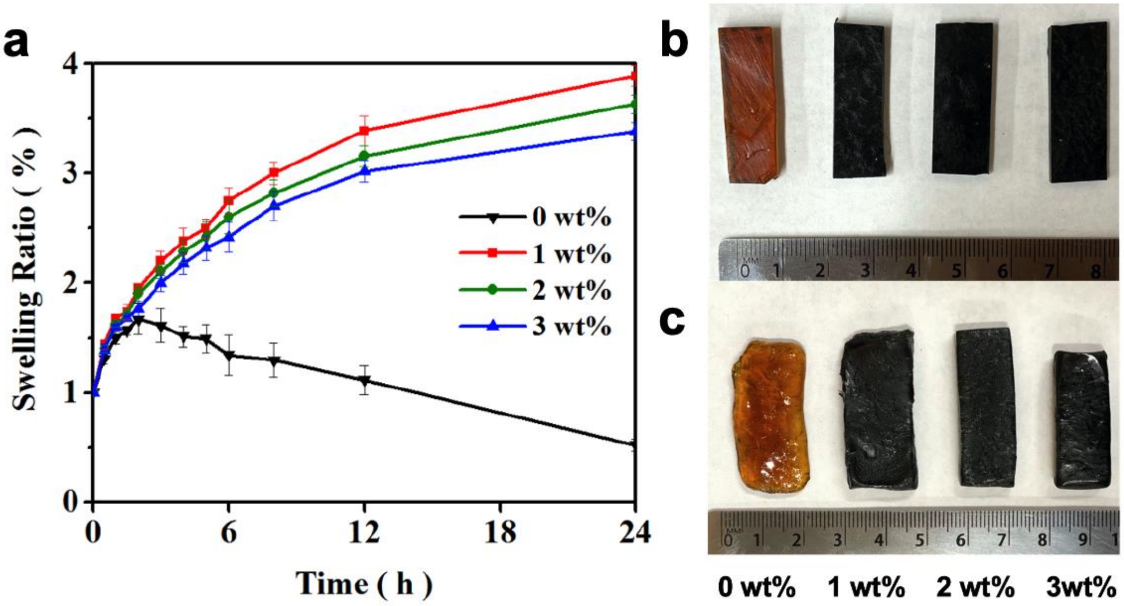

**Figure 5-6. (a) Swelling ratio for 0 wt%, 1 wt%, 2 wt% and 3 wt% DTDA-PU samples at room temperature. (b-c) Photographs of DTDA-PU with different MWCNTs-OH contents (b) before and (c) after being immersed in toluene for 6 hours at room temperature.**

Solvent resistance tests of the DTDA-PU/MWCNTs-OH composites were carried out to evaluate their durability. As shown in Figure 5-6a, the swelling ratio of pure DTDA-PU initially grew to 167.3% at the sixth hour, and then gradually dropped to 52.3% after 24 h of soaking. This result demonstrates that pure DTDA-PU was first absorbed by in the solvent, then dissolved. In contrast, the swelling ratio of all of the polyurethane-MWCNTs composites increased monotonically over 24h of soaking, with no indication of dissolution.

Figure 5-6b and Figure 5-6c show the photographs of the samples before and after 6 h of immersion in toluene at room temperature. After 6 h of immersion, the pure DTDA-PU sample became smaller and somewhat irregular in shape, while composite showed some swelling and retained their original cuboid shapes of samples. The swelling ratios of the DTDA-PU /MWCNTs-OH samples decreased as the contents of MWCNTs-OH increased. These results reflect the increase in polymer chain entanglement and cross-link density in the composites due to the reaction between -OH groups on the nanotubes and -NCO groups on the IPDI [223], which is corresponding to previous DSC and DMA results. The incorporation of MWCNTs with DTDA-PU improves their solvent resistance and the long-term stability and durability of these printing materials in various applications.

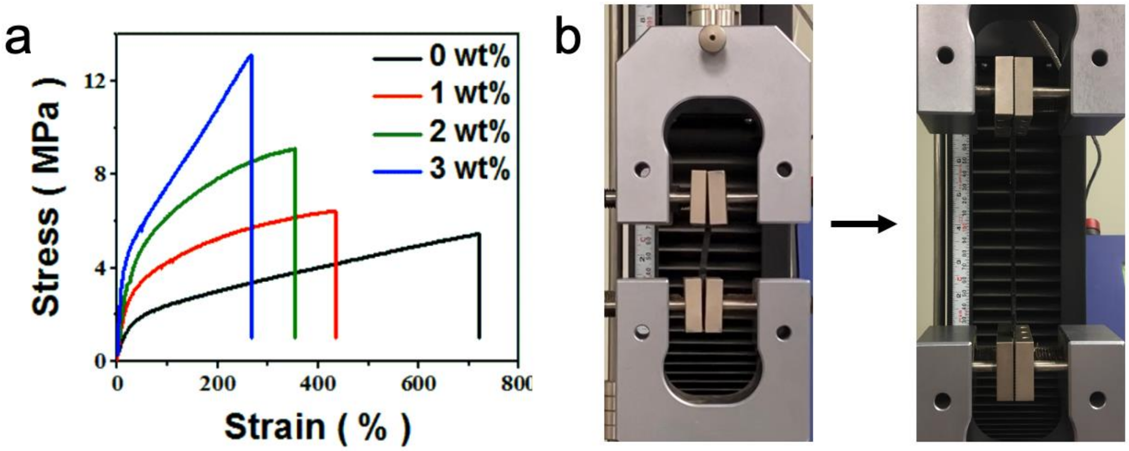

**Figure 5-7. (a) The tensile stress-strain curves of DTDA-PU composites. (b) Photographs showing the unstretched and stretched 2 wt% DTDA-PU.**

**Table 5-1. Young's modulus, tensile strength at break, and elongation at break of DTDA-PU composites and pure samples.**

| Content of MWCNTs-OH (wt%) | Young's Modulus (MPa) | Tensile Strength at Break (MPa) | Elongation at Break (%) |
|---|---|---|---|
| 0 | 6.3 ± 0.5 | 5.5 ± 0.4 | 720 ± 20 |
| 1 | 15.5 ± 0.7 | 6.5 ± 0.2 | 435 ± 36 |
| 2 | 20.9 ± 1.4 | 9.1 ± 0.3 | 353 ± 27 |
| 3 | 54.1 ± 2.7 | 12.8 ± 0.8 | 268 ± 21 |

The mechanical properties of DTDA-PU/MWCNTs-OH were studied via tensile tests. Figure 5-8 presents the stress-strain curves of 1 wt%, 2 wt%, 3 wt%, and pure DTDA-PU. The trends of four stress-strain curves are similar, with the stiffness and the tensile strength of the composites improving monotonically as the MWCNTs-OH contents increases. The detailed mechanical properties of the four samples are listed in Table 5-1. The ultimate tensile strength and Young's modulus of samples both increased with increasing MWCNTs-OH contents. In particular, Young's modulus of 1 wt%, 2 wt%, and 3 wt% DTDA-PU was about 2.4, 3.3, and 8.6 times higher than the pure DTDA-PU, respectively. The results indicate that the addition of nanotubes makes materials stiffer and harder to be stretched [224]. This effect is likely due to the tight bonding between the polymer-nanotubes interfaces, consistent with the previous SEM results [155, 225]. When the polymers and nanotubes are tightly bound with no interfacial slip, fractures of the material easily occur at high stress, leading to decreasing in the elongations at break [219]. On the other hand, the strength of the materials significantly improves. Our results show that incorporation of MWCNTs-OH improves the mechanical properties of DTDA-PU /MWCNTs-OH, and so increases the potential applications of 3D printed products with these materials.

### 5.2.3 Rheological Behavior of DTDA-PU/MWCNTs-OH Composites

The rheological behavior of DTDA-PU/MWCNTs-OH is an important parameter in assessing their printability, especially for DIW 3D printing used in this work. The temperature-dependent and shear rate-dependent viscosity of DTDA-PU/MWCNTs-OH were studied to characterize the printability of materials and to guide the choice of 3D printer settings. As shown in Figure 5-8, the viscosities of both pure DTDA-PU and composites decreased by roughly an order of magnitude as the temperature was increased from 120 °C to 150 °C. This performance directly relates to the breaking of disulfide bonds in polymer networks as the temperature rises. Although DTDA-PU/MWCNTs-OH already presented clear softening and liquidity at 120 °C, indicating that some disulfide bonds were already breaking, their viscosities at this temperature were too high for them to be used for DIW 3D printing applications [149, 152]. According to the literature, most DIW printing inks provide high printing accuracy when their viscosities are about 100 Pa·s [146]. A large fraction of disulfide bonds in the polymer networks must be broken to achieve this low viscosity with the DTDA-PU/MWCNTs-OH composites [186]. A high 3D printing temperature is thus required to increase the mobility of polymer chain [226].

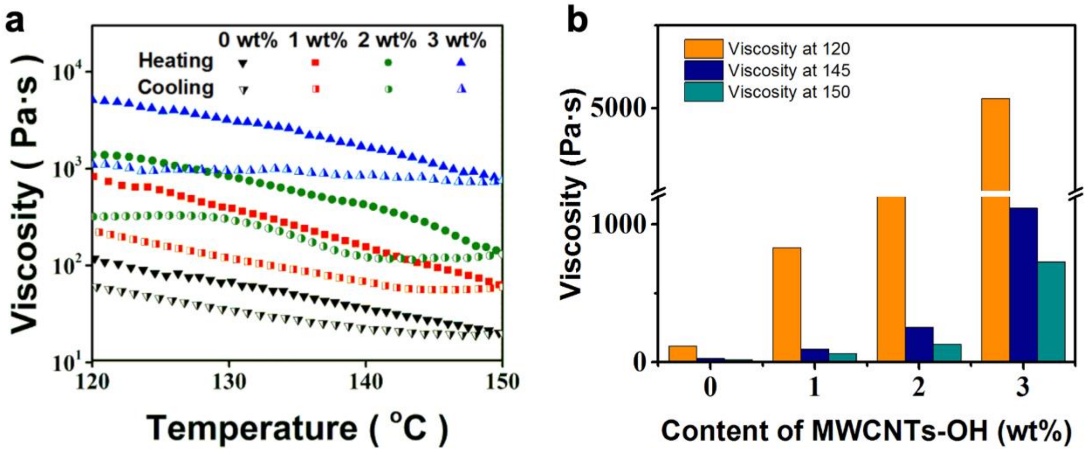

**Figure 5-8. (a) Temperature-dependent viscosity curves of DTDA-PU/ MWCNTs-OH. (b) The comparison of viscosities at 120 °C, 145 °C and 150 °C. The different colours and symbols indicate different MWCNTs-OH contents and different temperature, as shown in the legends.**

On the other hand, at a high temperature of 150 °C, the viscosity of pure DTDA-PU was 20 Pa·s, which was too low to be conducive for shape retention during the printing process [227]. The viscosities of the 1 wt% and 2 wt% DTDA-PU composites were about 61 Pa·s and 139 Pa·s at 150 °C, which are close to the requirement of printing materials. It is also evident from Figure 5-8 that the viscosities of composites increase as the context of MWCNTs-OH increases, reflecting the fact that MWCNTs-OH incorporation can increase the polymer crosslinking and limit polymer chain mobility [223]. Considering both the temperature-dependent viscosity results and the temperature range of our DIW printer (25 °C - 160 °C), we infer that a suitable printing temperature range for composite materials would be between 140 °C and 150 °C, depending on the MWCNTs contents.

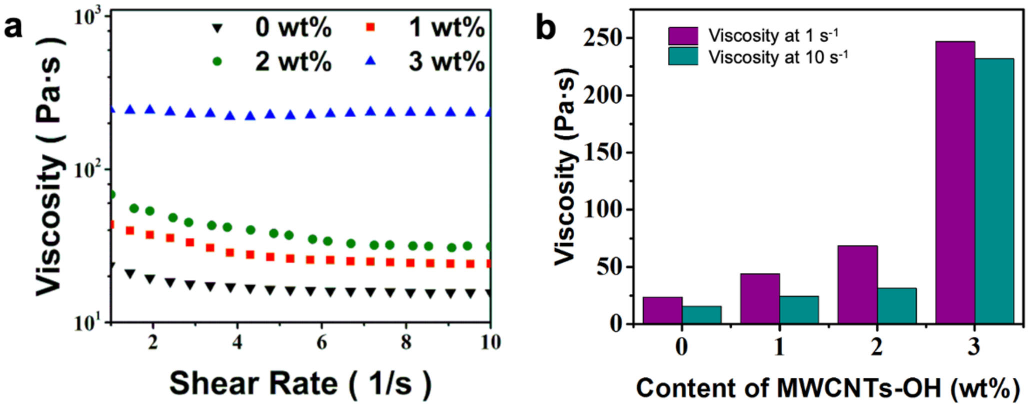

**Figure 5-9. (a) Share rate-dependent viscosity curves of DTDA-PU/ MWCNTs-OH. (b) The comparison of viscosities at 1 $s^{-1}$ and 10 $s^{-1}$. The different colours and symbols indicate different MWCNTs-OH contents and different share rate, as shown in the legends.**

The viscosity changes during the cooling process impacts the performance of solidification after the ink has been extruded from the hot nozzle, which determines the accuracy and resolution of the 3D printing process. As seen in Figure 5-8, the viscosities of all samples clearly increase during the cooling down process. Due to the reversibility of disulfide bonds, the broken disulfide bonds in the liquid ink tended to repolymerize once the temperature decreased[186], and the mobility of polymer networks gradually decreased [146]. The hysteresis is observed because the breaking and reformation of the disulfide bonds are also time-dependent, and the cooling rate was fast compared to the timescales required for the disulfide bonds in the polymer to reach equilibrium [228, 229]. This behavior guarantees that the viscosity of DTDA-PU/MWCNTs-OH increases as the ink is cooled after extrusion, and thus an additional gas cooling system was unnecessary. However, adjusting printing speed is required to prevent ink overflow and allow solidification of printed samples [230, 231].

The rheological behavior under shear stress of the printing ink during the extrusion process also plays an essential role in high-performance DIW 3D printing. Since the shear rate experienced by the ink during the extrusion varies substantially, the dependence of the viscosity of DTDA-PU/MWCNTs-OH on shear rate was also studied. Shear-thinning behavior would allow more rapid extrusion of the ink through micro nozzles under ambient conditions and help retain the shape of the printed part when flow ceases [232]. As illustrated in Figure 5-9, the viscosity of all DTDA-PU/MWCNTs-OH composites except for 3 wt% DTDA-PU decreased with an increase in the shear rate at a constant temperature at 145 °C. The viscosities of 2 wt% and 1 wt% DTDA-PU/MWCNTs-OH under the share rate at 10 $s^{-1}$ are about half of their viscosities under the share rate at 1 $s^{-1}$. On the other hand, the viscosity of the 3 wt% DTDA-PU remained approximately constant over this range of shear rate. The shear rates experienced by ink during printing is typically about 50 $s^{-1}$ [227], somewhat higher than our measured range. These tests are only for predicting the trends during the practical printing processes. The shear-thinning behavior of both 1 wt% and 2 wt% DTDA-PU/MWCNTs-OH should improve their printability in actual printing.

### 5.2.4 3D Printability and Recyclability of DTDA-PU/MWCNTs-OH Composites

By comparing all previous results, 2 wt% DTDA-PU, with good mechanical performance and suitable viscosity for DIW 3D printing, was chosen for the following printing tests. Figure 5-10 illustrates the DIW 3D printer printing process. A model of the Hanging

Gardens of Babylon was printed. This model was chosen because it incorporated various geometries and features that allow evaluation of the printing quality. Other CAD models were also printed and can be found in Appendices. The same model was also printed with pure DTDA-PU for comparison. As seen in Figure 5-11a, both printed samples were consistent with the CAD model, and small features such as stairs and columns were well preserved. A few details on the pure DTDA-PU printed sample were slightly distorted. For example, the curves on the bottom edge and the sag on the second-floor cantilever beam are marked out by red circles and shown at higher magnification in the insets of Figure 5-11a. In contrast, the 2 wt% DTDA-PU printed sample showed better details and higher resolution.

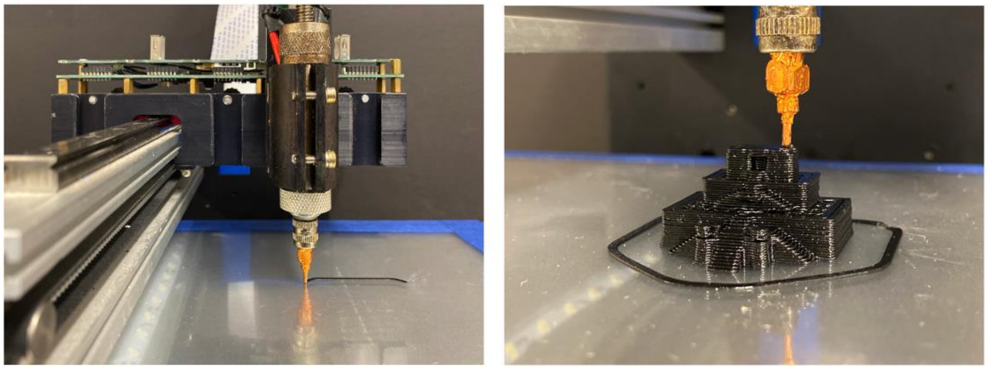

**Figure 5-10. Photographs of DIW 3D printer working process. The beginning (left) and finishing (right) of the printing process.**

Figure 5-11b presents detailed photos of this 2 wt% DTDA-PU printed model captured by the optical microscope under different magnification. The printed samples showed layer structure on the macroscale, whereas interface gaps between layers were not visible on the micro-level image. In extrusion-based 3D printing, the gap between layers dramatically reduces the mechanical performance of printed parts and further limits their service life [105, 151]. However, the disulfide bond metathesis occurring during thickening and solidifying of the printed composite can effectively provide the adhesion between layers and even eliminate the interfaces between layers to improve the quality of the printed object. These tests indicate that the 2 wt% DTDA-PU possesses good printing performance. We now study the recyclability of the products printed with this material.

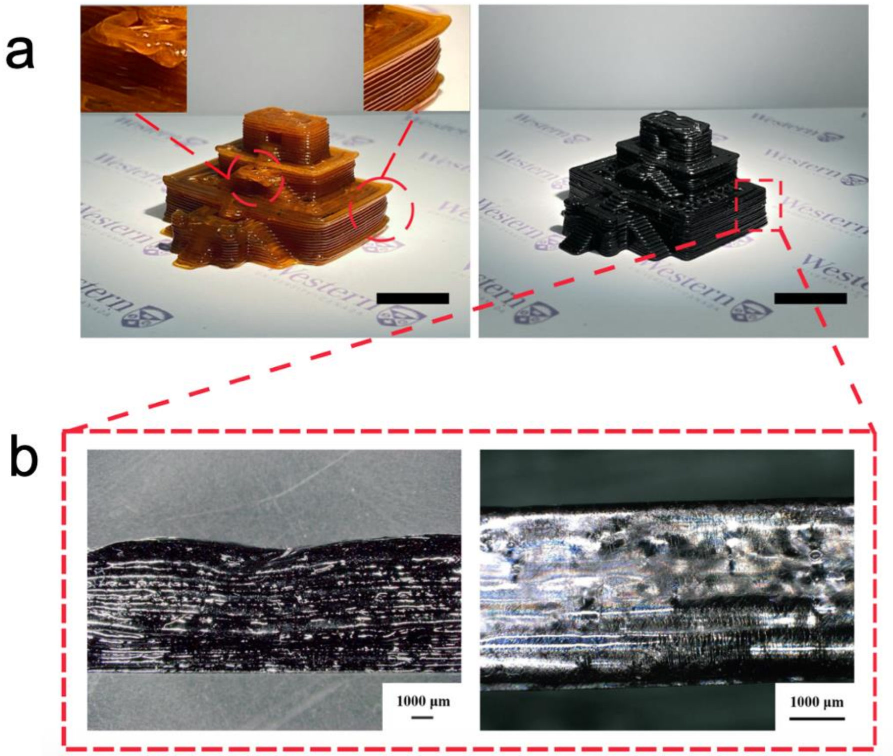

**Figure 5-11. (a) Photographs of the Hanging Gardens of Babylon model printed with pure (left) and 2 wt% DTDA-PU (right) with inset about bottom edge and the second-floor cantilever beam of the pure DTDA-PU printed sample. Scale bars: 10 mm. (b) Partial enlarged view of the 2 wt% DTDA-PU printed models captured by optical microscopy under different magnification. Scale bars: 1000 μm.**

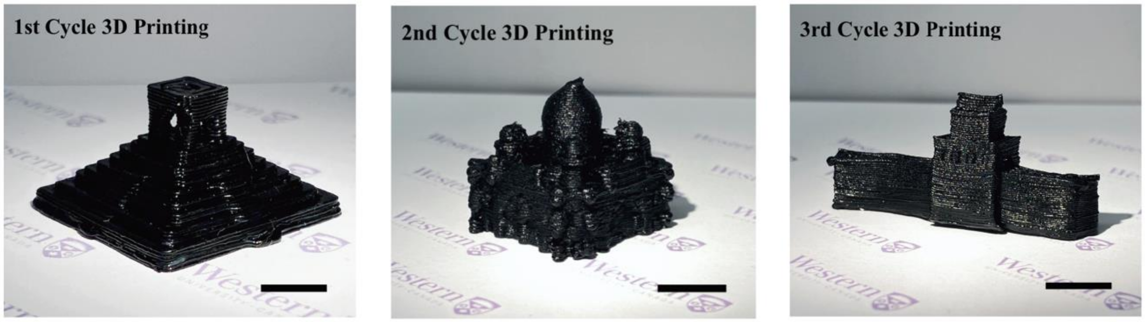

**Figure 5-12. Images of three cycles of printed architectures. From left to right are the printed models of Chichen Itza, Taj Mahal, the Great Wall of China. Scale bars: 10 mm.**

Recycling 3D printed parts is another fundamental method to reduce the amount of polymer waste from 3D printing. In this work, DTDA-PU/MWCNTs-OH 3D printed waste was directly recycled by three steps: crushing, reloading and reprinting. Failed printed parts were first crushed into small pieces. The material pieces were loaded into the syringe of the 3D printer and preheated at 120 °C for 15 min then used to print new 3D structures. The printhead temperature and the build platform temperature were set at 145 °C and 25 °C, consistent with the settings used when printing the initial material. Figure 5-12 demonstrates the recyclability of 2 wt% DTDA-PU. Models of Chichen Itza, Taj Mahal and the Great Wall of China were crushed and reprinted three times. All of the objects printed using recycled polymers were high quality, and detailed features were well preserved. For example, small windows in the watchtower of the Great Wall model are presented in the third cycle printed model. Since the material recycling mechanism is based on reversible dynamic disulfide bonds, the recycling process is not expected to change the material properties or the 3D printing performance [191]. The consistent performance of the printing ink ensured high resolution and accuracy of the end printed models even after the material was recycled three times.

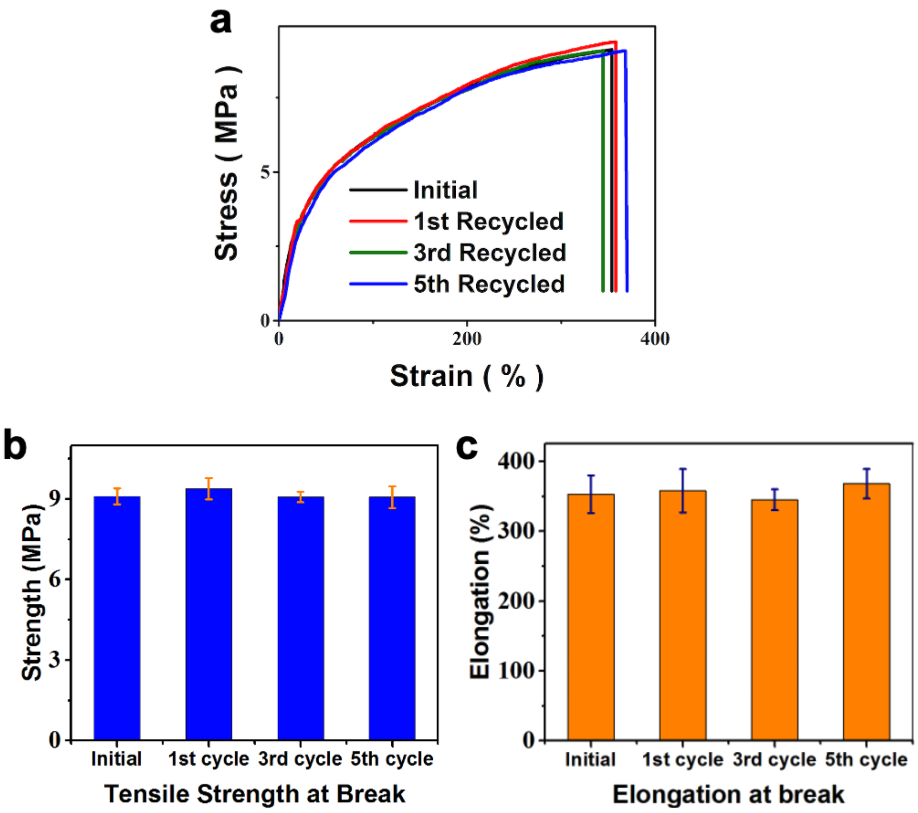

**Figure 5-13. (a) Typical tensile testing curves of the initial material and the third cycle recycled material, and their comparison of (b) tensile strength at break and (c) elongation at break.**

In Figure 5-13, the stress-strain curves of first, third and fifth cycle recycled samples are compared with that of the originally printed sample. The stress-strain curves of all samples are similar. The tensile strength at fracture of the fifth cycle recycled samples was about 9.07 MPa, within the margin of error of the strength of the original material (9.12 MPa). The tensile test results suggest that the material properties are consistent before and after recycling, which ensures the recyclability of the printing material. All the above results together demonstrate that 2 wt% DTDA-PU has the potential to achieve fully repairable and recyclable green 3D printing.

## 5.3 Summary

We have developed a sustainable 3D printing material based on the synergy of polyurethane and aromatic disulfide bond in previous chapters. In this part, to further improve the printing performance and broaden the application sphere, MWCNTs-OH have been incorporated to enhance the material properties and printability of DTDA-PU. The solvent resistance and tensile strength of DTDA-PU have significantly improved with the MWCNTs-OH incorporation. The integration of moderate MWCNTs-OH and dynamic disulfide bonds endows the as-prepared DTDA-PU/MWCNTs-OH with desirable shear-thinning behavior which is suitable for the DIW 3D printing process and excellent recycling performance. Combined with the above analysis, we chose the 2 wt% DTDA-PU as the printing material for the following practical 3D printing study.

In the practical printing tests, printed architectures from 2 wt% DTDA-PU present better printing resolution by comparison with pure DTDA-PU printed part. To recycle 3D printing waste, unwanted DTDA-PU/MWCNTs-OH printed components can be simply reloaded into the cartridge of DIW printer and reprinted multiple times with consistent performance. There is no marked difference between the mechanical properties of the original sample and the fifth cycle recycled sample. The following chapter will explore the applications based on the photothermal properties of DTDA-PU/MWCNTs-OH printing materials.

# Chapter 6

## 6 Photothermal Conversion Triggered Dynamic Disulfide Bonds of 3D Printed Polyurethane Composite

Based on dynamic covalent chemistry, the development of sustainable 3D printing manufacturing has explored disposal recycling in previous chapters. Despite this part, printed products repairing also plays an important role in extending the product service life, reducing waste and conserving the resource. For the heat-triggered repair process of damaged parts, heat energy may easily radiate on the uninjured parts and cause the dissociation of the whole printed sample. Therefore, we explored the NIR-triggered repair process relying on the photothermal conversion ability of MWCNTs. Furthermore, this photothermal conversion behavior of printed components can also be beneficial to their support removal processes. Our NIR-trigger contactless support removal technique opens up a new possibility of a fully automated 3D printing post-treatment process.

### 6.1 Introduction

As we mentioned before, manufacturing is the process that transforms raw materials into finished products to be used for some purposes. This process involves the raw materials acquisition, materials production, product manufacturing, product using and final disposal. Each step requires the utilization of resources and waste generation. The core content of sustainable manufacturing is reducing the waste of resources and achieving waste recycling. 3D printing technology features the product customization and on-demand manufacturing that effectively prevents resources wasting caused by the overproduction. Also, with the layer-by-layer manner, 3D printing inherently can avoid raw material wasting compared with traditional subtractive manufacturing. For further sustainable 3D printing development, we have provided a feasible solution for 3D printing waste recycling in previous chapters. Moreover, the full utilization of resources can also be contributed by extending the product service life and waste reduction. The repair option is important for products upon mechanical damage to extend their lifetime. Therefore, in this chapter, we discussed the practicability of 3D printed product repairing.

Repairable polymer systems have been realized with the dynamic covalent chemistry, which usually are known as the self-healing materials. The concept of self-healing is initially inspired by biology systems that refers to the ability of damaged materials to heal and restore to their original set of properties [233]. Healing mechanisms vary from extrinsic healing agents contained in materials to intrinsic dynamic covalent and noncovalent reactions [234]. Disulfide metathesis is the most widely used method to prepare self-healing polymer materials based on the dynamic covalent chemistry. The polyurethane based on aromatic disulfide bonds has been proven that can auto-repair at room temperature after 2 h [186]. However, the instant damage repair is looking forward to accommodating with the rapid prototyping feature of 3D printing.

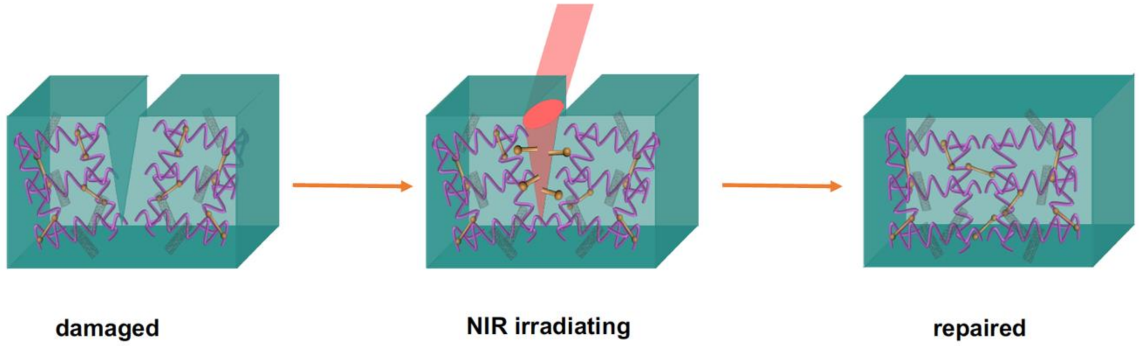

**Figure 6-1. Representation of the disulfide bond reaction during the in-situ repair process.**

The external stimuli can effectively accelerate the repair process of self-healing materials based on disulfide bonds. Heat energy can rapidly trigger the disulfide bond reaction and is easily accessible, while it can also easily radiate and diffuse to the surrounding area. The rapid prototyping of complex structures is one of the most important features of 3D printing technology. It would be hard to repair 3D printed objects with fine structures precisely with heat, since the heat energy diffusion may easily damage the 3D printed structures. Instead of using a heat source, a light source can be used to provide spatiotemporal control and locally precise activation for the repair process [141].

MWCNTs can effectively generate large amounts of heat via absorbing energy from NIR light. Based on this property, MWCNTs have been widely studied for their applications in anti-tumor therapy [235], desalination and wastewater treatment [236], actuators [237], and solar thermal energy harvest [238]. In our work, MWCNTs-OH can work as the light to heat convertor in DTDA-PU composite during the repair process. As shown in Figure 6-1, the MWCNTs-OH in the DTDA-PU matrix can effectively absorb near-infrared (NIR) light energy and convert it into heat energy, which then triggers the disulfide bond reaction. This property provides a basis for in-situ repair that can contribute to the 3D printing waste reduction and meet the sustainable 3D printing commitment of this work.

Since NIR can be remotely controllable and achieve point to point precise repair, we also explore a new approach of contactless 3D printing support removal in this work. For 3D printing, support structures are often necessary when the printing model has overhangs. Removal of the support is a tedious work and can be tricky on complex geometric designs. The controllability and accuracy of the NIR laser target in the developed strategy can provide a new approach for precise and rapid removal of support for 3D printing processes. All these works finally combine into a trinity sustainable 3D printing strategy that can realize the production waste reduction, product lifetime prolongation and failure products circulation.

## 6.2 Result and Discussion

### 6.2.1 Photothermal Behavior of DTDA-PU Composites.

The photothermal properties of DTDA-PU/MWCNTs-OH were studied using the FILR thermal imager. The experimental setup is shown in Figure 6-2. All sample photothermal tests were carried out in a homemade operation box. This box was opaque, with an observation window and a ventilation system to prevent harm due to high power NIR light and smoke emissions. An aluminum optical breadboard was used as the sample stage for vibration control. The H-laser was chosen as the light source and positioned 30 cm above the samples.

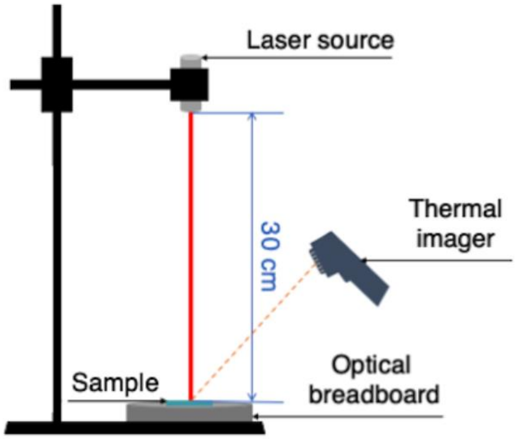

**Figure 6-2. Schematic illustration of the experimental setup. A 1 W 808nm NIR light source was used. The aluminum optical breadboard was used for vibration control. The operation stage was covered by an additional opaque case with a ventilation system for personal protection.**

For rapid repair, the rate of surface temperature rise under NIR irradiation is critical. As seen in Figure 6-3a, the temperature of the irradiated area is seen to increase rapidly within the first 30 s of illumination and then gradually stabilize in the following 30 s. After 1 min, the highest local temperatures of all DTDA-PU/MWCNTs-OH samples were all above 240 °C, which is well above the material flowing temperature and even the material printing temperature 145 °C. In contrast, the surface temperature of the pure DTDA-PU sample was only about 50 °C after 1 min high power NIR light irradiation (Figure 6-3b). This result indicates the higher MWCNTs-OH contents, the better energy converting behavior was. Therefore, the composites with high MWCNTs contents have the potential to achieve instant material repair with its ability to initiate material flow quickly.

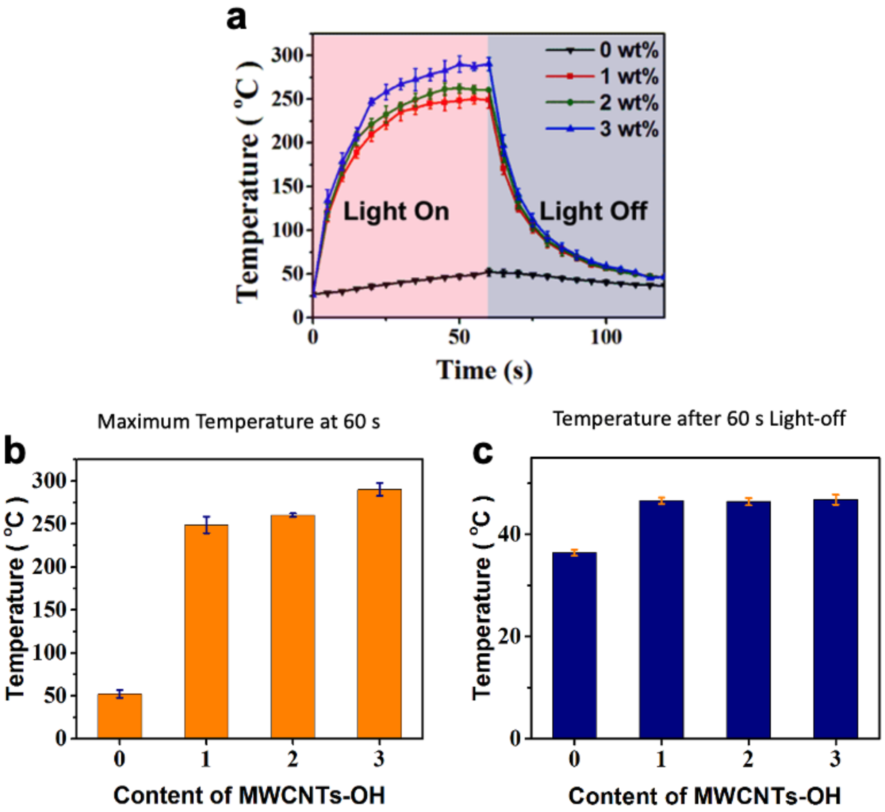

**Figure 6-3. (a) Surface temperature elevation of the DTDA-PU and their composites samples as a function of time with NIR light turns on for 60 s, then off. (b) The maximum temperatures of samples after 60 s NIR light irradiation. (c)The cooling down temperatures after light turn off for 60 s. Light spot diameter = 6 mm; working distance = 30 cm.**

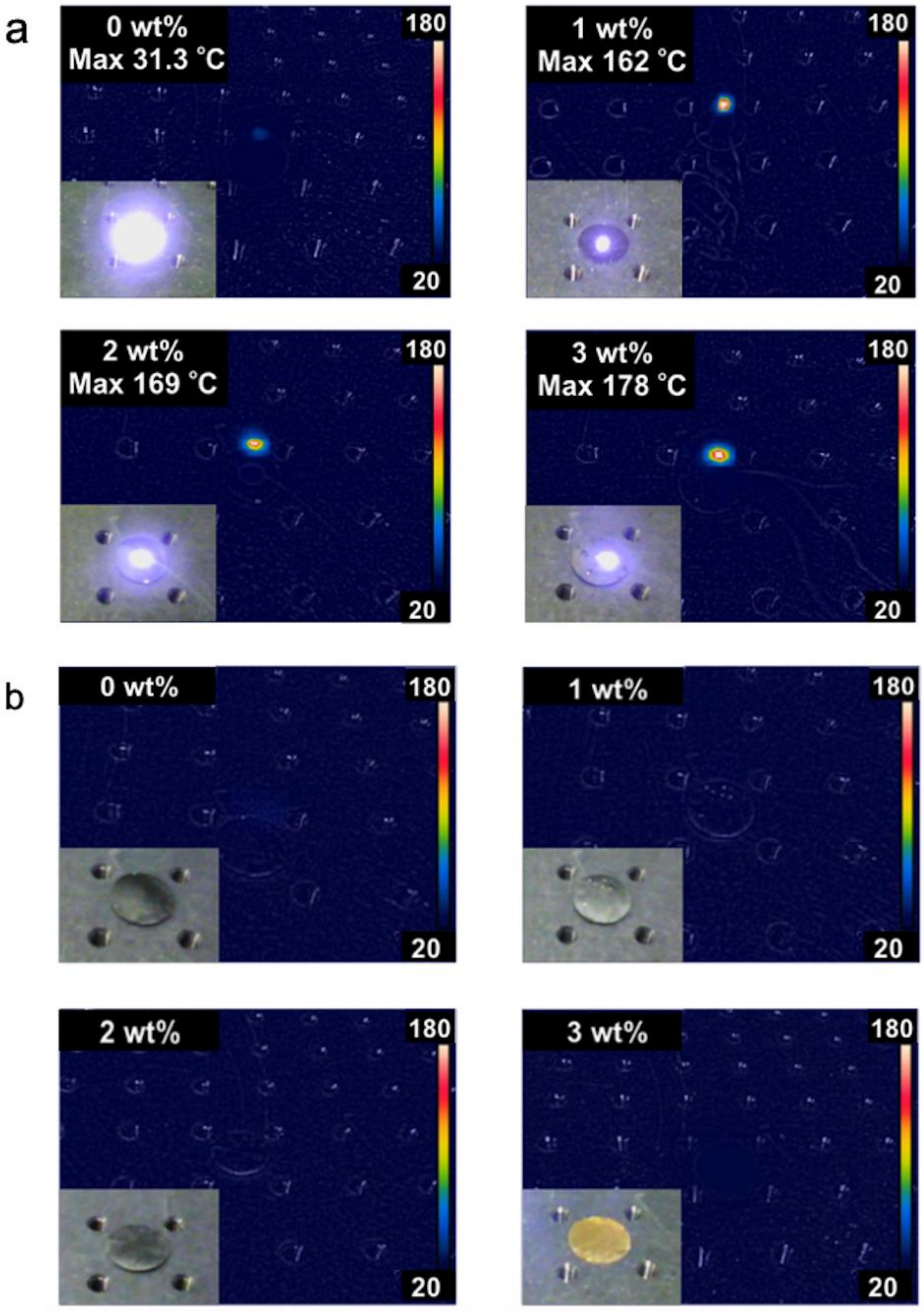
a
0 wt%
Max 31.3 °C
180
20
1 wt%
Max 162 °C
180
20
2 wt%
Max 169 °C
180
20
3 wt%
Max 178 °C
180
20
b
0 wt%
180
20
1 wt%
180
20
2 wt%
180
20
3 wt%
180
20

**Figure 6-4. Photothermal properties of DTDA-PU composites. Thermographic images of samples before (a) and after (b) NIR irradiation for 10 s with digital images of samples inset.**

However, excessive MWCNTs-OH content may cause local temperatures higher than desired, which would not only affect the controllability of the repair process but may also cause the polymer matrix to burn during the procedures. As the TGA analysis showed in Figure 5-3, the $T_{d5}$ of DTDA-PU/MWCNTs-OH composites were around 283 °C. When the material service temperature is above this, the material pyrolysis will begin. In Figure 6-3a, the highest surface temperature observed with the 3 wt% DTDA-PU was about 280 °C. As a result, the sample damage by pyrolysis is prone to happen for 3 wt% DTDA-PU during the material repair process. On the other hand, the temperature of the irradiated 2 wt% DTDA-PU remained below the pyrolysis temperature during the fast temperature rise. Consequently, this result combined with the above printing tests indicates that 2 wt% DTDA-PU is a qualified candidate as the recyclable and repairable printing material.

In addition, the photothermal controllability of DTDA-PU/MWCNTs-OH also benefits the fast cooling and solidifying of printed parts during the repair process. The instant temperature dropping after the repair process is expected to avoid the repaired sample deformation before solidification. In Figure 6-2, the temperatures of the irradiation area drastically declined once the laser was turned off and tended to room temperature after 30 s. Corresponding with the rheological behavior of DTDA-PU/MWCNTs-OH in Figure 5-9, the material viscosities can increase with temperature decrease after NIR light turn. Therefore, instant solidification can be achieved after the repair process. This rapid cooling behavior can effectively prevent the material deformation and ensure the precise in-situ repair.

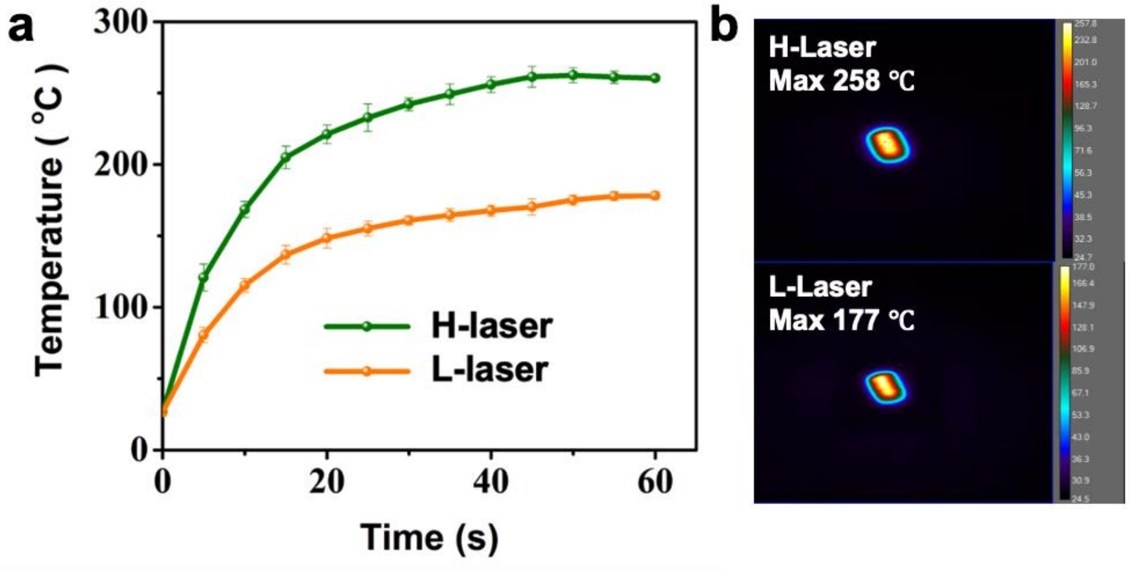

**Figure 6-5. (a) Temperature elevation of 2 wt% DTDA-PU under H-laser (1 W) and L-laser (0.5 W); spot diameter = 6 mm; working distance = 30 cm. (b) Thermographic images of the 2 wt% DTDA-PU after H-Laser and L-Laser irradiation for 60 s.**

It is also important to study the temperature gradient that developed on the sample surface under laser irradiation, which will affect the possible precision of sample repairs [106]. Figure 6-4a shows thermal images of the sample surfaces after 10 s of laser irradiation. All composites showed a clear increase in the local temperatures of the irradiated area, compared with their thermal images before irradiation (Figure 6-3b). In contrast, the temperature change of the untargeted areas was not observable. This result demonstrates that, over short times, the increase of the surface temperature and the melting of the material can be accurately limited to the area targeted by the laser. Thus, combining high directivity of NIR laser, the precise in-situ repair of DTDA-PU composite printed samples is feasible.

For the printing samples with fine features, high-intensity laser irradiation may over promote polymer chain movement and lead to local deformation, which is adverse to the precise repair [105, 151]. Thus, the choice of laser power, laser working distance, and irradiation time all need to be adjusted according to the practical situations. The surface temperature increases of 2 wt% DTDA-PU under L-laser irradiation was also recorded here. The temperature elevation curves under L-laser and H-laser irradiation are compared in Figure 6-5a. In both cases, the irradiated area heats up rapidly and then gradually tends to equilibrium after 30 s. The L-laser data show a lower temperature increase than the H-laser data due to the lower irradiation energy. This result can provide guidance for our following repair study of damaged printed components in various situations.

### 6.2.2 In-situ Repairability of DTDA-PU Composite Printed Samples

The repair of 3D printed parts is expected to extend service life and reduce printing waste. Considering the complex geometry of 3D printed products, the spatiotemporal controllability of the NIR laser can effectively limit unwanted deformations during the repair processes [141, 145]. In the previous section, we have discussed the material photothermal behavior. Here, the practical repair tests for damaged samples are presented. Since the damage situations of 3D printed components in real life are varied and complicated; therefore, before we discussed the damage repair of printed parts, the material repairability was first well studied.

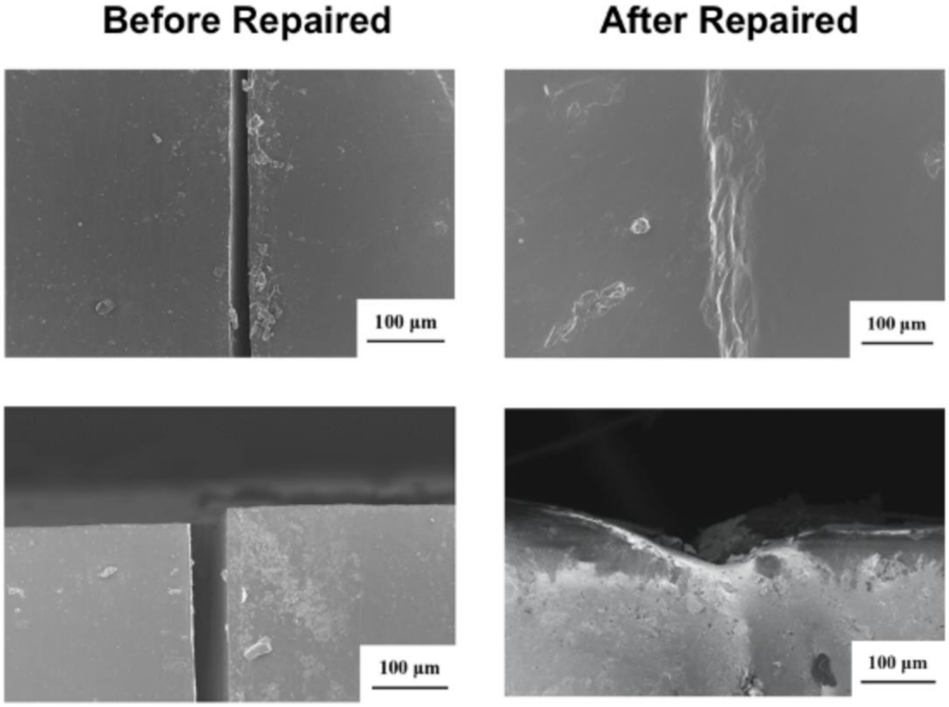

**Figure 6-6. Top view (see pictures above) and cross-sectional view (see pictures below) of the SEM images of damaged 2 wt% DTDA-PU before and after being repaired. Scale bar: 100 μm.**

SEM imaging and tensile tests were performed on repaired 2 wt% DTDA-PU samples to assess the effect of NIR laser-induced repair. To evaluate the repairability of DTDA-PU/MWCNTs-OH, the as-prepared 2 wt% DTDA-PU sample was cut into two slices. The two slices were then placed in close contact, and the interface between the two aligned pieces exposed to the NIR laser at room temperature. Figure 6-6 presents the SEM images of the top view and cross-sectional view of the scratch before and after being repaired. After in-situ photothermal repair, only a thin scar was left on the sample surface. During the irradiation process, high-intensity light energy was converted into heat energy to trigger the disulfide bond breaking, which led to the material melting and filling the scratch. Once the light was turned off, the material cooled, and disulfide bonds reformed to solidify the polymer and complete the repair process. The SEM images indicate that damage on printed parts can be precisely targeted and repaired in-situ.

Tensile tests of as-printed and repaired samples were carried out to evaluate the healing efficiency of 2 wt% DTDA-PU (Figure 6-7). The healing efficiency is defined as the ultimate tensile strength ratio of the repaired sample to the original sample ($\eta = \sigma_{\text{healed}} / \sigma_{\text{virgin}}$, where σ is the strength of the virgin sample and the healed sample). As shown in Figure 6-7b, the ultimate tensile strength of the original sample was about 9.12 MPa. After the first cycle repair, the maximum strength of the repaired sample was about 8.81 MPa, and the healing efficiency was about 95.6%. To verify the repeatability of the repair process, we scratched and repaired at the same position for two and three times, then calculated healing efficiency through the results of their tensile tests. Following the second and third cycle repair, the healing efficiencies decreased to about 92.4% and 86.3%, respectively. Compared with the change in maximum tensile strength, their changes in elongation at break is more obvious (Figure 6-7c). The maximum elongation of the third cycle repaired sample was about 79.5% of the original sample.  The drop in healing efficiency may be due to the deformation of the material in the scratch area caused by repeated melting and solidification [239]. All these results show that the 2 wt% DTDA-PU materials can be quickly and precisely repaired using the light-triggered disulfide bond reaction.

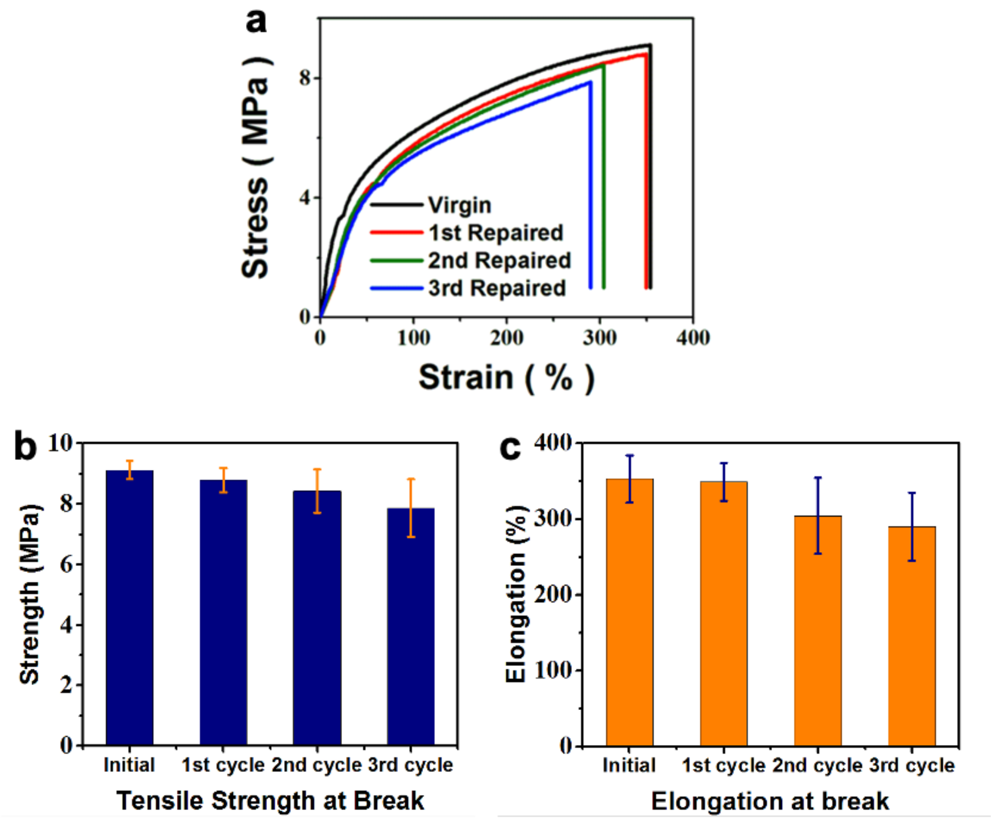

**Figure 6-7. (a) Stress-strain curves of 2 wt% DTDA-PU for three damaged-repaired cycles, and their comparison of (b) tensile strength at break and (c) elongation at break.**

Based on the above studies, we put forward two repair procedures corresponding to real-life damage situations of 3D printed components and studied their performance. According to previous photothermal behavior of 2 wt% DTDA-PU with H-laser and L-laser presented in Figure 6-5, different laser sources and operation methods were used with varied damage situations. For large cracks or cut-off specimens, e.g., the broken bridge model shown in Figure 6-8a, the H-laser was positioned 30 cm above the sample. To ensure complete repair, the edges of the two broken pieces edges were aligned manually and then repaired with the laser.

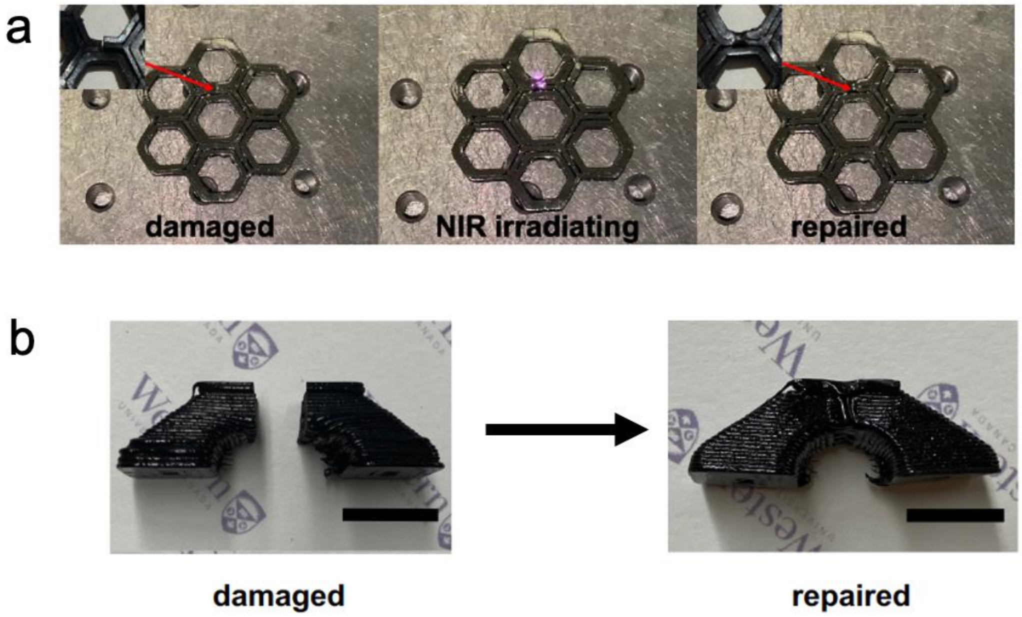

**Figure 6-8 Repair processes of 2 wt% DTDA-PU printed parts. (a) Photographs of a damaged and repaired printed arch bridge sample. Scale bars: 10 mm. (b) Photographs of a damaged and repaired 2 wt% DTDA-PU printing honeycomb sample. The detailed images are shown as insets.**

On the other hand, for a scratch or crack on a thin structure or in an inaccessible area, e.g., the crack on the inner part of the honeycomb model shown in Figure 6-8b, the L-laser was chosen as the light source to in-situ repair the sample. The L-laser was set about 30 cm above the sample and targeted on the crack. After laser irradiation for 30 s, the target area material melted and filled the crack. When the laser turned off, the sample quickly solidified and achieved the in-situ repair. Both types of repair procedures achieved excellent results and can be applied to most practical situations.

### 6.2.3 Laser Assisted Non-physical Support Removal Technique

The remotely controllable photothermal system can be applied for the removal of a support structure in the post-process of 3D printing. Support structures are very common for printing objects with overhangs and other complex geometrical features. For these complex printed parts, removing the support structure is not only labor-intensive but also prone to error, which dramatically increases the 3D printing defective rate. The NIR laser-aided support removal technology is an effective approach to address this problem. Figure 6-9a illustrates the operation setting. To evaluate the laser-assisted support structure cleaning processing, the H-laser was set about 5 cm away from the printing part and aligned with the joint of the support structure. After 5 s irradiation, the support part was detached from the main structure.

The choice of high-wattage NIR laser and close working distance resulted in the repaid temperature rise of the material. Material flow and even decomposition happened within a short time. The whole support removal process was recorded by a video camera. As presented in Figure 6-9b, the support structure melted after 3 s laser irradiation. Thanks to the thin features of the 3D printing support, the further melting led the support structure to collapse and detach from the main structure after 5 s. The smoke released during the removal demonstrated the burning and loss of the target area material, which also assisted the support structure detaching. This result demonstrates that the NIR laser can be used to precisely target and detach the support structure. This procedure is more controllable than the traditional manual support removal method, and therefore can accelerate the 3D printing post-process and reduce the printed product defective rate. This application also shows the feasibility of the automated support removal process, adding to the potential to achieve fully automated 3D printing technology.

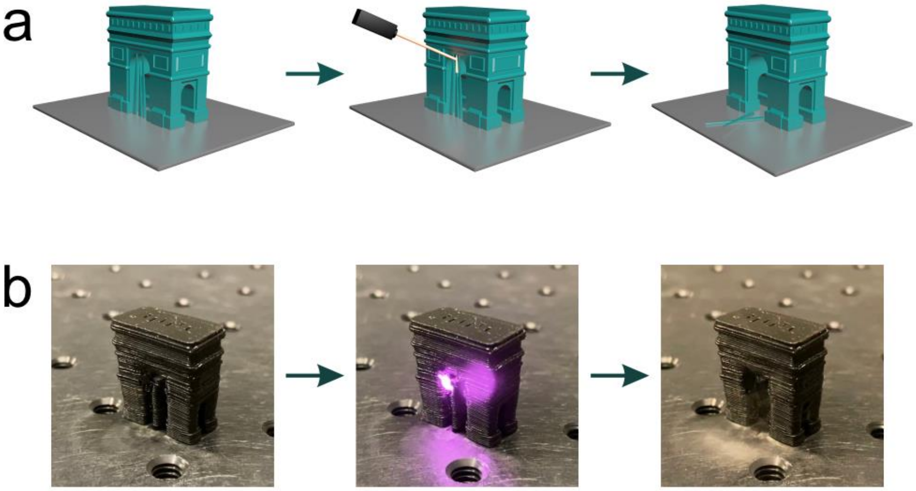

**Figure 6-9. The process of precisely removing the support structure of 2 wt% DTDA-PU printed the Arc de Triomphe model. (a) Schema. (b) Photographs.**

## 6.3 Summary

Our objective of sustainable 3D printing development is focused on both waste recycling and resource conservation. In the previous chapters, we have developed a simple and high customized 3D printing waste recycling procedure. In this chapter, we are focused on the actions that target on resource conservation. The precise in-situ repair of broken 3D printing parts can become very practicable for prolonging the lifetime of the printed components, which can not only reduce the printing waste but also save the resource invested for new printed products. The incorporation of MWCNTs-OH improves the printing performance and also can provide the printed samples with the photothermal activity that allows for in-situ repair. The real-time photothermal behavior of DTDA-PU composites with different contents of MWCNTs-OH was recorded by a thermal imager. The results indicate that the in-situ repair of printed products can be precisely triggered by NIR light. The healing efficiency was as high as 86.3% after three repairs. Two different repair procedures were discussed based on various printed structures and damage conditions.

The same controllable, contactless and precise targeting of the NIR laser, which is needed for the repair processes, can also be applied to the removal of 3D printed support structures. The support removal procedure is inescapable post-processing of 3D printing. This process wastes a mass of labor-power and most likely causes the printing failure. The procedure optimization with contactless NIR laser control can effectively reduce the product defective rate and potentially improve the 3D printing post-process to achieve full automation. Thus, the printed waste can effectively be controlled at the source. We hope that this study can pave the way for the development of a more sustainable 3D printing industry and lead to a transition from the current intensive resource consumption mode to a more rational utilization mode.

# Chapter 7

# 7 Conclusions and Future Work

This chapter includes the summary of results and contributions in this dissertation and personal opinions and suggestions for future work.

## 7.1 Conclusions

3D printing is a crucial manufacturing technology with great potential that promises to reduce production costs as well as to shorten product development cycle time. In addition, it has the advantages of freeform design, manufacturing capability, and supervision-free processing. Nowadays, more and more materials, such as metals, polymers, glass, etc. can be used to produce customized parts by 3D printing. Due to the low cost, lightweight, high performance and durability, 3D printable polymers are widely used for a variety of applications. However, the growing usage of 3D printing and the fast update of polymeric parts have resulted in tremendous growth of polymer waste and environmental problems over the past few decades. Herein, my Ph.D. work focused on devising a green 3D printing strategy based on dynamic covalent polymers for 3D printing technology to hold the promise of sustainable development. We are dedicated to reforming the current lifecycle for 3D printing materials “material to product to waste” into a circular, sustainable 3D printing economy (Figure 7-1).

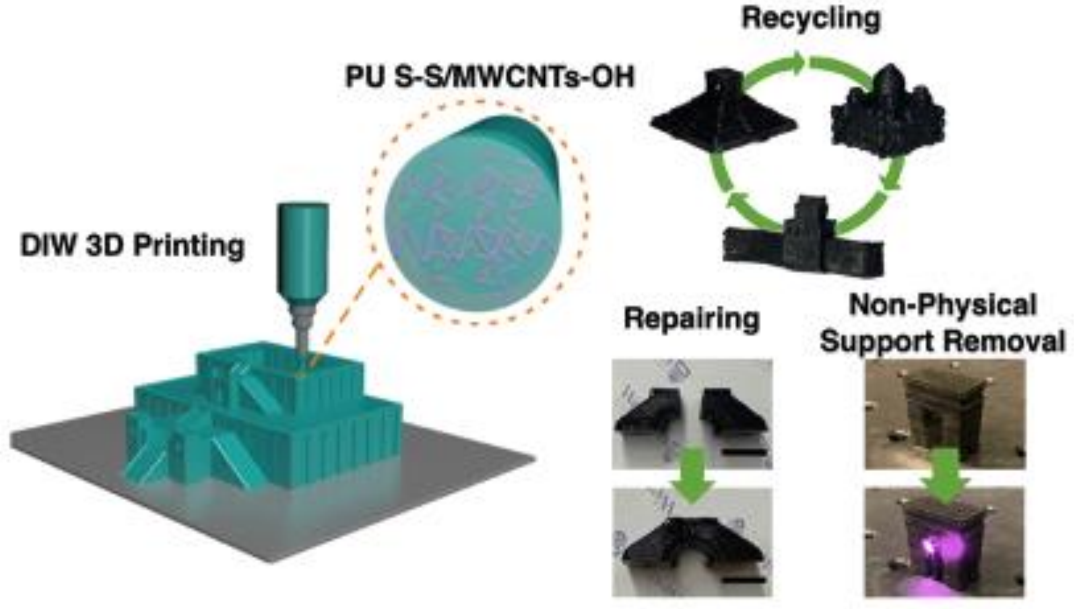

**Figure 7-1. The sustainable 3D printing strategy of the trinity of recycling printing wastes, repairing damaged parts, reducing processing defects.**

Four different polymer networks with dynamic covalent chemistry, FA-Epoxy, CADH-Epoxy, TEMPS-PU and DTDA-PU, were synthesized and characterized. These four materials are different in dynamic covalent chemistries, polymer structures and the molecule structures of dynamic covalent compounds. Through the synthesis and characterization of these materials, we can compare these materials intuitively and select out the suitable material as our recyclable and repairable printing materials. Although these materials all present accessibility for waste recycling, different mechanisms of dynamic covalent reactions determined their recycling conditions. Compared with transesterification-based material FA-Epoxy, disulfide-based materials have incomparable advantages in mild recycling conditions.

Beside dynamic covalent chemistry, the structures of polymer networks and the various formulas make a big difference in materials properties. From the polymer network structure, CADH-Epoxy with the bisphenol-based oxirane groups showed rigid polymer behavior due to the high crosslinking degree. In comparison, TEMPS-PU and DTDA-PU as the polyurethane-based polymer presented high elasticity due to their long chains and low crosslinking degree. In addition, from formulas of monomers with disulfide, DTDA-PU with aromatic disulfide bonds shows more stable thermal recyclability than TEMPS-PU with heterocyclic disulfide. After the comprehensive analysis and comparison, DTDA-PU printing material was selected as the research candidate for our study on sustainable 3D printing strategy due to its competitive mechanical properties, excellent printability and stable recyclability.

In order to further improve the printing performance and expand the applications of our printing strategy, MWCNTs-OH were introduced in DTDA-PU networks. The -OH groups of MWCNTs-OH participate in the reaction with IPDI and ensure the uniform distribution of MWCNTs in the DTDA-PU matrix. The evenly distributed MWCNTs-OH not only play the reinforcement role but also increase the polymer chain entanglement and cross-link density. Therefore, the solvent resistance and tensile strength of composite significantly improved with the increase of MWCNTs-OH contents.

In addition, MWCNTs, as the photothermal conversion material, provide a prime approach to precisely in-situ repair the printed parts. Spatiotemporal controllability is a strong advantage of light energy compared with other energy forms and allows localized repair of 3D printed parts without the structural damage. Based on the systemic analysis of the photothermal behavior of DTDA-PU/MWCNTs-OH composites, we put forward two repair procedures to deal with different structures of printed parts and varied damage situations. Moreover, to reduce the defective rate of printing parts and promote post-processing automation, a new approach of contactless supporting structure removal was demonstrated in this work in the end. This sustainable 3D printing strategy shows the trinity of recycling printing wastes, repairing damaged parts, reducing processing defects. We can envision that our work paves the way toward environmentally friendly, energy-efficient and highly customization revolutions in 3D printing technology.

## 7.2 Future Work

The major driving force of 3D printing technology development has been its promise of sustainable manufacturing. Our objective of this dissertation is to establish a sustainable 3D printing strategy to eliminate pollution of the environment and effectively utilize resources. Some recyclable and repairable 3D printing strategies have been reported in previous research works summarized in Chapter 1. However, most of the reported works are hard to achieve a compact and instant recycling and repair process. Although our work provides an accessible, energy-efficient approach for environmentally friendly 3D printing strategy via DIW printing of polyurethanes with dynamic disulfide bonds, a more universal solution for various types of printing materials and printing methods is still expected to adapt to all aspects of applications.

The FA-Epoxy, CADH-Epoxy and TEMPS-PU have certain defects separately as mentioned in Chapter 2 and Chapter 3. We think their further improvement is achievable.

The 3D printing of FA-Epoxy can be further studied with the development of printing technique. The high operation temperature and solvent evaporation should be the key issue that need to discuss. For the poor mechanical performance of CADH-Epoxy, beside changing the applications field, the addition of the chain-extenders could introduce the flexible segments in the epoxy resins to decrease degree of crosslinking and improve ductility. For the poor stability of TEMPS-PU under prolonged heating, the printing method adjustment from DIW 3D printing method to FDM 3D printing method may solve the problem. Unlike the DIW 3D printer used in this work, which was continuous heating the materials to remain the printable viscosity, FDM 3D printing will limit the heating area at the printing nozzle. This printing method will significantly reduce the material oxidation due to overheating.

Besides extrusion-based 3D printing method, photopolymerization based 3D printing technology is the most prevalent technique for the thermoset fabrication. Since its working mechanism is based on the polymerization of low viscosity photopolymers in the presence of photoinitiators, the printed component can only be thermoset polymers. Therefore, the recycling of this printing waste faces challenges. Based on our proposed extrusion-based disulfide-based printing materials, the polyurethane acrylate synthesis route with disulfide bonds can be designed and implemented. The predictable challenges should be centered on two aspects: the high viscosity of prepolymer due to the long chain of polyurethane acrylate and the disulfide bond stability under high energy density UV light exposure. Thus, it will be necessary to choose diluent and photoinitiators selectively.

# References

[1] K. Hitomi, "Manufacturing strategy for future production moving toward manufacturing excellence," *International journal of technology management,* vol. 14, no. 6-8, pp. 701-711, 1997.

[2] K. Hitomi, *Manufacturing systems engineering: a unified approach to manufacturing technology, production management and industrial economics*. Routledge, 2017.

[3] H. W. Stoll, "Design for manufacture: an overview," 1986.

[4] A. B. Badiru, *Handbook of industrial and systems engineering*. CRC Press, 2005.

[5] F. Jovane *et al.*, "The incoming global technological and industrial revolution towards competitive sustainable manufacturing," *CIRP annals,* vol. 57, no. 2, pp. 641-659, 2008.

[6] A. Skowroński, "A civilization based on sustainable development: its limits and prospects," *Sustainable Development,* vol. 16, no. 2, pp. 117-125, 2008.

[7] S. Imperatives, "Report of the World Commission on Environment and Development: Our common future," *Accessed Feb,* vol. 10, 1987.

[8] R. Emas, "The concept of sustainable development: definition and defining principles," *Brief for GSDR,* vol. 2015, 2015.

[9] A. Jayal, F. Badurdeen, O. Dillon Jr, and I. Jawahir, "Sustainable manufacturing: Modeling and optimization challenges at the product, process and system levels," *CIRP Journal of Manufacturing Science and Technology,* vol. 2, no. 3, pp. 144-152, 2010.

[10] I. Jawahir and O. Dillon Jr, "Sustainable manufacturing processes: new challenges for developing predictive models and optimization techniques," in *Proceedings of the first international conference on sustainable manufacturing, Montreal, Canada*, 2007, pp. 1-19.

[11] B. P. Conner *et al.*, "Making sense of 3-D printing: Creating a map of additive manufacturing products and services," *Additive Manufacturing,* vol. 1, pp. 64-76, 2014.

[12] D. Chen, S. Heyer, S. Ibbotson, K. Salonitis, J. G. Steingrímsson, and S. Thiede, "Direct digital manufacturing: definition, evolution, and sustainability implications," *Journal of Cleaner Production,* vol. 107, pp. 615-625, 2015.

[13] S. H. Huang, P. Liu, A. Mokasdar, and L. Hou, "Additive manufacturing and its societal impact: a literature review," *The International Journal of Advanced Manufacturing Technology,* vol. 67, no. 5-8, pp. 1191-1203, 2013.

[14] S. Ford and M. Despeisse, "Additive manufacturing and sustainability: an exploratory study of the advantages and challenges," *Journal of cleaner Production,* vol. 137, pp. 1573-1587, 2016.

[15] C. Kohtala, "Addressing sustainability in research on distributed production: an integrated literature review," *Journal of Cleaner Production,* vol. 106, pp. 654-668, 2015.

[16] I. Astm, "ASTM52900-15 Standard Terminology for Additive Manufacturing—General Principles—Terminology," *ASTM International, West Conshohocken, PA,* vol. 3, no. 4, p. 5, 2015.

[17] A. Ambrosi and M. Pumera, "3D-printing technologies for electrochemical applications," *Chemical Society Reviews,* vol. 45, no. 10, pp. 2740-2755, 2016.

[18] H. Lipson, "Standard specification for additive manufacturing file format (AMF) version 1.1," *ASTM International,* vol. 10, 2013.

[19] T. D. Ngo, A. Kashani, G. Imbalzano, K. T. Nguyen, and D. Hui, "Additive manufacturing (3D printing): A review of materials, methods, applications and challenges," *Composites Part B: Engineering,* vol. 143, pp. 172-196, 2018.

[20] H. Bikas, P. Stavropoulos, and G. Chryssolouris, "Additive manufacturing methods and modelling approaches: a critical review," *The International Journal of Advanced Manufacturing Technology,* vol. 83, no. 1-4, pp. 389-405, 2016.

[21] F. Causa, P. A. Netti, and L. Ambrosio, "A multi-functional scaffold for tissue regeneration: the need to engineer a tissue analogue," *Biomaterials,* vol. 28, no. 34, pp. 5093-5099, 2007.

[22] B. Derby, "Printing and prototyping of tissues and scaffolds," *Science,* vol. 338, no. 6109, pp. 921-926, 2012.

[23] M. D. Symes *et al.*, "Integrated 3D-printed reactionware for chemical synthesis and analysis," *Nature chemistry,* vol. 4, no. 5, pp. 349-354, 2012.

[24] C. W. Hull, "Apparatus for production of three-dimensional objects by stereolithography," ed: Google Patents, 1986.

[25] E. MacDonald and R. Wicker, "Multiprocess 3D printing for increasing component functionality," *Science*, vol. 353, no. 6307, 2016.

[26] F. Calignano *et al.*, "Overview on additive manufacturing technologies," *Proceedings of the IEEE*, vol. 105, no. 4, pp. 593-612, 2017.

[27] T. Marquardt and E. Zheng, "History of 3D printing," *Fonte: Maker Space: https://blogs. lawrence. edu/makerspace/history/Monnerat, H*, 2012.

[28] Y. He, Y. Wu, J. z. Fu, Q. Gao, and J. j. Qiu, "Developments of 3D printing microfluidics and applications in chemistry and biology: a review," *Electroanalysis,* vol. 28, no. 8, pp. 1658-1678, 2016.

[29] J. R. Tumbleston *et al.*, "Continuous liquid interface production of 3D objects," *Science*, vol. 347, no. 6228, pp. 1349-1352, 2015.

[30] A. Bagheri and J. Jin, "Photopolymerization in 3D printing," *ACS Applied Polymer Materials,* vol. 1, no. 4, pp. 593-611, 2019.

[31] M. Zarek, M. Layani, I. Cooperstein, E. Sachyani, D. Cohn, and S. Magdassi, "3D printing of shape memory polymers for flexible electronic devices," *Advanced Materials,* vol. 28, no. 22, pp. 4449-4454, 2016.

[32] B. Berman, "3-D printing: The new industrial revolution," *Business horizons,* vol. 55, no. 2, pp. 155-162, 2012.

[33] M. Feygin and S. S. Pak, "Laminated object manufacturing apparatus and method," ed: Google Patents, 1999.

[34] M. Feygin and B. Hsieh, "Laminated object manufacturing (LOM): a simpler process," in *1991 International Solid Freeform Fabrication Symposium*, 1991.

[35] H. Windsheimer, N. Travitzky, A. Hofenauer, and P. Greil, "Laminated Object Manufacturing of Preceramic ‐ Paper ‐ Derived Si? SiC Composites," *Advanced Materials,* vol. 19, no. 24, pp. 4515-4519, 2007.

[36] I. Gibson, D. W. Rosen, and B. Stucker, "Sheet lamination processes," in *Additive Manufacturing Technologies*: Springer, 2010, pp. 223-252.

[37] R. Dehoff and S. Babu, "Characterization of interfacial microstructures in 3003 aluminum alloy blocks fabricated by ultrasonic additive manufacturing," *Acta Materialia,* vol. 58, no. 13, pp. 4305-4315, 2010.

[38] P. M. Bhatt, A. M. Kabir, M. Peralta, H. A. Bruck, and S. K. Gupta, "A robotic cell for performing sheet lamination-based additive manufacturing," *Additive Manufacturing*, vol. 27, pp. 278-289, 2019.

[39] C. R. Deckard, "Method and apparatus for producing parts by selective sintering," ed: Google Patents, 1989.

[40] M. Grasso and B. M. Colosimo, "Process defects and in situ monitoring methods in metal powder bed fusion: a review," *Measurement Science and Technology,* vol. 28, no. 4, p. 044005, 2017.

[41] X. Xu, S. Meteyer, N. Perry, and Y. F. Zhao, "Energy consumption model of Binder-jetting additive manufacturing processes," *International Journal of Production Research,* vol. 53, no. 23, pp. 7005-7015, 2015.

[42] E. Sachs, M. Cima, P. Williams, D. Brancazio, and J. Cornie, "Three dimensional printing: rapid tooling and prototypes directly from a CAD model," 1992.

[43] H. Fayazfar *et al.*, "A critical review of powder-based additive manufacturing of ferrous alloys: Process parameters, microstructure and mechanical properties," *Materials & Design,* vol. 144, pp. 98-128, 2018.

[44] Y. Bai and C. B. Williams, "An exploration of binder jetting of copper," *Rapid Prototyping Journal,* 2015.

[45] A. Bailey, A. Merriman, A. Elliott, and M. Basti, "Preliminary testing of nanoparticle effectiveness in binder jetting applications," in *27th Annual International Solid Freeform Fabrication Symposium,* 2016, pp. 1069-1077.

[46] P. Bidare, I. Bitharas, R. Ward, M. Attallah, and A. J. Moore, "Fluid and particle dynamics in laser powder bed fusion," *Acta Materialia,* vol. 142, pp. 107-120, 2018.

[47] M. Ziaee and N. B. Crane, "Binder jetting: A review of process, materials, and methods," *Additive Manufacturing,* vol. 28, pp. 781-801, 2019.

[48] M. Molitch-Hou, "Overview of additive manufacturing process," in *Additive Manufacturing*: Elsevier, 2018, pp. 1-38.

[49] T. Wang, Y. Zhu, S. Zhang, H. Tang, and H. Wang, "Grain morphology evolution behavior of titanium alloy components during laser melting deposition additive manufacturing," *Journal of Alloys and Compounds,* vol. 632, pp. 505-513, 2015.

[50] R. Koike *et al.*, "Graphical evaluation method for void distribution in direct energy deposition," *Procedia Manuf,* vol. 6, pp. 105-112, 2016.

[51] F. Li, Z. Wang, and X. Zeng, "Microstructures and mechanical properties of Ti6Al4V alloy fabricated by multi-laser beam selective laser melting," *Materials Letters,* vol. 199, pp. 79-83, 2017.

[52] I. Gibson, D. W. Rosen, and B. Stucker, "Guidelines for process selection," in *Additive Manufacturing Technologies*: Springer, 2010, pp. 333-356.

[53] G. B. Kim *et al.*, "Three-dimensional printing: basic principles and applications in medicine and radiology," *Korean journal of radiology,* vol. 17, no. 2, pp. 182-197, 2016.

[54] X. Shen and H. E. Naguib, "A robust ink deposition system for binder jetting and material jetting," *Additive Manufacturing*, vol. 29, p. 100820, 2019.

[55] Y. L. Yap, C. Wang, S. L. Sing, V. Dikshit, W. Y. Yeong, and J. Wei, "Material jetting additive manufacturing: An experimental study using designed metrological benchmarks," *Precision engineering*, vol. 50, pp. 275-285, 2017.

[56] J. Dilag, T. Chen, S. Li, and S. A. Bateman, "Design and direct additive manufacturing of three-dimensional surface micro-structures using material jetting technologies," *Additive Manufacturing*, vol. 27, pp. 167-174, 2019.

[57] B. J. De Gans, P. C. Duineveld, and U. S. Schubert, "Inkjet printing of polymers: state of the art and future developments," *Advanced materials*, vol. 16, no. 3, pp. 203-213, 2004.

[58] J. Z. Gul *et al.*, "3D printing for soft robotics–a review," *Science and Technology of advanced MaTerialS*, vol. 19, no. 1, pp. 243-262, 2018.

[59] J. Pearce, C. Blair, K. Laciak, R. Andrews, A. Nosrat, and I. Zelenika-Zovko, "3-D printing of open source appropriate technologies for self-directed sustainable development," 2010.

[60] D. Bourell *et al.*, "Materials for additive manufacturing," *CIRP Annals*, vol. 66, no. 2, pp. 659-681, 2017.

[61] S. Singh, S. Ramakrishna, and R. Singh, "Material issues in additive manufacturing: A review," *Journal of Manufacturing Processes*, vol. 25, pp. 185-200, 2017.

[62] D. Herzog, V. Seyda, E. Wycisk, and C. Emmelmann, "Additive manufacturing of metals," *Acta Materialia,* vol. 117, pp. 371-392, 2016.

[63] T. Debroy *et al.*, "Scientific, technological and economic issues in metal printing and their solutions," *Nature materials,* p. 1, 2019.

[64] A. Deshpande and K. Hsu, "Acoustoplastic metal direct-write: towards solid aluminum 3D printing in ambient conditions," *Additive Manufacturing,* vol. 19, pp. 73-80, 2018.

[65] C. Buchanan and L. Gardner, "Metal 3D printing in construction: A review of methods, research, applications, opportunities and challenges," *Engineering Structures,* vol. 180, pp. 332-348, 2019.

[66] S. Morsali *et al.*, "Multi-physics simulation of metal printing at micro/nanoscale using meniscus-confined electrodeposition: Effect of nozzle speed and diameter," *Journal of Applied Physics,* vol. 121, no. 21, p. 214305, 2017.

[67] N. T. Aboulkhair, M. Simonelli, L. Parry, I. Ashcroft, C. Tuck, and R. Hague, "3D printing of Aluminium alloys: Additive Manufacturing of Aluminium alloys using selective laser melting," *Progress in Materials Science,* vol. 106, p. 100578, 2019.

[68] J. H. Martin, B. D. Yahata, J. M. Hundley, J. A. Mayer, T. A. Schaedler, and T. M. Pollock, "3D printing of high-strength aluminium alloys," *Nature,* vol. 549, no. 7672, pp. 365-369, 2017.

[69] L. Zhou *et al.*, "Microstructure and tensile property of a novel AlZnMgScZr alloy additively manufactured by gas atomization and laser powder bed fusion," *Scripta Materialia,* vol. 158, pp. 24-28, 2019.

[70] X. Wang, Q. Guo, X. Cai, S. Zhou, B. Kobe, and J. Yang, "Initiator-integrated 3D printing enables the formation of complex metallic architectures," *ACS applied materials & interfaces,* vol. 6, no. 4, pp. 2583-2587, 2014.

[71] D. Zhang, J. Xiao, Y. Qiu, J. Yang, and Q. Guo, "Initiator-integrated 3-D printing of magnetic object for remote controlling application," *IEEE Transactions on Magnetics,* vol. 53, no. 5, pp. 1-9, 2017.

[72] D. Zhang, J. Xiao, W. Yu, Q. Guo, and J. Yang, "Hierarchical metal/polymer metamaterials of tunable negative Poisson’s ratio fabricated by initiator-integrated 3D printing (i3DP)," *Nanotechnology,* vol. 29, no. 50, p. 505704, 2018.

[73] C. Xu, B. Quinn, L. L. Lebel, D. Therriault, and G. L’Espérance, "Multi-material direct ink writing (DIW) for complex 3D metallic structures with removable supports," *ACS applied materials & interfaces,* vol. 11, no. 8, pp. 8499-8506, 2019.

[74] Y. Wen *et al.*, "3D printed porous ceramic scaffolds for bone tissue engineering: a review," *Biomaterials science,* vol. 5, no. 9, pp. 1690-1698, 2017.

[75] N. Travitzky *et al.*, "Additive manufacturing of ceramic ‐ based materials," *Advanced engineering materials,* vol. 16, no. 6, pp. 729-754, 2014.

[76] I. Cooperstein, S. C. Indukuri, A. Bouketov, U. Levy, and S. Magdassi, "3D Printing of Micrometer ‐ Sized Transparent Ceramics with On ‐ Demand Optical ‐ Gain Properties," *Advanced Materials,* p. 2001675, 2020.

[77] Z. Weng, J. Wang, T. Senthil, and L. Wu, "Mechanical and thermal properties of ABS/montmorillonite nanocomposites for fused deposition modeling 3D printing," *Materials & Design,* vol. 102, pp. 276-283, 2016.

[78] C.-C. Kuo *et al.*, "Preparation of starch/acrylonitrile-butadiene-styrene copolymers (ABS) biomass alloys and their feasible evaluation for 3D printing applications," *Composites Part B: Engineering,* vol. 86, pp. 36-39, 2016.

[79] Q. Chen, J. D. Mangadlao, J. Wallat, A. De Leon, J. K. Pokorski, and R. C. Advincula, "3D printing biocompatible polyurethane/poly (lactic acid)/graphene oxide nanocomposites: anisotropic properties," *ACS applied materials & interfaces,* vol. 9, no. 4, pp. 4015-4023, 2017.

[80] Z. Liu, Y. Wang, B. Wu, C. Cui, Y. Guo, and C. Yan, "A critical review of fused deposition modeling 3D printing technology in manufacturing polylactic acid parts," *The International Journal of Advanced Manufacturing Technology,* vol. 102, no. 9-12, pp. 2877-2889, 2019.

[81] N. B. Palaganas *et al.*, "3D printing of photocurable cellulose nanocrystal composite for fabrication of complex architectures via stereolithography," *ACS applied materials & interfaces,* vol. 9, no. 39, pp. 34314-34324, 2017.

[82] A. Chiappone *et al.*, "3D printed PEG-based hybrid nanocomposites obtained by sol–gel technique," *ACS applied materials & interfaces,* vol. 8, no. 8, pp. 5627-5633, 2016.

[83] R. Liska *et al.*, "Photopolymers for rapid prototyping," *Journal of Coatings Technology and Research,* vol. 4, no. 4, pp. 505-510, 2007.

[84] J. Yue *et al.*, "3D‐Printable antimicrobial composite resins," *Advanced functional materials,* vol. 25, no. 43, pp. 6756-6767, 2015.

[85] A. Al Mousawi *et al.*, "3-Hydroxyflavone and N-phenylglycine in high performance photoinitiating systems for 3D printing and photocomposites synthesis," *Macromolecules,* vol. 51, no. 12, pp. 4633-4641, 2018.

[86] A. Al Mousawi *et al.*, "Carbazole derivatives with thermally activated delayed fluorescence property as photoinitiators/photoredox catalysts for LED 3D printing technology," *Macromolecules,* vol. 50, no. 13, pp. 4913-4926, 2017.

[87] C. Decker, T. N. T. Viet, D. Decker, and E. Weber-Koehl, "UV-radiation curing of acrylate/epoxide systems," *Polymer,* vol. 42, no. 13, pp. 5531-5541, 2001.

[88] S. C. Ligon-Auer, M. Schwentenwein, C. Gorsche, J. Stampfl, and R. Liska, "Toughening of photo-curable polymer networks: a review," *Polymer Chemistry,* vol. 7, no. 2, pp. 257-286, 2016.

[89] J. J. Martin, B. E. Fiore, and R. M. Erb, "Designing bioinspired composite reinforcement architectures via 3D magnetic printing," *Nature communications,* vol. 6, no. 1, pp. 1-7, 2015.

[90] L. S. Dimas, G. H. Bratzel, I. Eylon, and M. J. Buehler, "Tough composites inspired by mineralized natural materials: computation, 3D printing, and testing," *Advanced Functional Materials,* vol. 23, no. 36, pp. 4629-4638, 2013.

[91] A. V. Do, B. Khorsand, S. M. Geary, and A. K. Salem, "3D printing of scaffolds for tissue regeneration applications," *Advanced healthcare materials,* vol. 4, no. 12, pp. 1742-1762, 2015.

[92] H.-W. Kang, S. J. Lee, I. K. Ko, C. Kengla, J. J. Yoo, and A. Atala, "A 3D bioprinting system to produce human-scale tissue constructs with structural integrity," *Nature biotechnology,* vol. 34, no. 3, pp. 312-319, 2016.

[93] S. Tibbits, "4D printing: multi‐material shape change," *Architectural Design,* vol. 84, no. 1, pp. 116-121, 2014.

[94] Q. Ge, A. H. Sakhaei, H. Lee, C. K. Dunn, N. X. Fang, and M. L. Dunn, "Multimaterial 4D printing with tailorable shape memory polymers," *Scientific reports,* vol. 6, p. 31110, 2016.

[95] M. Zarek, N. Mansour, S. Shapira, and D. Cohn, "4D printing of shape memory ‐ based personalized endoluminal medical devices," *Macromolecular rapid communications,* vol. 38, no. 2, p. 1600628, 2017.

[96] D. Kokkinis, M. Schaffner, and A. R. Studart, "Multimaterial magnetically assisted 3D printing of composite materials," *Nature communications,* vol. 6, no. 1, pp. 1-10, 2015.

[97] K. Malachowski *et al.*, "Stimuli ‐ responsive theragrippers for chemomechanical controlled release," *Angewandte Chemie International Edition,* vol. 53, no. 31, pp. 8045-8049, 2014.

[98] S. E. Bakarich, R. Gorkin III, M. I. H. Panhuis, and G. M. Spinks, "4D printing with mechanically robust, thermally actuating hydrogels," *Macromolecular rapid communications,* vol. 36, no. 12, pp. 1211-1217, 2015.

[99] A. S. Gladman, E. A. Matsumoto, R. G. Nuzzo, L. Mahadevan, and J. A. Lewis, "Biomimetic 4D printing," *Nature materials,* vol. 15, no. 4, pp. 413-418, 2016.

[100] S. C. Ligon, R. Liska, J. r. Stampfl, M. Gurr, and R. Mülhaupt, "Polymers for 3D printing and customized additive manufacturing," *Chemical reviews,* vol. 117, no. 15, pp. 10212-10290, 2017.

[101] T. Li, J. Aspler, A. Kingsland, L. M. Cormier, and X. Zou, "3d printing–a review of technologies, markets, and opportunities for the forest industry," *J. Sci. Technol. For. Prod. Process,* vol. 5, no. 2, p. 30, 2016.

[102] M. Hong and E. Y.-X. Chen, "Chemically recyclable polymers: a circular economy approach to sustainability," *Green Chemistry,* vol. 19, no. 16, pp. 3692-3706, 2017.

[103] J. M. Winne, L. Leibler, and F. E. Du Prez, "Dynamic covalent chemistry in polymer networks: a mechanistic perspective," *Polymer Chemistry,* vol. 10, no. 45, pp. 6091-6108, 2019.

[104] J. Deng *et al.*, "Vitrimer Elastomer‐Based Jigsaw Puzzle‐Like Healable Triboelectric Nanogenerator for Self‐Powered Wearable Electronics," *Advanced Materials,* 2018.

[105] Z. Yang, Q. Wang, and T. Wang, "Dual-triggered and thermally reconfigurable shape memory graphene-vitrimer composites," *ACS applied materials & interfaces,* vol. 8, no. 33, pp. 21691-21699, 2016.

[106] Q.-T. Li *et al.*, "Photothermal conversion triggered precisely targeted healing of epoxy resin based on thermoreversible diels–alder network and amino-functionalized carbon nanotubes," *ACS applied materials & interfaces,* vol. 9, no. 24, pp. 20797-20807, 2017.

[107] W. Denissen, J. M. Winne, and F. E. Du Prez, "Vitrimers: permanent organic networks with glass-like fluidity," *Chemical Science,* vol. 7, no. 1, pp. 30-38, 2016.

[108] C. J. Kloxin, T. F. Scott, B. J. Adzima, and C. N. Bowman, "Covalent adaptable networks (CANs): a unique paradigm in cross-linked polymers," *Macromolecules,* vol. 43, no. 6, pp. 2643-2653, 2010.

[109] Y. Jin, C. Yu, R. J. Denman, and W. Zhang, "Recent advances in dynamic covalent chemistry," *Chemical Society Reviews,* vol. 42, no. 16, pp. 6634-6654, 2013.

[110] C. J. Kloxin and C. N. Bowman, "Covalent adaptable networks: smart, reconfigurable and responsive network systems," *Chemical Society Reviews,* vol. 42, no. 17, pp. 7161-7173, 2013.

[111] W. Zou, J. Dong, Y. Luo, Q. Zhao, and T. Xie, "Dynamic covalent polymer networks: from old chemistry to modern day innovations," *Advanced Materials,* vol. 29, no. 14, p. 1606100, 2017.

[112] M. Stern and A. Tobolsky, "Stress-time-temperature relations in polysulfide rubbers," *Rubber Chemistry and Technology,* vol. 19, no. 4, pp. 1178-1192, 1946.

[113] A. V. Tobolsky, "Stress relaxation studies of the viscoelastic properties of polymers," *Journal of Applied Physics,* vol. 27, no. 7, pp. 673-685, 1956.

[114] R. Osthoff, A. Bueche, and W. Grubb, "Chemical stress-relaxation of polydimethylsiloxane elastomers1," *Journal of the American Chemical Society,* vol. 76, no. 18, pp. 4659-4663, 1954.

[115] P. Zheng and T. J. McCarthy, "A surprise from 1954: siloxane equilibration is a simple, robust, and obvious polymer self-healing mechanism," *Journal of the American Chemical Society,* vol. 134, no. 4, pp. 2024-2027, 2012.

[116] A. M. Asadirad, S. p. Boutault, Z. Erno, and N. R. Branda, "Controlling a polymer adhesive using light and a molecular switch," *Journal of the American Chemical Society,* vol. 136, no. 8, pp. 3024-3027, 2014.

[117] P. A. Pratama, M. Sharifi, A. M. Peterson, and G. R. Palmese, "Room temperature self-healing thermoset based on the Diels–Alder reaction," *ACS applied materials & interfaces,* vol. 5, no. 23, pp. 12425-12431, 2013.

[118] R. Nishiyabu, Y. Kubo, T. D. James, and J. S. Fossey, "Boronic acid building blocks: tools for self assembly," *Chemical Communications,* vol. 47, no. 4, pp. 1124-1150, 2011.

[119] L. Zhu, S. H. Shabbir, M. Gray, V. M. Lynch, S. Sorey, and E. V. Anslyn, "A Structural Investigation of the N− B Interaction in an o-(N, N-Dialkylaminomethyl) arylboronate System," *Journal of the American Chemical Society,* vol. 128, no. 4, pp. 1222-1232, 2006.

[120] D. Montarnal, M. Capelot, F. Tournilhac, and L. Leibler, "Silica-like malleable materials from permanent organic networks," *Science,* vol. 334, no. 6058, pp. 965-968, 2011.

[121] M. Capelot, D. Montarnal, F. Tournilhac, and L. Leibler, "Metal-catalyzed transesterification for healing and assembling of thermosets," *Journal of the american chemical society,* vol. 134, no. 18, pp. 7664-7667, 2012.

[122] Z. Q. Lei, H. P. Xiang, Y. J. Yuan, M. Z. Rong, and M. Q. Zhang, "Room-temperature self-healable and remoldable cross-linked polymer based on the dynamic exchange of disulfide bonds," *Chemistry of Materials,* vol. 26, no. 6, pp. 2038-2046, 2014.

[123] W. M. Xu, M. Z. Rong, and M. Q. Zhang, "Sunlight driven self-healing, reshaping and recycling of a robust, transparent and yellowing-resistant polymer," *Journal of Materials Chemistry A,* vol. 4, no. 27, pp. 10683-10690, 2016.

[124] P. Vongvilai, M. Angelin, R. Larsson, and O. Ramström, "Dynamic combinatorial resolution: direct asymmetric lipase ‐ mediated screening of a dynamic nitroaldol library," *Angewandte Chemie,* vol. 119, no. 6, pp. 966-968, 2007.

[125] H. Seki, S. Kuwabara, H. Kudo, and T. Nishikubo, "Condensation reaction of phenols with 1, 5-pentanedial for synthesis of noria-like ladder-cyclic oligomer by dynamic covalent chemistry mechanism," *Chemistry Letters,* vol. 40, no. 5, pp. 464-466, 2011.

[126] G. C. Vougioukalakis and R. H. Grubbs, "Ruthenium-based heterocyclic carbene-coordinated olefin metathesis catalysts," *Chemical reviews,* vol. 110, no. 3, pp. 1746-1787, 2010.

[127] C. Zhang, Q. Wang, H. Long, and W. Zhang, "A highly C70 selective shape-persistent rectangular prism constructed through one-step alkyne metathesis," *Journal of the American Chemical Society,* vol. 133, no. 51, pp. 20995-21001, 2011.

[128] J. P. Moerdyk and C. W. Bielawski, "Diamidocarbenes as versatile and reversible [2+ 1] cycloaddition reagents," *Nature Chemistry,* vol. 4, no. 4, pp. 275-280, 2012.

[129] K. C. Nicolaou, S. A. Snyder, T. Montagnon, and G. Vassilikogiannakis, "The Diels–Alder reaction in total synthesis," *Angewandte Chemie International Edition,* vol. 41, no. 10, pp. 1668-1698, 2002.

[130] X. Chen *et al.*, "A thermally re-mendable cross-linked polymeric material," *Science,* vol. 295, no. 5560, pp. 1698-1702, 2002.

[131] P. Du, X. Liu, Z. Zheng, X. Wang, T. Joncheray, and Y. Zhang, "Synthesis and characterization of linear self-healing polyurethane based on thermally reversible Diels–Alder reaction," *RSC advances,* vol. 3, no. 35, pp. 15475-15482, 2013.

[132] Y.-L. Liu, C.-Y. Hsieh, and Y.-W. Chen, "Thermally reversible cross-linked polyamides and thermo-responsive gels by means of Diels–Alder reaction," *Polymer,* vol. 47, no. 8, pp. 2581-2586, 2006.

[133] L. Polgar, M. Van Duin, A. Broekhuis, and F. Picchioni, "Use of Diels–Alder chemistry for thermoreversible cross-linking of rubbers: the next step toward

recycling of rubber products?," *Macromolecules,* vol. 48, no. 19, pp. 7096-7105, 2015.

[134] J. P. Brutman, P. A. Delgado, and M. A. Hillmyer, "Polylactide vitrimers," *ACS Macro Letters,* vol. 3, no. 7, pp. 607-610, 2014.

[135] A. Rekondo, R. Martin, A. R. de Luzuriaga, G. Cabañero, H. J. Grande, and I. Odriozola, "Catalyst-free room-temperature self-healing elastomers based on aromatic disulfide metathesis," *Materials Horizons,* vol. 1, no. 2, pp. 237-240, 2014.

[136] J. Canadell, H. Goossens, and B. Klumperman, "Self-healing materials based on disulfide links," *Macromolecules,* vol. 44, no. 8, pp. 2536-2541, 2011.

[137] P. Chakma and D. Konkolewicz, "Dynamic covalent bonds in polymeric materials," *Angewandte Chemie International Edition,* vol. 58, no. 29, pp. 9682-9695, 2019.

[138] S. P. Black, J. K. Sanders, and A. R. Stefankiewicz, "Disulfide exchange: exposing supramolecular reactivity through dynamic covalent chemistry," *Chemical Society Reviews,* vol. 43, no. 6, pp. 1861-1872, 2014.

[139] J. Bennett, H. Sieper, and P. Tavs, "2, 2, 6, 6-tetramethylpiperidyl-1-thiyl: A stable new radical," *Tetrahedron,* vol. 23, no. 4, pp. 1697-1699, 1967.

[140] B. D. Fairbanks, S. P. Singh, C. N. Bowman, and K. S. Anseth, "Photodegradable, photoadaptable hydrogels via radical-mediated disulfide fragmentation reaction," *Macromolecules,* vol. 44, no. 8, pp. 2444-2450, 2011.

[141] D. Habault, H. Zhang, and Y. Zhao, "Light-triggered self-healing and shape-memory polymers," *Chemical Society Reviews,* vol. 42, no. 17, pp. 7244-7256, 2013.

[142] B. T. Michal, C. A. Jaye, E. J. Spencer, and S. J. Rowan, "Inherently photohealable and thermal shape-memory polydisulfide networks," *ACS Macro Letters,* vol. 2, no. 8, pp. 694-699, 2013.

[143] C. B. Highley, C. B. Rodell, and J. A. Burdick, "Direct 3D printing of shear‐thinning hydrogels into self‐healing hydrogels," *Advanced Materials,* vol. 27, no. 34, pp. 5075-5079, 2015.

[144] M. Fevre, G. O. Jones, M. Zhang, J. M. García, and J. L. Hedrick, "Melt‐Processable Dynamic‐Covalent Poly (hemiaminal) Organogels as Scaffolds for UV‐Induced Polymerization," *Advanced Materials,* vol. 27, no. 32, pp. 4714-4718, 2015.

[145] J. R. Davidson, G. A. Appuhamillage, C. M. Thompson, W. Voit, and R. A. Smaldone, "Design paradigm utilizing reversible Diels–Alder reactions to enhance the mechanical properties of 3D printed materials," *ACS applied materials & interfaces,* vol. 8, no. 26, pp. 16961-16966, 2016.

[146] K. Yang *et al.*, "Diels–Alder reversible thermoset 3D printing: isotropic thermoset polymers via fused filament fabrication," *Advanced Functional Materials,* vol. 27, no. 24, p. 1700318, 2017.

[147] N. Zheng *et al.*, "Mechano‐Plastic Pyrolysis of Dynamic Covalent Polymer Network toward Hierarchical 3D Ceramics," *Advanced Materials,* vol. 31, no. 11, p. 1807326, 2019.

[148] X. Li *et al.*, "Self-healing polyurethane elastomers based on a disulfide bond by digital light processing 3D printing," *ACS Macro Letters,* vol. 8, no. 11, pp. 1511-1516, 2019.

[149] Q. Shi *et al.*, "Recyclable 3D printing of vitrimer epoxy," (in English), *Materials Horizons,* vol. 4, no. 4, pp. 598-607, Jul 1 2017.

[150] B. Zhang, K. Kowsari, A. Serjouei, M. L. Dunn, and Q. Ge, "Reprocessable thermosets for sustainable three-dimensional printing," *Nature communications,* vol. 9, no. 1, pp. 1-7, 2018.

[151] Y. Zhang, X.-Y. Yin, M. Zheng, C. Moorlag, J. Yang, and Z. L. Wang, "3D printing of thermoreversible polyurethanes with targeted shape memory and precise in situ self-healing properties," *Journal of Materials Chemistry A,* vol. 7, no. 12, pp. 6972-6984, 2019.

[152] J. A. Lewis, "Direct ink writing of 3D functional materials," *Advanced Functional Materials,* vol. 16, no. 17, pp. 2193-2204, 2006.

[153] J. Zhang, C. Li, Y. Wang, R.-X. Zhuo, and X.-Z. Zhang, "Controllable exploding microcapsules as drug carriers," *Chemical Communications*, vol. 47, no. 15, pp. 4457-4459, 2011.

[154] V. G. Rocha, E. Saiz, I. S. Tirichenko, and E. García-Tuñón, "Direct ink writing advances in multi-material structures for a sustainable future," *Journal of Materials Chemistry A*, vol. 8, no. 31, pp. 15646-15657, 2020.

[155] P. R. Griffiths and J. A. De Haseth, *Fourier transform infrared spectrometry*. John Wiley & Sons, 2007.

[156] N. E. Zafeiropoulos, *Interface engineering of natural fibre composites for maximum performance*. Elsevier, 2011.

[157] Y. Picó, *Chemical analysis of food: Techniques and applications*. Academic Press, 2012.

[158] O. Olabisi and K. Adewale, *Handbook of thermoplastics*. CRC press, 2016.

[159] T. Wu *et al.*, "Additively manufacturing high-performance bismaleimide architectures with ultraviolet-assisted direct ink writing," *Materials & Design*, vol. 180, p. 107947, 2019.

[160] D. Ratna, *Handbook of thermoset resins*. ISmithers Shawbury, UK, 2009.

[161] S. J. Rowan, S. J. Cantrill, G. R. Cousins, J. K. Sanders, and J. F. Stoddart, "Dynamic covalent chemistry," *Angewandte Chemie International Edition*, vol. 41, no. 6, pp. 898-952, 2002.

[162] W. Zhang and Y. Jin, *Dynamic covalent chemistry: principles, reactions, and applications*. John Wiley & Sons, 2017.

[163] J. M. Lehn, "Dynamic combinatorial chemistry and virtual combinatorial libraries," *Chemistry–A European Journal,* vol. 5, no. 9, pp. 2455-2463, 1999.

[164] T. Maeda, H. Otsuka, and A. Takahara, "Dynamic covalent polymers: reorganizable polymers with dynamic covalent bonds," *Progress in Polymer Science,* vol. 34, no. 7, pp. 581-604, 2009.

[165] J. Hu, S. K. Gupta, J. Ozdemir, and M. H. Beyzavi, "Applications of Dynamic Covalent Chemistry Concept toward Tailored Covalent Organic Framework Nanomaterials: A Review," *ACS Applied Nano Materials,* vol. 3, no. 7, pp. 6239-6269, 2020.

[166] W. Dang, M. Kubouchi, S. Yamamoto, H. Sembokuya, and K. Tsuda, "An approach to chemical recycling of epoxy resin cured with amine using nitric acid," *Polymer,* vol. 43, no. 10, pp. 2953-2958, 2002.

[167] Y. Sato, Y. Kondo, K. Tsujita, and N. Kawai, "Degradation behaviour and recovery of bisphenol-A from epoxy resin and polycarbonate resin by liquid-phase chemical recycling," *Polymer Degradation and Stability,* vol. 89, no. 2, pp. 317-326, 2005.

[168] S. Hirose, T. Hatakeyama, and H. Hatakeyama, "Glass transition and thermal decomposition of epoxy resins from the carboxylic acid system consisting of ester-carboxylic acid derivatives of alcoholysis lignin and ethylene glycol with

various dicarboxylic acids," *Thermochimica acta*, vol. 431, no. 1-2, pp. 76-80, 2005.

[169] A. Cherdoud‐Chihani, M. Mouzali, and M. Abadie, "Study of crosslinking acid copolymer/DGEBA systems by FTIR," *Journal of applied polymer science,* vol. 87, no. 13, pp. 2033-2051, 2003.

[170] Q. Shi, K. Yu, M. L. Dunn, T. Wang, and H. J. Qi, "Solvent assisted pressure-free surface welding and reprocessing of malleable epoxy polymers," *Macromolecules,* vol. 49, no. 15, pp. 5527-5537, 2016.

[171] C. Ramírez, M. Rico, A. Torres, L. Barral, J. López, and B. Montero, "Epoxy/POSS organic–inorganic hybrids: ATR-FTIR and DSC studies," *European Polymer Journal*, vol. 44, no. 10, pp. 3035-3045, 2008.

[172] M. G. González, J. C. Cabanelas, and J. Baselga, "Applications of FTIR on epoxy resins-identification, monitoring the curing process, phase separation and water uptake," *Infrared Spectroscopy-Materials Science, Engineering and Technology,* vol. 2, pp. 261-284, 2012.

[173] S. Bauhuber, C. Hozsa, M. Breunig, and A. Göpferich, "Delivery of nucleic acids via disulfide‐based carrier systems," *Advanced Materials,* vol. 21, no. 32‐33, pp. 3286-3306, 2009.

[174] C. Xu, Y. Huang, L. Tang, and Y. Hong, "Low-initial-modulus biodegradable polyurethane elastomers for soft tissue regeneration," *ACS applied materials & interfaces,* vol. 9, no. 3, pp. 2169-2180, 2017.

[175] C. Hepburn, *Polyurethane elastomers*. Springer Science & Business Media, 2012.

[176] G. Yin *et al.*, "Dielectric elastomer generator with improved energy density and conversion efficiency based on polyurethane composites," *ACS applied materials & interfaces,* vol. 9, no. 6, pp. 5237-5243, 2017.

[177] T. Zhao *et al.*, "4D printing of shape memory polyurethane via stereolithography," *European Polymer Journal,* vol. 101, pp. 120-126, 2018.

[178] W. C. Danen and D. D. Newkirk, "Nitrogen-centered free radicals. IX. The ease of formation of thionitroxide radicals," *Journal of the American Chemical Society,* vol. 98, no. 2, pp. 516-520, 1976.

[179] K. Matyjaszewski and J. Xia, "Atom transfer radical polymerization," *Chemical reviews,* vol. 101, no. 9, pp. 2921-2990, 2001.

[180] A. Takahashi, R. Goseki, and H. Otsuka, "Thermally Adjustable Dynamic Disulfide Linkages Mediated by Highly Air‐Stable 2, 2, 6, 6‐Tetramethylpiperidine‐1‐sulfanyl (TEMPS) Radicals," *Angewandte Chemie International Edition,* vol. 56, no. 8, pp. 2016-2021, 2017.

[181] Y. Yang, Z. Pei, X. Zhang, L. Tao, Y. Wei, and Y. Ji, "Carbon nanotube–vitrimer composite for facile and efficient photo-welding of epoxy," *Chemical Science,* vol. 5, no. 9, pp. 3486-3492, 2014.

[182] X. An *et al.*, "Aromatic diselenide crosslinkers to enhance the reprocessability and self-healing of polyurethane thermosets," *Polymer Chemistry,* vol. 8, no. 23, pp. 3641-3646, 2017.

[183] U. Lafont, H. Van Zeijl, and S. Van Der Zwaag, "Influence of cross-linkers on the cohesive and adhesive self-healing ability of polysulfide-based thermosets," *ACS applied materials & interfaces,* vol. 4, no. 11, pp. 6280-6288, 2012.

[184] V. Garcia-Pacios, Y. Iwata, M. Colera, and J. M. Martín-Martínez, "Influence of the solids content on the properties of waterborne polyurethane dispersions obtained with polycarbonate of hexanediol," *International journal of adhesion and adhesives,* vol. 31, no. 8, pp. 787-794, 2011.

[185] G. Trovati, E. A. Sanches, S. C. Neto, Y. P. Mascarenhas, and G. O. Chierice, "Characterization of polyurethane resins by FTIR, TGA, and XRD," *Journal of Applied Polymer Science,* vol. 115, no. 1, pp. 263-268, 2010.

[186] S. M. Kim *et al.*, "Superior toughness and fast self‐healing at room temperature engineered by transparent elastomers," *Advanced Materials,* vol. 30, no. 1, p. 1705145, 2018.

[187] P. J. Haines, *Thermal methods of analysis: principles, applications and problems*. Springer Science & Business Media, 2012.

[188] N. Alves, J. Mano, and J. G. Ribelles, "Molecular mobility in polymers studied with thermally stimulated recovery. II. Study of the glass transition of a

semicrystalline PET and comparison with DSC and DMA results," *Polymer,* vol. 43, no. 13, pp. 3627-3633, 2002.

[189] A. Shrivastava, *Introduction to plastics engineering*. William Andrew, 2018.

[190] X. Sheng, J. K. Lee, and M. R. Kessler, "Influence of cross-link density on the properties of ROMP thermosets," *Polymer,* vol. 50, no. 5, pp. 1264-1269, 2009.

[191] R. Martin, A. Rekondo, A. R. de Luzuriaga, G. Cabañero, H. J. Grande, and I. Odriozola, "The processability of a poly (urea-urethane) elastomer reversibly crosslinked with aromatic disulfide bridges," *Journal of Materials Chemistry A,* vol. 2, no. 16, pp. 5710-5715, 2014.

[192] W. F. Su, K. Chen, and S. Tseng, "Effects of chemical structure changes on thermal, mechanical, and crystalline properties of rigid rod epoxy resins," *Journal of Applied Polymer Science,* vol. 78, no. 2, pp. 446-451, 2000.

[193] J. Herzberger, J. M. Sirrine, C. B. Williams, and T. E. Long, "Polymer design for 3D printing elastomers: Recent advances in structure, properties, and printing," *Progress in Polymer Science,* vol. 97, p. 101144, 2019.

[194] M. Wehner *et al.*, "An integrated design and fabrication strategy for entirely soft, autonomous robots," *Nature,* vol. 536, no. 7617, pp. 451-455, 2016.

[195] T. J. Hinton, A. Hudson, K. Pusch, A. Lee, and A. W. Feinberg, "3D printing PDMS elastomer in a hydrophilic support bath via freeform reversible

embedding," *ACS biomaterials science & engineering,* vol. 2, no. 10, pp. 1781-1786, 2016.

[196] N. X. Williams, S. Noyce, J. A. Cardenas, M. Catenacci, B. J. Wiley, and A. D. Franklin, "Silver nanowire inks for direct-write electronic tattoo applications," *Nanoscale,* vol. 11, no. 30, pp. 14294-14302, 2019.

[197] P. Jiang *et al.*, "Direct ink writing with high-strength and swelling-resistant biocompatible physically crosslinked hydrogels," *Biomaterials science,* vol. 7, no. 5, pp. 1805-1814, 2019.

[198] X. Wan, L. Luo, Y. Liu, and J. Leng, "Direct Ink Writing Based 4D Printing of Materials and Their Applications," *Advanced Science,* vol. 7, no. 16, p. 2001000, 2020.

[199] Z. Mao *et al.*, "Direct‐Ink Written Shape‐Morphing Film with Rapid and Programmable Multimotion," *Advanced Materials Technologies*, vol. 5, no. 2, p. 1900974, 2020.

[200] L. Li, Q. Lin, M. Tang, A. J. Duncan, and C. Ke, "Advanced Polymer Designs for Direct‐Ink‐Write 3D Printing," *Chemistry –A European Journal,* vol. 25, no. 46, pp. 10768-10781, 2019.

[201] D. Therriault, S. R. White, and J. A. Lewis, "Chaotic mixing in three-dimensional microvascular networks fabricated by direct-write assembly," *Nature materials,* vol. 2, no. 4, pp. 265-271, 2003.

[202] J. Zhu, Q. Zhang, T. Yang, Y. Liu, and R. Liu, "3D printing of multi-scalable structures via high penetration near-infrared photopolymerization," *Nature communications,* vol. 11, no. 1, pp. 1-7, 2020.

[203] A. M'barki, L. Bocquet, and A. Stevenson, "Linking rheology and printability for dense and strong ceramics by direct ink writing," *Scientific reports,* vol. 7, no. 1, pp. 1-10, 2017.

[204] H. Yuk and X. Zhao, "A new 3D printing strategy by harnessing deformation, instability, and fracture of viscoelastic inks," *Advanced Materials,* vol. 30, no. 6, p. 1704028, 2018.

[205] D. J. Fortman, R. L. Snyder, D. T. Sheppard, and W. R. Dichtel, "Rapidly reprocessable cross-linked polyhydroxyurethanes based on disulfide exchange," *ACS Macro Letters,* vol. 7, no. 10, pp. 1226-1231, 2018.

[206] S. Nevejans, N. Ballard, M. Fernández, B. Reck, and J. M. Asua, "Flexible aromatic disulfide monomers for high-performance self-healable linear and cross-linked poly (urethane-urea) coatings," *Polymer,* vol. 166, pp. 229-238, 2019.

[207] M. Pepels, I. Filot, B. Klumperman, and H. Goossens, "Self-healing systems based on disulfide–thiol exchange reactions," *Polymer Chemistry,* vol. 4, no. 18, pp. 4955-4965, 2013.

[208] J. Brandrup, E. H. Immergut, E. A. Grulke, A. Abe, and D. R. Bloch, *Polymer handbook*. Wiley New York, 1999.

[209] X. Wang, M. Jiang, Z. Zhou, J. Gou, and D. Hui, "3D printing of polymer matrix composites: a review and prospective," *Composites Part B: Engineering,* vol. 110, pp. 442-458, 2017.

[210] B. T. Astrom, *Manufacturing of polymer composites*. CRC press, 1997.

[211] S. Iijima, "Helical microtubules of graphitic carbon," *nature,* vol. 354, no. 6348, pp. 56-58, 1991.

[212] K.-t. Lau, C. Gu, and D. Hui, "A critical review on nanotube and nanotube/nanoclay related polymer composite materials," *Composites Part B: Engineering,* vol. 37, no. 6, pp. 425-436, 2006.

[213] M. S. Shaffer and A. H. Windle, "Fabrication and characterization of carbon nanotube/poly (vinyl alcohol) composites," *Advanced materials,* vol. 11, no. 11, pp. 937-941, 1999.

[214] S. Peng *et al.*, "3D Printing Mechanically Robust and Transparent Polyurethane Elastomers for Stretchable Electronic Sensors," *ACS Applied Materials & Interfaces*, vol. 12, no. 5, pp. 6479-6488, 2020.

[215] J. Zhu, J. Kim, H. Peng, J. L. Margrave, V. N. Khabashesku, and E. V. Barrera, "Improving the dispersion and integration of single-walled carbon nanotubes in epoxy composites through functionalization," *Nano letters,* vol. 3, no. 8, pp. 1107-1113, 2003.

[216] X. Wang, J. Li, H. Song, H. Huang, and J. Gou, "Highly stretchable and wearable strain sensor based on printable carbon nanotube layers/polydimethylsiloxane composites with adjustable sensitivity," *ACS applied materials & interfaces,* vol. 10, no. 8, pp. 7371-7380, 2018.

[217] J. Shen, W. Huang, L. Wu, Y. Hu, and M. Ye, "The reinforcement role of different amino-functionalized multi-walled carbon nanotubes in epoxy nanocomposites," *Composites Science and Technology,* vol. 67, no. 15-16, pp. 3041-3050, 2007.

[218] L.-c. Tang, H. Zhang, J.-h. Han, X.-p. Wu, and Z. Zhang, "Fracture mechanisms of epoxy filled with ozone functionalized multi-wall carbon nanotubes," *Composites science and technology,* vol. 72, no. 1, pp. 7-13, 2011.

[219] R. E. Gorga and R. E. Cohen, "Toughness enhancements in poly (methyl methacrylate) by addition of oriented multiwall carbon nanotubes," *Journal of polymer science part B: Polymer physics,* vol. 42, no. 14, pp. 2690-2702, 2004.

[220] M. Wong, M. Paramsothy, X. Xu, Y. Ren, S. Li, and K. Liao, "Physical interactions at carbon nanotube-polymer interface," *Polymer,* vol. 44, no. 25, pp. 7757-7764, 2003.

[221] H.-C. Kuan, C.-C. M. Ma, W.-P. Chang, S.-M. Yuen, H.-H. Wu, and T.-M. Lee, "Synthesis, thermal, mechanical and rheological properties of multiwall carbon nanotube/waterborne polyurethane nanocomposite," *Composites Science and Technology,* vol. 65, no. 11-12, pp. 1703-1710, 2005.

[222] G. Camino, G. Tartaglione, A. Frache, C. Manferti, and G. Costa, "Thermal and combustion behaviour of layered silicate–epoxy nanocomposites," *Polymer Degradation and Stability,* vol. 90, no. 2, pp. 354-362, 2005.

[223] J. N. Coleman, U. Khan, W. J. Blau, and Y. K. Gun'ko, "Small but strong: a review of the mechanical properties of carbon nanotube–polymer composites," *Carbon,* vol. 44, no. 9, pp. 1624-1652, 2006.

[224] J. N. Coleman, U. Khan, and Y. K. Gun'ko, "Mechanical reinforcement of polymers using carbon nanotubes," *Advanced materials,* vol. 18, no. 6, pp. 689-706, 2006.

[225] C. Zeng, N. Hossieny, C. Zhang, B. Wang, and S. M. Walsh, "Morphology and tensile properties of PMMA carbon nanotubes nanocomposites and nanocomposites foams," *Composites science and technology,* vol. 82, pp. 29-37, 2013.

[226] U. F. Fritze and M. von Delius, "Dynamic disulfide metathesis induced by ultrasound," *Chemical Communications,* vol. 52, no. 38, pp. 6363-6366, 2016.

[227] B. G. Compton and J. A. Lewis, "3D‐printing of lightweight cellular composites," *Advanced materials,* vol. 26, no. 34, pp. 5930-5935, 2014.

[228] D. H. Turkenburg, H. van Bracht, B. Funke, M. Schmider, D. Janke, and H. R. Fischer, "Polyurethane adhesives containing Diels–Alder‐based thermoreversible bonds," *Journal of Applied Polymer Science,* vol. 134, no. 26, 2017.

[229] R. J. Sheridan and C. N. Bowman, "Understanding the process of healing of thermoreversible covalent adaptable networks," *Polymer Chemistry,* vol. 4, no. 18, pp. 4974-4979, 2013.

[230] S. Lin *et al.*, "Synthetic Multifunctional Graphene Composites with Reshaping and Self‐Healing Features via a Facile Biomineralization‐Inspired Process," *Advanced Materials,* vol. 30, no. 34, p. 1803004, 2018.

[231] S. Hong *et al.*, "3D printing of highly stretchable and tough hydrogels into complex, cellularized structures," *Advanced materials,* vol. 27, no. 27, pp. 4035-4040, 2015.

[232] Z. Jiang *et al.*, "Direct Ink Writing of Poly (tetrafluoroethylene)(PTFE) with Tunable Mechanical Properties," *ACS applied materials & interfaces,* vol. 11, no. 31, pp. 28289-28295, 2019.

[233] R. P. Wool, "Self-healing materials: a review," *Soft Matter,* vol. 4, no. 3, pp. 400-418, 2008.

[234] C. E. Diesendruck, N. R. Sottos, J. S. Moore, and S. R. White, "Biomimetic self‐healing," *Angewandte Chemie International Edition,* vol. 54, no. 36, pp. 10428-10447, 2015.

[235] Z. Zhang *et al.*, "Electrospun PLA/MWCNTs composite nanofibers for combined chemo-and photothermal therapy," *Acta biomaterialia,* vol. 26, pp. 115-123, 2015.

[236] Y. Wang, C. Wang, X. Song, S. K. Megarajan, and H. Jiang, "A facile nanocomposite strategy to fabricate a rGO–MWCNT photothermal layer for efficient water evaporation," *Journal of Materials Chemistry A,* vol. 6, no. 3, pp. 963-971, 2018.

[237] D. Hua *et al.*, "3D printing of shape changing composites for constructing flexible paper-based photothermal bilayer actuators," *Journal of Materials Chemistry C,* vol. 6, no. 8, pp. 2123-2131, 2018.

[238] J. Qu, R. Zhang, Z. Wang, and Q. Wang, "Photo-thermal conversion properties of hybrid CuO-MWCNT/H2O nanofluids for direct solar thermal energy harvest," *Applied Thermal Engineering,* vol. 147, pp. 390-398, 2019.

[239] D. Y. Wu, S. Meure, and D. Solomon, "Self-healing polymeric materials: a review of recent developments," *Progress in polymer science,* vol. 33, no. 5, pp. 479-522, 2008.

# Appendices

**Appendix A**: The CAD models of the 3D printed parts in Figure 4-5, in turn, are (a) octopus, (b) the Eiffel Tower, (c) Tiantan and (d) Arc de Triomphe.

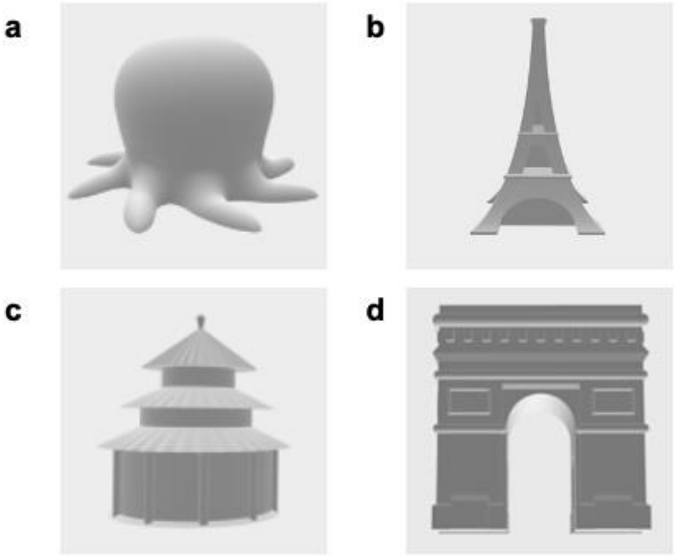

**Appendix B**: The CAD models of the 3D printed parts in Figure 4-7, in turn, are (a) Chinese "Fu" character, (b) butterfly and (c) honeycomb.

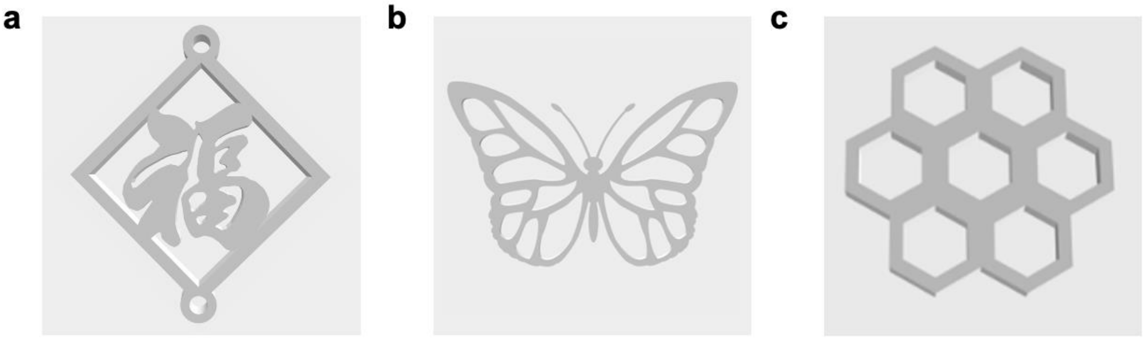

**Appendix C**: The CAD model of the 3D printed part in Figure 5-11 is Hanging Gardens of Babylon.

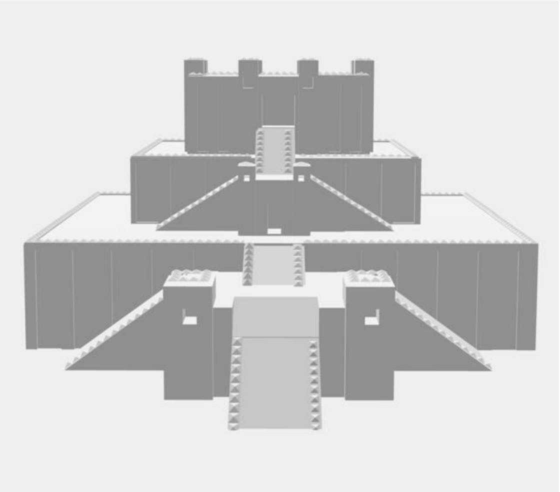

**Appendix D**: The CAD models of the 3D printed parts in Figure 5-12, in turn, are (a) Chichen Itza, (b) Taj Mahal, and (c) the Great Wall of China.

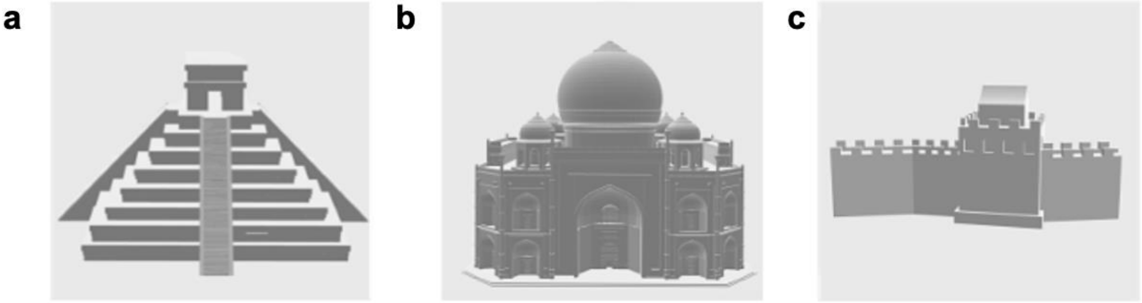

## **Appendix E**: The CAD models of the 3D printed parts in Figure 6-8, in turn, are (a) honeycomb and (b) arch bridge.

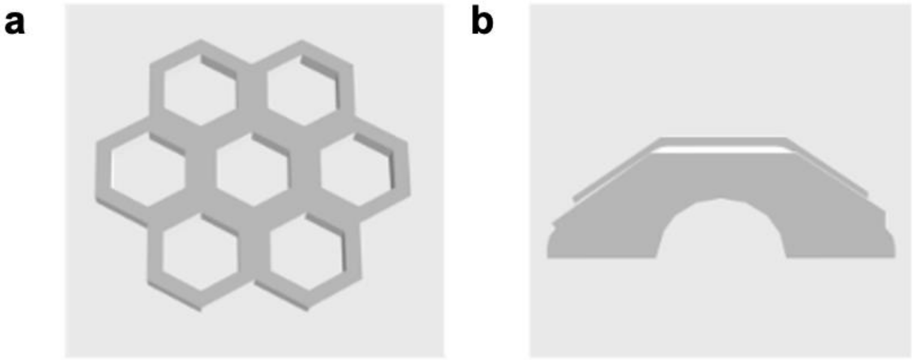

# Curriculum Vitae

## Mingyue Zheng

## Education

- Western University | Mechanical and Materials Engineering | Ph.D.
  2015.09-2020.12 (Canada)

- Tianjin University | Material Science and Engineering | Bachelor
  2011.09-2015.09 (Tianjin)

## Research Experience

**Ph.D. Degree** **Western University** **2015.09-2020.12**

- Supervised by Professor Jun Yang

- Designed the synthetical routes of recyclable and repairable disulfide-based polyurethane 3D printing materials, scaled up experiments, and improved production processes, analyzed the chemical and physical properties of materials, added fillers to targeted modify the performance of materials

**Bachelor's Degree** **Tianjin University** **2014.07-2014.09**

***Protease-responsive polypeptide-based functional hydrogels (Graduation Project)***

- Based on Michael reaction synthesized protease-responsive functional polypeptide hydrogels; got proficient with the skills of SDS-PAGE gel electrophoresis, standard sterile operation and bacteria & cell culture techniques

***Synthesis and characterization of thermal sensitive star-branched polymer***

- Based on RAFT mechanism, synthesized three different grafting density HPEI-g-PNIPA; studied their solubility changes under different temperature

## Other Experience

**Teaching Assistant** **Western University** **2016.09-2020.04**

- Served as a teaching assistant for Engineering Materials courses and Robotics Automation courses for four years. In charge of Lab courses, summarized and reflected the problems, improved the quality of teaching

| | | |
|---|---|---|
| **Volunteer** | **Banting House National Historic Site** | **2016.11-2019.04** |

## Publications and Conference

- Zheng, M., Guo, Q., Yin, X., Getangama, N., de Bruyn. J., Xiao, J., ... & Yang, J.
  Direct ink writing of recyclable and in situ repairable photothermal polyurethane for sustainable 3D printing development. **Journal of Materials Chemistry A,** DOI: 10.1039/d0ta11341g
- Zhang, Y., Yin, X. Y., Zheng, M., Moorlag, C., Yang, J., & Wang, Z. L. (2019). 3D printing of thermoreversible polyurethanes with targeted shape memory and precise in situ self-healing properties. **Journal of Materials Chemistry A**, 7(12), 6972-6984.
- Zhang, D., Xiao, J., Bai, Y., Guo, Q., Zheng, M., Liu, M., ... & Yang, J. (2020). Introducing Bioinspired Initiator into Resins for In Situ Repairing of 3D-Printed Metallic Structures. **ACS Applied Materials & Interfaces**, 12(43), 49073-49079.
- Zheng, M.& Yang, J. 3D Printing Materials with Recyclable and Precise In-Situ Self-Healing Properties. **The 2019 Canadian Society for Mechanical Engineering and the CFD Society of Canada (CSME-CFDSC 2019)**
-